ISTANBUL TECHNICAL UNIVERSITY ★ GRADUATE SCHOOL OF SCIENCE ENGINEERING AND TECHNOLOGY

ON STEADY-STATE PERFORMANCE ESTIMATION OF THREE-PHASE INDUCTION MOTORS

M.Sc. THESIS

Rami AL-SAMARAAE

Department of Electrical Engineering

Electrical Engineering Program

MARCH 2018

ISTANBUL TECHNICAL UNIVERSITY ★ GRADUATE SCHOOL OF SCIENCE ENGINEERING AND TECHNOLOGY

ON STEADY-STATE PERFORMANCE ESTIMATION OF THREE-PHASE INDUCTION MOTORS

M.Sc. THESIS

Rami AL-SAMARAAE
(504151089)

Department of Electrical Engineering

Electrical Engineering Program

Thesis Advisor: Assoc. Prof. Özgür ÜSTÜN

MARCH 2018

ISTANBUL TEKNİK ÜNİVERSİTESİ ★ FEN BİLİMLERİ ENSTİTÜSÜ

ÜÇ FAZLI ASENKRON MOTORLARIN SÜREKLİ-HAL PERFORMANS KESTİRİMİ

YÜKSEK LİSANS TEZİ

Rami AL-SAMARAAE
(504151089)

Elektrik Mühendisliği Anabilim Dalı

Elektrik Mühendisliği Programı

Tez Danışmanı: Doç. Dr. Özgür ÜSTÜN

MART 2018

Rami Rafil AL-SAMARAAE, a M.Sc. student of İTU Graduate School of Science Engineering and Technology student ID 504151089, successfully defended the thesis/dissertation entitled “ON STEADY-STATE PERFORMANCE ESTIMATION OF THREE-PHASE INDUCTION MOTORS”, which he prepared after fulfilling the requirements specified in the associated legislations, before the jury whose signatures are below.

Thesis Advisor :	**Assoc. Prof. Özgür ÜSTÜN** Istanbul Technical University	.....
Jury Members :	**Asst. Prof. Murat YILMAZ** Istanbul Technical University	.....
	Asst. Prof. Salih Barış ÖZTÜRK Okan University	.....

Date of Submission : 19 MARCH 2018
Date of Defense : 23 MARCH 2018

FOREWORD

I am heartily thankful to my supervisor Assoc. Prof. Özgür ÜSTÜN, whose encouraged, supervised, supported me from the preliminary to the concluding level, and for his cooperation, to complete my research. I want to thank Res. Asst. M. Onur GÜLBAHÇE, for his support and encouragement. My committee members Asst. Prof. Murat YILMAZ and Asst. Prof. Salih Barış ÖZTÜRK thank you for your advice, perspective, and ability to help me focus on the right path.

Throughout my life, my beloved family is acknowledged for their unconditional and endless love, and support, also for giving me this opportunity to study abroad. None of my accomplishments would have been possible without them.

I want to thank my friends for their all-time love and support through this venture. Finally, I want to thanks all those people who helped me in all their capacity in many different ways to complete this work.

MARCH 2018 RAMI AL-SAMARAAE
(Engineer)

TABLE OF CONTENTS

Page

ABBREVIATIONS

4G : Fourth Generation
AC : Alternating Current
CF : Crest Factor
DAQ : Data Acquisition Card
DC : Direct Current
EMF : Electromotive Force
FFT : Fast Fourier Transform
IE : International Efficiency
IEC : International Electrotechnical Commission
IEEE : Institute of Electrical and Electronics Engineers
IoT : Internet of Things
LTE : Long Term Evolution
MA : Moving Average Filtering
MMF : Magnetomotive Force
NEMA : National Electrical Manufacturers Association
OLS : Ordinary Least Squares
RMS : Root Mean Square
THD : Total Harmonic Distortion
TLS : Total Least Square

SYMBOLS

a	: Turns ratio
α	: Angle of deviation from the direction of the principal stresses
$\cos\varphi$	: Power factor
E_1	: Per-phase induced voltage (counter-emf) in the stator winding
E_2	: Per-phase induced voltage in the rotor winding at a standstill
E_1'	: The initial voltage behind the transient reactance
E_2'	: Per-phase induced voltage referred to stator
f_1	: Line (Supply) frequency
f_2	: Slip frequency
G_c	: Per-phase stator core-loss conductance
I_1, i_1	: Per-phase stator and line current
i_{1d}, i_{1q}, i_{10}	: Stator-currents in dq-component
I_2'	: Per-phase rotor current referred to stator
I_2, i_2	: Rotor current
i_{2d}, i_{2q}, i_{20}	: Rotor-currents in dq-component
i_A, i_B, i_C	: Current for rotor phases A, B, and C
i_a, i_b, i_c	: Current for stator phases a, b, and c
I_c	: Core-loss current
I_{dc}	: DC current
I_{SC}	: Current of Full-load (blocked-rotor) test
I_m	: Magnetizing current
I_{NL}	: Current of no-load test
I_o	: Excitation current
J	: Moment of inertia of the rotor and the mechanical equipment coupled to it
L'	: Transient inductance
L_1	: Stator self-inductance
L_2	: Rotor self-inductance
M_1	: Mutual inductance between stator windings
M_2	: Mutual inductance between rotor windings
N_1	: Number of stator windings (Turns)
N_2	: Number of rotor windings (Turns)
n_m	: Mechanical shaft speed of the rotor in rpm
n_s	: Synchronous speed (i.e., the speed of magnetic fields) in rpm
η	: Motor efficiency
θ_0	: Shaft-position angle
θ_2	: Displacement angle between the rotor phases and the stator phases
θ_s	: Displacement angle between the rotor phase-A and the d-axis
ρ	: The differential operator d/dt
p	: Numbers of poles
p_1	: An instantaneous power input
$P_{1,cu}$	: Total stator copper losses

$\mathbf{P_{2,cu}}$: Total rotor copper losses
$\mathbf{P_{core}}$: Total core losses
$\mathbf{P_d}$: Total mechanical power developed
$\mathbf{PF_{SC}}$: Full-load power factor
$\mathbf{PF_{NL}}$: No-load power factor
$\mathbf{P_{FW}}$: Friction and windage losses
$\mathbf{P_g}$: Total air-gap power
$\mathbf{P_{in}}$: Electrical input power to the motor stator
$\mathbf{P_{in\text{-}SC}}$: Electrical input power to the motor stator in Full-load (blocked-rotor) test
$\mathbf{P_{in\text{-}NL}}$: Electrical input power to the motor stator in no-load test
$\mathbf{P_{loss}}$: Total power losses
$\mathbf{P_m}$: Total mechanical power developed
$\mathbf{P_{out}}$: Output power
$\mathbf{P_{rot}}$: Total rotational losses
$\mathbf{P_{stray}}$: Stray losses
$\mathbf{R_1}$, $\mathbf{r_1}$: Per-phase stator winding resistance
$\mathbf{R_2}$, $\mathbf{r_2}$: Per-phase rotor winding resistance
$\mathbf{R_2'}$: Rotor winding resistance per-phase referred to stator
$\mathbf{R_{ab}}$: Resultant resistance of parallel R_c and R_2'
$\mathbf{R_c}$: Per-phase stator core-loss resistance
$\mathbf{R_{dc}}$: DC resistance
$\mathbf{R_{in}}$: Total resistance in exact equivalent circuit
$\mathbf{R_{TH}}$: Thevenin equivalent resistance
$\boldsymbol{s}$: Slip
$\mathbf{S_{max}}$: Slip for maximum torque
$\mathbf{T}$: Electromagnetic torque
$\mathbf{t}$: Time
$\mathbf{T'}$: Short-circuit time constant
$\mathbf{T_0'}$: Time constant of the rotor circuit alone
$\mathbf{T_d}$: Developed torque
$\mathbf{T_{max}}$: Maximum (pull-out) torque
$\mathbf{T_{out}}$: Output torque (Shaft torque)
$\mathbf{T_{start}}$: Starting Torque
$\mathbf{V_1}$, $\mathbf{v_1}$: Per-phase stator terminal voltage
$\mathbf{V_{10}}$: The prefault rms terminal voltage
$\mathbf{v_{1d}}$, $\mathbf{v_{1q}}$: Stator-voltages in dq-component
$\mathbf{V_2}$, $\mathbf{v_2}$: Per-phase rotor terminal voltage
$\mathbf{v_{2d}}$, $\mathbf{v_{2q}}$: Rotor-voltages in dq-component
$\mathbf{V_A}$, $\mathbf{V_B}$, $\mathbf{V_C}$: Rotor terminal voltage for phases A, B, and C
$\mathbf{V_a}$, $\mathbf{V_b}$, $\mathbf{V_c}$: Stator terminal voltage for phases a, b, and c
$\mathbf{V_{dc}}$: DC voltage
$\mathbf{V_{L\text{-}SC}}$: Line voltage of Full-load (blocked-rotor) test
$\mathbf{V_{L\text{-}NL}}$: Line voltage of no-load test
$\mathbf{V_m}$: Voltage across magnetizing branch
$\mathbf{V_{p\text{-}SC}}$: Phase voltage of Full-load (blocked-rotor) test
$\mathbf{V_{p\text{-}NL}}$: Phase voltage of no-load test
$\mathbf{V_{TH}}$: Thevenin equivalent voltage
$\boldsymbol{\omega_m}$: Mechanical shaft speed of rotor in rad/s
$\boldsymbol{\omega_s}$: Synchronous speed in rad/s

ω_0 : Shaft angular velocity
ω_2 : Rotor angular velocity
X' : Transient reactance
X_1 : Per-phase stator leakage reactance
X_2 : Per-phase rotor leakage inductive reactance
X'_2 : Rotor winding inductance per-phase referred to stator
X_{ab} : Resultant reactance of parallel X_m and X'_2
X_{SC} : Full load equivalent reactance
X_{in} : Total reactance in exact equivalent circuit
X_m : Per-phase stator magnetizing reactance
X_{TH} : Thevenin equivalent reactance
z_1 : Impedance of stator parameters (R_1+X_1)
z_2 : Impedance of stator parameters (R_2+X_2)
Z_{ab} : Impedance of magnetizing branch (R_c+X_m)
Z_{eq} : Equivalent impedance
Z_{SC} : Total impedance of Full-load (blocked-rotor) test
Z_{in} : Total impedance in exact equivalent circuit
Z_{NL} : Total impedance of no-load test
λ_1 : Flux-linkage of stator
λ_{1d}, λ_{1q} : Stator Flux-linkage in dq-components
λ_2 : Flux-linkage of rotor
λ_{2d}, λ_{2q} : Rotor Flux-linkage in dq-components
λ_A, λ_B, λ_C : Flux-linkage for rotor phases A, B, and C
λ_a, λ_b, λ_c : Flux-linkage for stator phases a, b, and c

LIST OF TABLES

Page

LIST OF FIGURES

Page

ON STEADY-STATE PERFORMANCE ESTIMATION OF THREE-PHASE INDUCTION MOTORS

SUMMARY

In industry, more than 85 % of the used motors are induction motors, because of two main reasons: rugged in construction and low cost when comparing it to other motors. Recently, increasing higher efficiency interests and protective maintenance trends lead the on-line performance monitoring of induction motors. If it is intended to monitor performances of all motors, this can be only done by using cheaper sensors and by processing the captured information to provide a performance monitoring calculation in a central unit. For this reason, there are multiple types of research on the performance monitoring devices, which are using LTE/4G IoT technology. It is possible to estimate the motor performance by means of captured terminal quantities and motor parameters. The aim of this thesis is to define input and output steady-state performance values of an induction motor via information from simple terminal voltage and current sensors.

Since motor parameters are required to estimate performance, by on-line and off-line techniques can determine the motor parameters. By conducting some fundamental tests (no-load, and blocked-rotor), the motor equivalent circuit parameters can be defined. The target of this study is to predict the performance of an induction motor by using only terminal quantities.

The experimental work and estimation calculations are applied for a 4-pole, 2.2 kW three-phase squirrel cage induction motor. First, the fundamental tests such as no-load and blocked-rotor tests are conducted and the performance of the motor is monitored experimentally. Then corrected no-load test is conducted to find the more accurate value of core loss resistor and frictional losses. So motor equivalent circuit parameters and motor heating are defined.

By using VisSim software, motor input impedance calculation and power distribution algorithms are formed and variation of the input equivalent impedance with the motor slip is obtained. A basic algorithm is developed to calculate the input powers, i.e. input apparent, active and reactive powers from the terminal voltage and current values.

In this study, a simple method that is based on total equivalent impedance of T-equivalent circuit is proposed as a scientific contribution. The essence of the method is to find out the relation between equivalent impedance and slip. To extract the slip from the impedance expression is required a substantial of a burden of calculation. Thus, this problem is solved by using a quadratic equation of equivalent impedance that is a function of slip. A MATLAB curve fitting algorithm is used to define input impedance-slip variation with a quadratic equation. The coefficients of the quadratic equation are depending on the motor equivalent circuit parameters. These coefficients can be obtained from the manufacturer or found by means of fundamental tests. So all these calculations including the terminal powers and slip

can be done via a microprocessor with a simple code. By adding frictional and stray losses, the output power and shaft torque can be defined. By doing so, the efficiency and loading can be monitored on-line.

In the thesis, the tested and calculated results are in agreement. Therefore, it is shown that the performance of an induction motor can be estimated by using only terminal measurements and simple calculations. For future work, it will be searched the ways of determining motor parameters during operation and without implementing any tests. Moreover, the temperature dependency of the related parameters will analyze thoroughly.

ÜÇ FAZLI ASENKRON MOTORLARIN SÜREKLİ HAL PERFORMANS KESTİRİMİ

ÖZET

Endüstride kullanılan motorların yüzde seksen beşinden fazlası asenkron motorlardır. Bu yoğun kullanımın temel nedenleri, sağlam yapıları ve diğer motorlara göre daha ucuz olmalarıdır. Son yıllarda artan yüksek verim arayışları ve önleyici bakım araştırmaları, asenkron motorların performanslarının sürekli gözlenmesi gibi çözüm arayışları getirmiştir. Eğer tüm motorların performanslarının gözlenmesi amaçlanıyorsa, bu ancak ucuz sensörler ve bu sensörlerin algıladıkları bilgileri önce işleyerek ardından ana bir hesaplama birimine göndermesi ile olanaklı olabilir. Bu amaçla günümüzde LTE/4G haberleşmeli IoT (Internet of Things) modülleri ile performans gözleyici cihazlarla ilgili araştırmalar yapılmaktadır. Yalnızca alınan giriş büyüklükleri bilgileri ile asenkron motorun performansı tahmin edilebilir. Bu tezin amacı, basit ve ucuz gerilim ve akım sensörleri kullanılarak yalnızca giriş bilgilerinin ölçülmesi ve motor parametreleri yardımı ile motor çıkış büyüklüklerinin belirlenmesidir.

Motor performansının kestirimi için motor eşdeğer devre parametrelerinin belirlenmesi gerektiğinden, bu parametreler çevrim içi ya da çevrim dışı belirlenebilir. Temel deneyler olarak adlandırılan boşta ve kısa devre (kilitli rotor) deneyleri ile motor eşdeğer devre parametreleri belirlenebilir. Bu çalışmanın hedefi eşdeğer devre parametreleri yardımı ile yalnızca giriş büyüklüklerini kullanarak bir asenkron motorun sürekli hal performansının kestirimidir.

Hesaplamalar ve deneysel çalışma için 380 V, 4 kutup, 2.2 kW gücünde üç fazlı bir asenkron motor kullanılmıştır. Öncelikle motorun performans ve temel deneyleri (boşta ve kilitli rotor) yapılmış ve motor performansı deneysel olarak gözlenmiştir. Ayrıca hem sürtünme kayıplarının hem de doğru demir direnci değerlerinin belirlenmesini sağlayan düzeltilmiş boşta deney de gerçekleştirilmiştir. Motor eşdeğer devre parametreleri ve motorun ısınması da ayrıca belirlenmiştir.

Ardından VisSim yazılımı ortamında, motor giriş eşdeğer empedansı ve motor güç dağılımı algoritmaları oluşturulmuş ve giriş empedansının kayma ile değişimi ortaya konulmuştur. Ayrıca motor giriş gerilimi ve akımından motor giriş aktif, reaktif ve görünür güçlerini belirleyen basit algoritmalar kurulmuştur. Ardından MATLAB ortamında eğri uydurma algoritmaları kullanılarak giriş eşdeğer empedansının kayma ile değişimi ikinci dereceden modellenmiştir. İkinci dereceden denklemin katsayıları motorun eşdeğer devre parametrelerine bağlıdır. Bu katsayılar doğrudan üretici tarafından ya da yapılacak olan deneylerle belirlenebilir. Bu sayede, seçilecek olan işlemciye yazılacak basit bir gömülü yazılım ile giriş güç hesaplama ve eşdeğer empedanstan kayma değerini belirleme işlemleri yaptırılabilir. Sürtünme ve ek kayıpların ilavesi ile motor çıkış gücü ve mil momenti belirlenebilir. Bu sayede motorun verimi ve yüklenme durumu sürekli olarak gözlenebilir.

Tezde elde edilen deneysel sonuçlar ve yapılan kestirim hesaplamaları yakın sonuçlar vermiştir. Bu anlamda, asenkron motorların sürekli hal performanslarının çok basit sensörler ve hesaplamalar kullanılarak yapılabileceği ortaya konulmuştur. İleri çalışmalarda, eşdeğer devre parametrelerinin herhangi bir deney yapmaksızın, motorun işletmesi sırasında belirlenmesine yönelik çalışmalar yapılacaktır. Ayrıca giriş eşdeğer empedansının sıcaklıkla olan değişiminin de hesaba katılacağı basit ve hızlı algoritmalar tasarlanacaktır.

1. INTRODUCTION

1.1 Purpose of Thesis

As it is known, induction motors are most widely used electric motors in the industry. Most of the rolling mill applications are applied by three-phase cage induction motors. Statistics show that 45-47% of the global electricity consumed by electrical motors (Waide and Brunner, 2011). And that usage of the electric motor is mainly covered by induction motors. By 2019, the expected market volume of induction motors is predicted as an approximate 16 Million USD (Research and Markets, 2015). Heating and ventilating systems, pump and compressor systems are the main application areas for induction motors. The reason for this remarkable tendency is based on the simple and cheaper structure of induction motors. Using an aluminum or copper cage instead of permanent magnet assembly brings an undeniable advantage for induction motors. According to the nature of the application, induction motors can be line fed or inverter fed. There is a significant number of line fed induction motors which are used mainly in ventilating, pump and compressor systems.

In recent years, seek for higher efficiency motor usage for energy saving is rapidly increasing and this approach is affecting induction motor designs. Nowadays, IE4 efficiency class motors take to the stage in presence of widely used IE3 motors while IE2 motors are rapidly losing their grounds. New ferromagnetic core materials and copper cages which bring lower iron and copper losses become dominant in induction motor designs. Another effort is directed to investigate the proper motor usage for specific applications. The main question is: Is the motor used the right motor for the application? What if a smaller and higher efficiency motor is used? Researchers are showing that a great number of induction motors can be replaced by a lower rated power motor and use a higher efficiency class motor, e.g. IE4 instead of IE3, may lead substantial energy and cost saving when the lifespan cost of the motor is considered.

Thus, performance monitoring of induction motors is an essential task to find out the quality of motor operation. A performance monitoring task can be done thoroughly by using a voltmeter, ampere meter, and power meters and also shaft torque and speed measurements. But this type of monitoring is not applicable if the total cost of measurement devices and complexity of the monitoring system are considered. In many years, the motor diagnostics is seen as a tough job, and it is mainly studied by academicians. But nowadays, capturing excessive data by means of IoT systems enables to find a proper solution to this problematic area. So, using simple measurements and a performance estimation algorithm is proper for a high number of motor performance predictions.

The total cost of energy and energy saving status of an electric motor can be monitored, and also data can be used for Big Data Analytics. For big data analytics, data sets can be captured from cheaper sensors and sent via an IoT module (local wireless or LTE/4G). The captured data are filtered and can be converted to useful information. So performance every induction motor which is equipped with cheaper sensors, a simple microprocessor, and an IoT module can be monitored. Also, the serious deviations from the expected performance of any induction such as higher currents, higher slip values motor can be evaluated as a failure mode and thus, motor diagnostics can be done properly. This situation means that big data analytics can be efficiently utilized in induction motor monitoring both for performance and health status.

By the usage of cheap current and voltage sensors and capturing current and voltage waveforms changing with time, all the terminal data of a three-phase induction motor such as apparent input power, the phase angle between terminal voltage and current, power factor, active and reactive input powers can be calculated approximately.

The performance estimation algorithm in this thesis is based on pure or near sinusoidal waveforms both for voltage and current, so it cannot be applied appropriately any induction motor driven by inverters or fed from non-sinusoidal sources. Two basic methods are proposed to find out the sinusoidal form of any waveform: The first check is based on FFT (Fast Fourier Transform) analysis which is giving reliable information of the captured waveforms are whether sinusoidal or not. For example, the estimation analysis can be done up to a specific THD limit such as 10% or lower. A simpler version is to check the Crest Factor (CF) of a

waveform which is approximately 1.4142 for a pure sinusoidal signal. CF is simply the ratio of peak and RMS values. So, of course, there can be other waveforms which have 1.4142 CF value. But in a regular AC grid, the most probable member of 1.4142 CF is a pure or near sinusoidal waveform.

The captured terminal measurements are processed to find out the all terminal quantities of 3 phase induction motor. For a balanced 3 phase source, single phase measurements are enough to get the aimed performance data. After the capturing process, by means of T- equivalent circuit parameters and some approximations, the operation slip of induction motor under attention can be defined. The T-equivalent circuit is a lumped-parameter model of an induction motor and known as Steinmetz equivalent circuit, and it is mainly used for steady-state evaluation of induction motors. Any steady-state value of currents, induced voltages, inner or loss powers and slip values can be defined by means of this circuit. So in this study, the performance estimation is for the mainly steady-state operation of induction motors. But using some additional estimation algorithms, the transient behavior of motors can be evaluated properly. Also from the terminal current history and the estimated value of stator winding resistance, the motor winding temperature can be predicted. As it is a well-known fact, the slip is the key parameter for induction motor steady-state performance. Slip value, shaft speed, estimated output mechanical power, estimated shaft torque and efficiency can be defined approximately.

The generated code of proposed simple algorithm can be embedded in a cheap microprocessor, and via an IoT module (local wireless or LTE/4G) the data sets can be transmitted to Big Data Analytics processors. Along with voltage and current measurements, temperature and vibration can also be sensed and used for the performance and health evaluation. And even the total energy consumption, efficiency and power loss amount can be monitored, for example, in a production plant. So all the data can be used for improvement purposes such as replacing motors with higher efficiency counterparts, replacing wrong selected motors with properly selected ones, monitoring the total cost of the production process, preventive maintenance and so on. The total cost of an induction motor during a lifetime can be found.

1.2 Literature Review

In this section, a brief description of what the researchers work done that related to the prediction and estimation of performance characteristics of the three-phase induction motor, by finding the equivalent circuit parameters of the motor.

The main parameters in the equivalent circuit of an induction motor are stator/rotor resistance, stator/rotor leakage inductance, rated magnetizing inductance and transient stator inductance.

Generally, methods of parameters estimation of an induction motor can be classified into three major categories, relying on the availability of data and for what the data is used:

1.2.1 Parameter estimation based on basic motor tests

According to Institute of Electrical and Electronics Engineers (IEEE) Standard 112, the induction motor parameters can be obtained from two primary tests no-load and locked rotor test. Temperature, saturation, and frequency all these factors affect the value of the induction motor parameters (IEEE Std. 112, 2004).

Salleh et al. (2013), shows that the induction motor parameters can be obtained through the no-load and blocked-rotor tests. The no-load test is achieved by applying rated voltage and frequency to the motor. In blocked-rotor test, a low voltage applied to the stator windings until rated current is reached. The measured data are taken from the measurements devices during these tests.

Jurkovic (2005) tried to find the most accurate parameters values of the motor. In addition to the no-load and blocked-rotor test, second no-load test performed under the same condition. Rated voltage and frequency is applied to the motor stator and the rotor of the induction motor is rotated at the synchronous speed with DC machine. Conclude that the results of the second no-load test are more accurate because the slip is now exactly zero. The second blocked-rotor test results are omitted because they are almost identically.

Gastli (1999), the proposed method to identify the equivalent circuit parameters is based on single-phase tests, by injecting single-phase AC current then measured the voltage, current, and power that absorbed by the motor. This approach is closed to

blocked-rotor test and provides results that related to the rotor resistance and leakage inductance. The single-phase tests are done on three types of induction motor equivalent circuit.

1.2.2 Parameter estimation based on software simulation

Ghule et al. (2013), proposed that a new off-line technique to predict performance characteristics from motor parameters and manufacturer's data. Current, speed, power factor, efficiency, and torque all these performance characteristics can be estimated by using an off-line technique from some mathematical formula relating to the equivalent circuit parameters. A couple of graphs represent the results of motor performance. Moreover, software programs are used to implement the three-phase squirrel cage induction motor tests, such as MATLAB/Simulink to calculate parameters values by using mathematical formula and ETAP to measure the parameters values. In this work, three types of tests are used, DC to determine the stator per phase resistance, no-load to determine the stator inductance and the power loss, and blocked-rotor to determine the rotor per phase resistance and the sum of the leakage inductances of the stator and rotor windings. It has been noticed that this approach is very simple and convenient to implement. However, there is a deviation between the calculated values and the measured values. As a result, the reasons for these differences as follow. During the operating condition, the machine parameters in the equivalent circuit hardly to remain constant. Due to increase in temperature both stator and rotor resistance increase linearly, relying on the temperature coefficient of the resistance materials. Because of the harmonics, there is skin effect that causes current crowding on the conductor, which leads to an increase in resistance and decrease of inductance. Concludes that, within the parameters, determination must be used indirect measurement methods and calculations from the data given by the reference or by the experimentally measured speed-torque characteristics. Moreover, because of this approach depending on motor nameplate and catalog, it can be applied to many equivalent circuit modifications.

Sehra et al. (2012) and Baranwal et al. (2014), described a way to get the motor parameters from the indirect test (no-load and blocked-rotor) and the motor performance from Thevenin equivalent circuit parameters. In addition, generating a graphical user interface (GUI) by using MATLAB program to obtain the

performance graphs. In a no-load test, rated voltage and frequency is applied to the stator terminals without any mechanical load. In a blocked-rotor test, applied 25% of the rated frequency and voltage until rated current is reached. In both tests current, voltage and power are measured at the motor input. After that, MATLAB is used to get desired performance characteristics. The results of GUI have a better result of various torque and decrease in the slip with an increase in efficiency. The graphs characteristics are in the form of speed-slip, torque-slip, efficiency-slip, and torque-speed. When compared the results with the normal operation have got on, improvement in efficiency, maximum torque, starting torque, and decreasing in the slip.

Ayasun and Nwankpa (2005), Pandey and Zope (2013), Basu (2015) and Hidayah et al. (2013), presents a MATLAB/Simulink model for a three-phase induction motor block. The motor model takes the inputs data from the tests result (no-load, blocked-rotor and DC resistance). Thereafter, the model is simulated to give the equivalent circuit parameters and operating characteristics. The induction motor block consists of three blocks: the circuit-parameter estimation block, the torque estimation block, and stator current-power-efficiency estimation block. The tests result shows that the various operating characteristics; these characteristics will predict the operational behavior of the motor.

Sangwan (2014), described a dynamic model and simulation of 40 hp three-phase induction motor. dq0 axis transformation is used to normalized stator and rotor parameters in the reference frame via MATLAB/Simulink.

Ratnani and Thosar (2014) and Soe et al. (2008), made a mathematical model for small 3 hp induction motor in the arbitrary frame, to understand the behavior of the motor in both transient and steady-state. Aktaibi et al. (2011), used the same model above, but the difference is two different rating motors are tasted small 3 hp and large 2250 hp induction motors. The simulation models are given both the torque and speed characteristics.

Calis and Caki (2014), presents virtual instrumentation typed engineering workbench (LabVIEW) software to design and develop an automated testing system for an induction motor. The Data Acquisition Card (DAQ) takes the output data from the experimental work; these data are used by LabVIEW user interface to find out the

motor parameters. The main menu of LabVIEW user interface consists of eight different tests that related to the motor parameters, equivalent circuit, and characteristics.

Singhal and Garg (2012), a method for online parameters determination and performance analysis for induction motor are proposed. The method used the virtual instrumentation techniques with the help of DAQ, and all the estimation algorithms are implemented in LabVIEW program. A new method presents called (Impedance Method) to measure motor speed without any kind of sensor. By using measurements of 4 sensors only at stator (input) side of the motor, online output power, torque, losses, and efficiency are measured.

1.2.3 Parameter estimation based on numerical methods

Daut et al. (2009), assumed that the efficiency value that presents in the market is 84%. Also, assumed that the power factor value for the 5 hp induction motor is 0.80; this method called backward calculation. The backwards calculation method is used to calculate the parameters of the motor. Based on Daut's work the value of each parameter calculated is nearly the value of the manufacturer's data. Moreover, noted that when the capacity of the induction motor increases the value of resistance decreases.

Wengerkievicz et al. (2017), presents a survey on the determination of circuit parameter from non-standard tests and manufacture catalog data by using six different analytical methodologies to improve the estimation results. The analytical methods are applied to five different motors, the motors rated power is 7.5, 18.5, 37, 55, and 75 kW. The analytical methods are simple and no need for numerical optimization routines; these methods are Natarajan-Misra's, Haque's, NEQ (for R1 and Pfw only), Sabharwal's, Lee's and Guimarães'. Each method has own precision. The smallest deviation for R1 can get from Guimarães' method, for R2 NM method, for Rc and Xm Haque's method, for X1, X2, and Pconst Lee's methods. Concludes that every method has the strength and weak points and results that are more accurate can be obtained by combining all methods into one method, to achieve smaller average deviation.

Imecs and Incze (2001), shows a simple estimation procedure from the machine nameplate. Analytical calculations based on two types of steady-state equivalent

circuits electrical and magnetically; these equivalent circuits yield the same results. Two simulations of motor dynamic d-q model are used for validation; thus, the simulation results are analyzed by the space-phasor theory.

Sangani (2015), suggested a new method to estimate the parameters and steady-state performance of induction motor, based on the equivalent circuit. The data are taken from the DC, no-load, and blocked-rotor tests. Numerical algorithm is used for parameters estimation (using Newton-Raphson method). Therefore, determining the steady-state performance of induction motor algebraically and graphically (using circle diagram).

Lee et al. (2012), offered a new iterative method to estimate the induction motor parameters using only the nameplate data and as regards motor behavior, typical assumptions are made. The proposed iterative solution method is containing a set of eight simultaneous equations solved by Gauss-Seidel algorithm.

Shaw and Leeb (1999), the authors' present three techniques for estimating the electrical and mechanical parameters of an induction motor. The methods depend on the initial estimation of the transient stator current measurements. The first two methods are used to estimate the electrical parameters; these methods are an Extrapolative method and Equation error method. The last one is to estimate the mechanical parameters of the motor; this method is General identification method.

Zamora and Garcia-Cerrada (2000), proposed that a method to estimate the motor parameters on-line and with using only stator voltage and current measurements. A set of algorithms such as moving average (MA) filtering, ordinary least squares (OLS) and total least square (TLS) used to identify the stator parameters. These parameters are stator resistance, stator inductance, and leakage inductance. Dynamic model used for 15 kW an induction motor. It has been found that, to estimate the stator parameters three motor operating region needs for the purpose of estimation. The stator resistance can be estimated when the rotor speed is very low, and torque is high, stator inductance estimation is possible at any rotor speed and low torque, finally, leakage inductance can only be accurately estimated if rotor speed and torque are high.

Natarajan and Misra (1989), Haque (1993) and Guimarães (2014), developed an approach to estimate induction motor parameters from the nameplate data and

manufacturer catalog data. Natarajan's method was the first papers on determining parameters from manufacturers' data by using a spreadsheet to solve a system of linear equations to find the motor parameters. Haque's method used these data to develop a set of nonlinear equations and solve it by an iterative Gauss-Seidel method. Guimarães's presented a novel methodology to obtain the parameters from straight and non-iterative equations.

1.3 Thesis Outline

This chapter shows the purpose of this work and a summary of the existing work being done on three-phase induction motor parameters and performance estimation. In Chapter 2, an overview of three-phase induction motor has been described such as steady-state, dynamic (mathematical) model, and transient model are introduced for the equivalent circuit beside the standard that related to an induction motor. In Chapter 3, demonstrates off-line and on-line proposed approaches to estimate motor parameters and identify motor performance. In Chapter 4, parameters and performance results from manufacturer data, experimental tests, and software simulation are evaluated and compared. In Chapter 5, methods explained for performance estimation study. Finally, Chapter 6 concludes with a brief summary of what the working end with and recommendations.

2. OVERVIEW OF THREE-PHASE INDUCTION MOTOR

2.1 Introduction

In 1891, Nikola Tesla presented an elementary form of polyphase induction motors. Two years later, Dobrovolsky exhibited a three-phase induction motor with a squirrel cage. Since then, many scientists and developers attempted to make detailed improvements to the induction motor. The induction motor has some limitations, e.g., inherent speed and power factor. Nevertheless, 85 % of the induction motors are used in industries (Say, 1976).

2.2 Steady-State Theory and Performance

2.2.1 Construction and operation principle

According to the National Electrical Manufacturers Association (NEMA) defines "An induction machine is an asynchronous machine that has a magnetic circuit interlinked with two electric circuits, or sets of circuits, rotating with respect to each other. Power is transferred from one circuit to the other by electromagnetic induction" (NEMA MG-1, 2012).

Figure 2.1 shows, a three-phase induction motor. An induction motor has two main parts, the fixed part, called stator; it consists of a core made up of laminations carrying slot-embedded conductors.

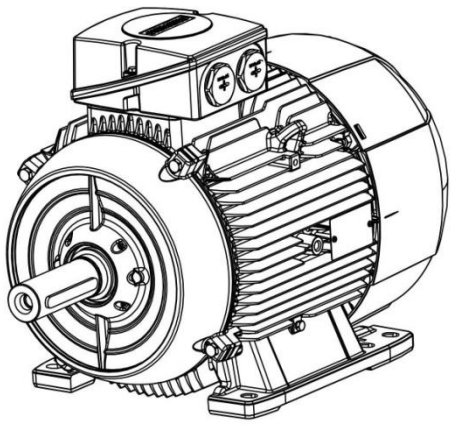

Figure 2.1 : Induction Motor (Siemens, 2003).

The moving part, called rotor as shown in Figure 2.2, air gap separated the rotor from the stator, and the rotor mounted on bearings. The rotor is either a squirrel cage type or wound rotor type.

Table 2.1 : Difference between Slip Ring and Squirrel Cage Induction Motor (Url-1).

Slip ring or phase wound Induction motor	Squirrel cage induction motor
Construction is complicated due to the presence of slip ring and brushes.	Construction is very simple.
The rotor winding is similar to the stator winding.	The rotor consists of rotor bars, which are permanently shorted with the help of end rings.
We can easily add rotor resistance by using slip ring and brushes.	Since the rotor bars are permanently shorted, it is not possible to add external resistance.
Due to the presence of external resistance, high starting torque can be obtained.	Staring torque is low and cannot be improved.
Slip ring and brushes are present.	Slip ring and brushes are absent.
Frequent maintenance is required due to the presence of brushes.	Less maintenance is required.
The construction is complicated, and the presence of brushes and slip ring makes the motor more costly.	The construction is simple and robust, and it is cheap as compared to slip ring induction motor.
This motor is rarely used only 10 % industry uses slip ring induction motor.	Due to its simple construction and low cost, the squirrel cage induction motor is widely used.
Rotor copper losses are high and hence less efficiency.	Less rotor copper losses, and hence high efficiency.
Speed control by rotor resistance method is possible.	Speed control by rotor resistance method is not possible.
Slip ring induction motor is used where high starting torque is required in hoists, cranes, and elevator.	Squirrel cage induction motor is used in lathes, drilling machine, fan, blower, and printing machines.

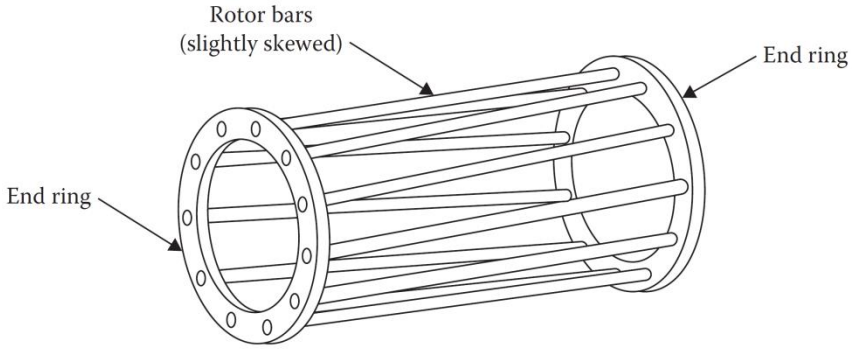

(a)

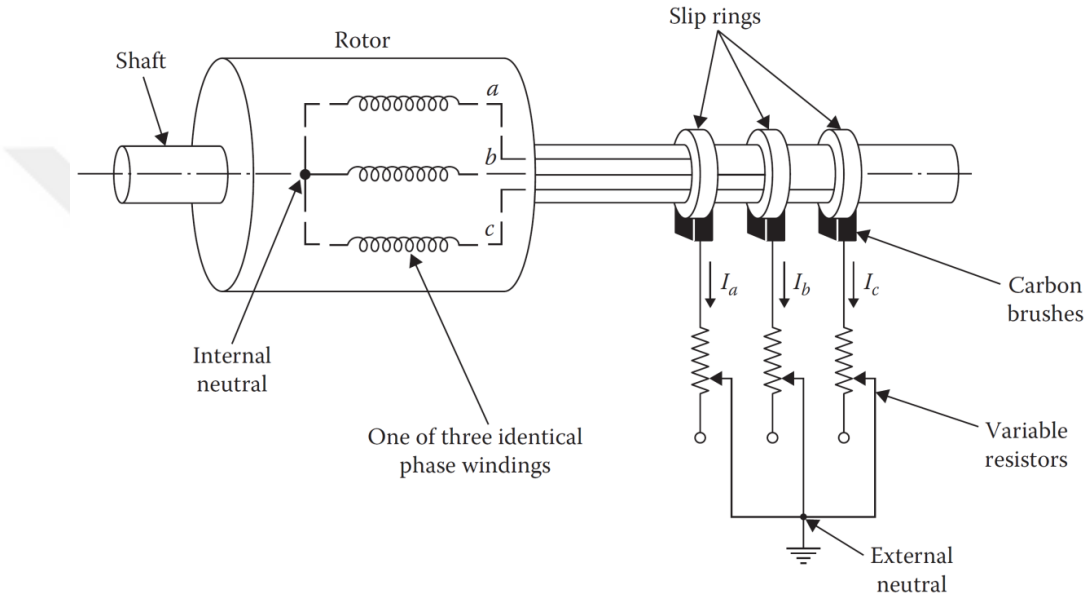

(b)

Figure 2.2 : (a) the squirrel-cage winding of a cage rotor of an induction motor and (b) Illustration of a three-phase wound-rotor winding with slip rings (Turan, 2012).

When applied three-phase current to the motor, the stator produces a rotating magnetic field, due to the moving magnetic field, currents are induced in the closed rotor circuit. The rotor magnetic field runs at a stator frequency, and the rotor shaft speed is not in synchronism with the rotating stator frequency. In this case, the difference between the speeds defined as a slip. In the most induction motors, the slip value varies from 1 % to 5 %. The interacting of the stator magnetic field with the rotor magnetic field caused a torque on the rotor, that torque gives the rotor the needed movement (Jones, 2013). Slip equation can express by the following equation:

$$s = \frac{n_s - n_m}{n_s} \tag{2.1}$$

2.2.2 Types of the induction motor

The induction motors are classified based on the number of the stator windings, and they are single-phase induction motor and three-phase induction motor (Parekh, 2003).

Table 2.2 : Difference between single-phase and three-phase induction motors (Url-2).

Basis	Single-phase	Three-phase
Supply	Uses single-phase supply	Uses three-phase supply
Starting	Not self-starting, need auxiliary winding	Self-starting
Starting Torque	Low	High
Maintenance	Easy to repair and maintain	Difficult to repair and maintain
Features	Simple in construction, reliable and economical as compared to three phase induction motors	Complex in construction and costly
Efficiency	Less	High
Power factor	Low	High
Examples	They are mostly used in domestic appliances such as mixer grinder, fans, compressors	Three phase induction motors are mostly used in industries

2.2.3 Equivalent circuit

Assume that a balanced wye connection, the currents applied are the line values and the voltages are the line-to-neutral values. When the current is applied to both stator and rotor windings, the resultant rotating magnetic fields in the air gap are rotating at the same speed, and they will develop air gap field rotating at the synchronous speed.

2.2.3.1 Exact equivalent circuit

2.2.3.1.1 Stator circuit model

In the Figure 2.3.a, shows the stator equivalent circuit. Because of the voltage drop due to the leakage impedance, the stator terminal voltage differs from the induced voltage in the stator windings.

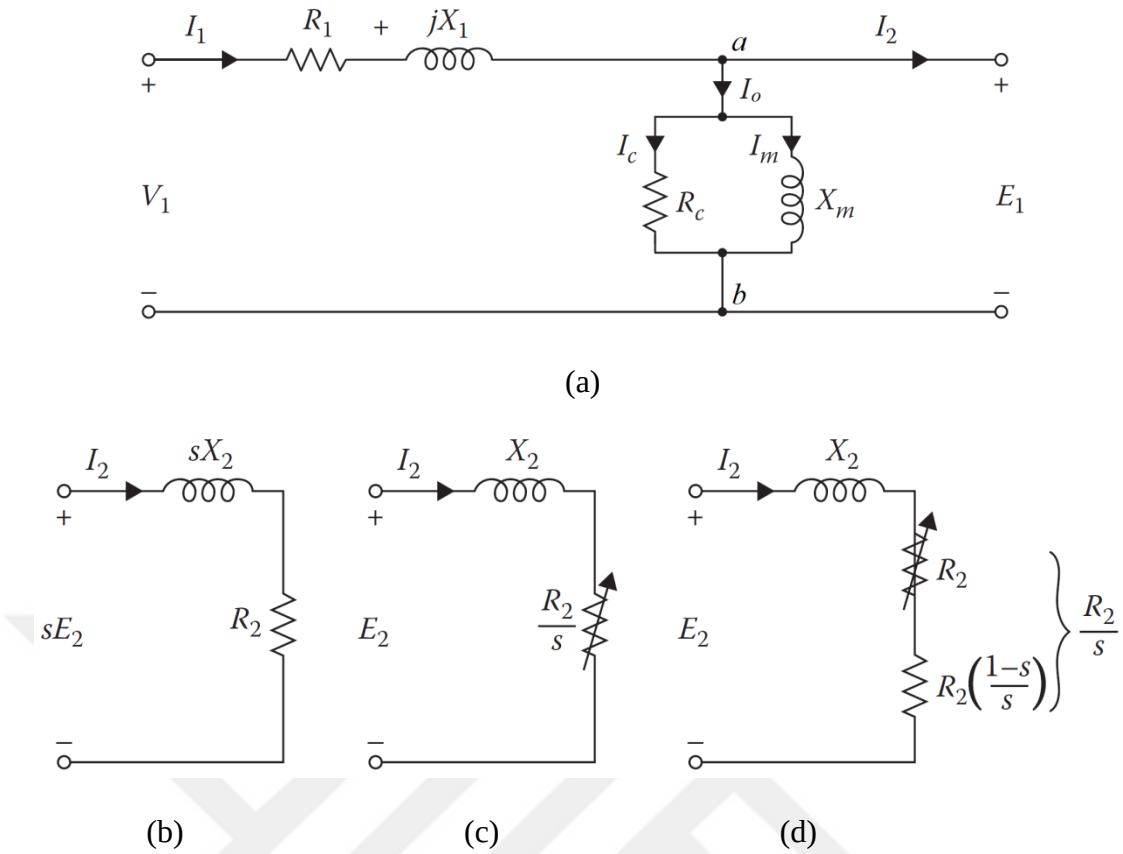

Figure 2.3 : Development of an induction motor per-phase stator and rotor-equivalent circuits (a) stator equivalent circuit, (b) actual rotor circuit, (c) rotor equivalent circuit, and (d) modified equivalent rotor circuit (Turan, 2012).

The stator voltage can be given in phasor form as

$$\bar{V}_1 = \overline{E_1} + \bar{I}_1(R_1 + jX_1) \tag{2.2}$$

I_2 and I_o represent the load component (rotor current) and excitation component, respectively, that separated from the stator current I_1. Thus, the load component (rotor current) I_2 produces the necessary mmf that rotates the rotor. The air-gap flux is the resultant of the excitation current I_o. Thus, the excitation impedance is low and therefore I_o it can be as high as 30%-50% of the full-load current. In the shunt branch of the equivalent circuit, there are two main components per-phase stator core-loss resistance R_c and per-phase stator magnetizing reactance X_m.

2.2.3.1.2 Rotor circuit model

In the Figure 2.3.b, shows the exact rotor circuit operating under load at a slip s. The equation of the rotor current per phase can be expressed as

$$\bar{I_2} = \frac{s\overline{E_2}}{R_2 + jsX_2} \tag{2.3}$$

The Figure 2.3.b shows that the impedance per-phase is R_2 + jsX_2 and the induced emf sE_2 produced the current I_2. Therefore, the total rotor copper loss can be written as

$$P_{2.cu} = 3I_2^2 R_2 \tag{2.4}$$

By dividing both the numerator and the denominator of the equation 2.3 by slip s, it can be rewritten as

$$\bar{I_2} = \frac{\overline{E_2}}{(R_2/s) + jX_2} \tag{2.5}$$

As a result, equation 2.5 represents the rotor equivalent circuit that shown in (Figure 2.3.c). In equations 2.3 and 2.5, the magnitude and phase angle of I_2 still unchanged .The current I_2 in equation 2.3 is at slip frequency f_2, while the current I_2 in equation 2.5 is at line frequency f_1.

In general, the slip is the difference between the synchronous speed of the magnetic field, and the shaft rotating speed. Therefore, every parameter has related to slip can changes with speed, such that the rotor leakage reactance sX_2 in equation 2.3 and the resistance R_2 in equation (2.5).

2.2.3.1.3 Complete equivalent circuit

The Figure 2.3.a, 2.3.c, and 2.3.d have the same line frequency f_1. Thus, it can draw the figures together. If however, the turns in the stator winding are different from the rotor winding; the E_1 and E_2 are different and the turns ratio α needs to be taken into account as shown in (Figure 2.4.a).

$$\alpha = {}^{N_1}/_{N_2} \tag{2.6}$$

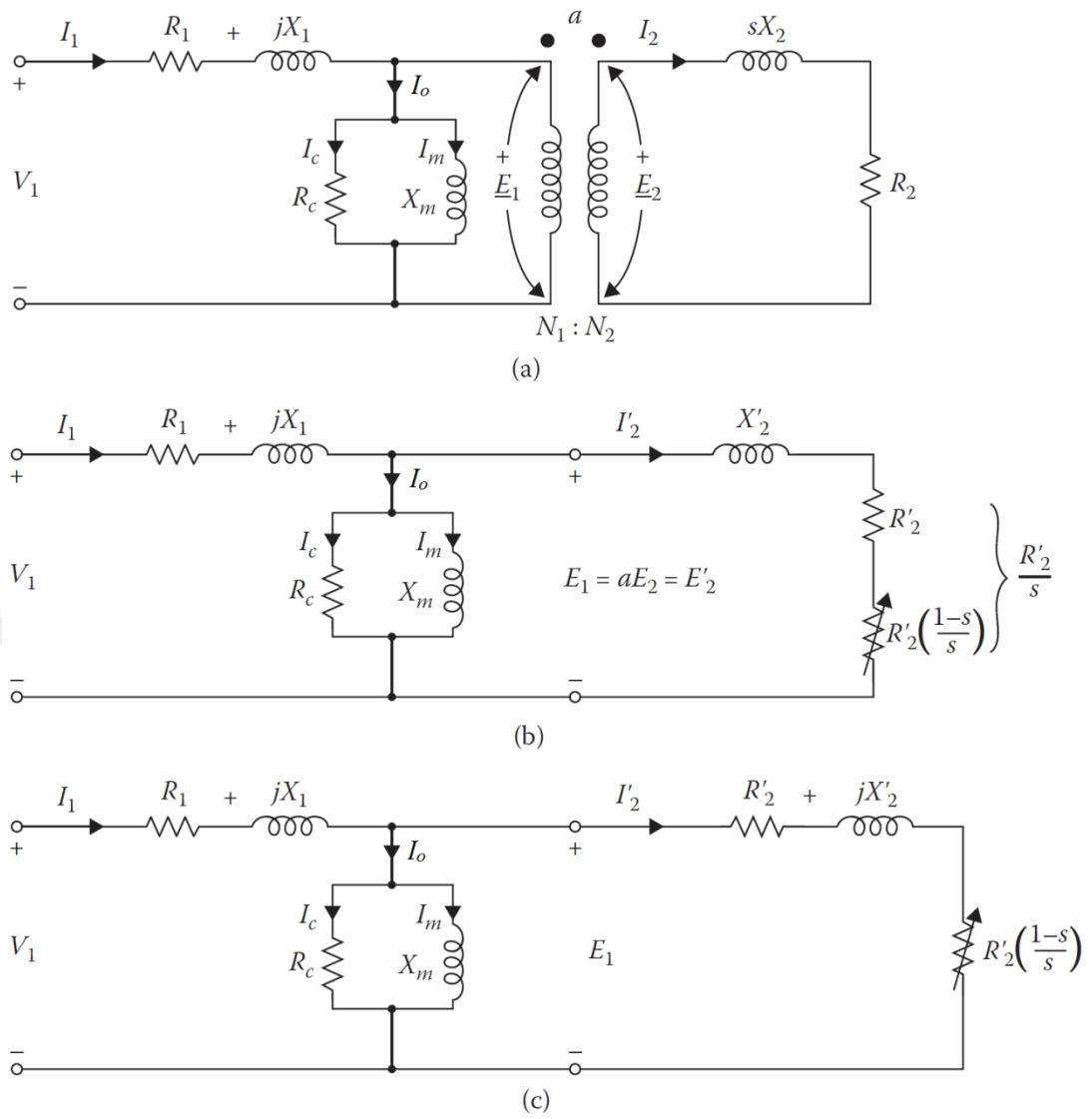

Figure 2.4 : Induction motor per-phase equivalent circuit: (a) transformer model of the induction motor, (b) exact equivalent circuit, and (c) alternative form of the equivalent circuit (Turan, 2012).

From the Figure 2.4.b and 2.4.c, note that the rotor parameters use the stator-referred quantities. Therefore,

$$Z_{in} = z_1 + (z_2 // Z_{ab}) = R_1 + jx_1 + \frac{1}{\frac{1}{R_c} + \frac{1}{jX_m} + \frac{1}{R_2'/s + jx_2'}} \tag{2.7}$$

$$= R_1 + jx_1 + R_{ab} + jX_{ab} = R_{in} + jX_{in}$$

$$I_2' = \frac{I_2}{a} \tag{2.8}$$

$$\bar{I_o} = \frac{\overline{E_1}}{R_c} - j\frac{\overline{E_1}}{X_m} \tag{2.9}$$

$$E_1 = aE_2 = E_2' = V_1\frac{Z_{ab}}{Z_{in}} \tag{2.10}$$

$$R_2' = a^2R_2 \tag{2.11}$$

$$X_2' = a^2X_2 \tag{2.12}$$

$$R_2'\left(\frac{1-s}{s}\right) = a^2R_2\left(\frac{1-s}{s}\right) \tag{2.13}$$

$$\bar{I_1} = \frac{\overline{V_1}}{Z_{in}}\left(\frac{R_{in}}{Z_{in}} - j\frac{X_{in}}{Z_{in}}\right) = \bar{I_1}\cos\theta_1 + j\bar{I_1}\sin\theta_1 \tag{2.14}$$

By the omitted the resistance R_c and lumping the core loss with the friction and windage losses, the equivalent circuit can be simplified as shown in (Figure 2.5).

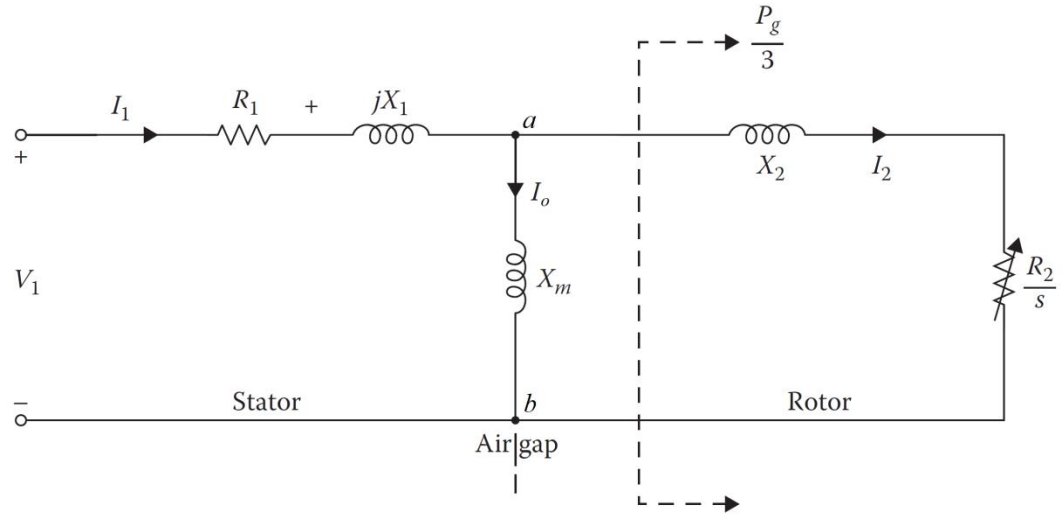

Figure 2.5 : Exact equivalent circuit omitted the core-loss resistor (Steinmetz model) (Turan, 2012).

2.2.3.2 Approximate equivalent circuit

The equivalent circuit can be simplified with quite little loss of accuracy, by assuming that $V_1 = E_1 = E_2$, it can move the magnetizing (shunt) branch to the machine terminals as shown in (Figure 2.6). Furthermore, more simplified can be achieved by omitting the resistance R_c.

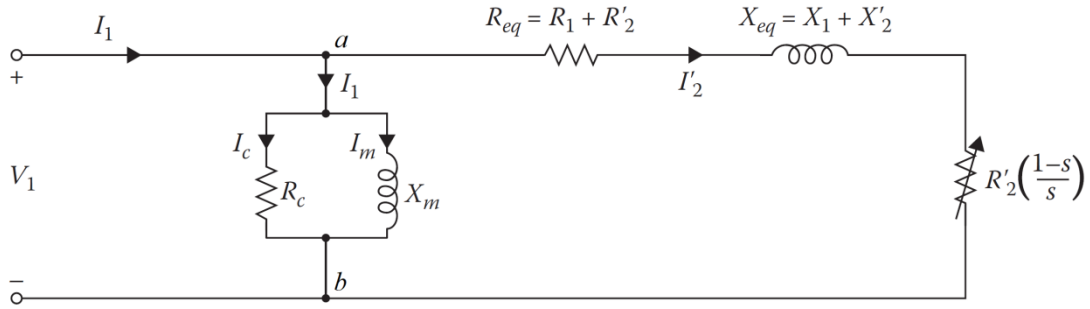

Figure 2.6 : Approximate equivalent circuit (Turan, 2012).

$$T_d = \frac{3V_1^2 R'_2}{2\pi\left(\frac{f_1}{p}\right)\left((R_1 + \frac{R'_2}{s})^2 + (X_1 + X'_2)^2\right)s} \tag{2.15}$$

$$\overline{I'_2} = \frac{\overline{V_1}}{(R_1 + \frac{R'_2}{s}) + j(X_1 + X'_2)} \tag{2.16}$$

$$\overline{I_o} = \frac{\overline{V_1}}{R_c} - j\frac{\overline{V_1}}{X_m} \tag{2.17}$$

$$I_1 = I'_2 + I_o \tag{2.18}$$

2.2.4 Performance calculations

Power, torque and efficiency equations are essential to determine the performance and parameters of an induction motor (Hindmarsh and Renfrew, 1996).

2.2.4.1 Power equations

Figure 2.4.c shows that the equivalent circuit of an induction motor, and thus power-flow diagram can be shown in (Figure 2.7). The electrical input power to the motor stator can be written as,

$$P_{in} = P_1 = \sqrt{3}V_1 I_1 \cos\varphi_1 = \sqrt{3}E_1 I'_2 \cos\varphi_2 + Stator\ loss \tag{2.19}$$

The total stator copper losses are

$$P_{1,cu} = 3I_1^2 R_1 \tag{2.20}$$

The total core losses can be found from

$$P_{core} = 3E_1^2 G_c = \frac{3E_1^2}{R_c} \tag{2.21}$$

Therefore, the total air-gap power given by

$$P_g = P_{in} - P_{1,cu} - P_{core} \tag{2.22a}$$

or

$$P_g = 3I_2^2 \frac{R_2}{s} = 3I_2'^2 \frac{R_2'}{s} = \sqrt{3}E_1 I_2' \cos\theta_2 \tag{2.22b}$$

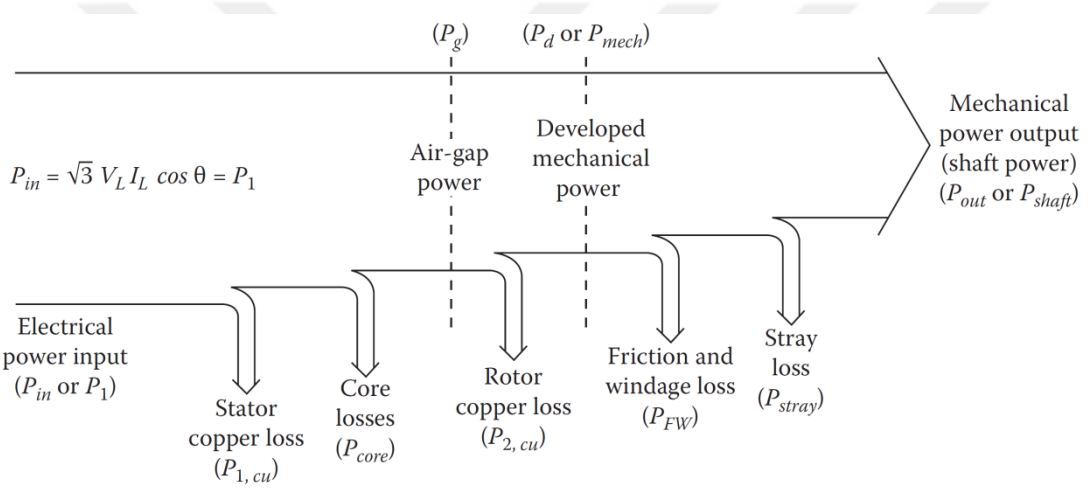

Figure 2.7 : Power-flow diagram of an induction motor, (Turan, 2012).

The total rotor copper losses are

$$P_{2,cu} = 3I_2^2 R_2 = sP_g \tag{2.23}$$

Thus, the total mechanical power developed can be expressed as

$$\begin{aligned} P_d = P_m = P_g - P_{2,cu} = P_g(1-s) = \left(\frac{1-s}{s}\right) 3I_2^2 R_2 \\ = \left(\frac{1-s}{s}\right) P_{2,cu} \end{aligned} \tag{2.24}$$

If the core losses are assumed to be constant, and the friction and windage losses and the stray losses are known, it can sum them together to get the rotational losses by the following equation

$$P_{rot} = P_{core} + P_{FW} + P_{stray} \tag{2.25}$$

Therefore, the output power can be written as

$$P_{out} = P_d - P_{rot} \tag{2.26}$$

2.2.4.2 Torque equations

The developed torque can be expressed by dividing the developed power by the shaft speed. Therefore,

$$T_d = \frac{3P_d}{\omega_m} = \frac{3P_g(1-s)}{\omega_s(1-s)} = \frac{3P_g}{\omega_s} = \frac{3I_2^2R_2}{s\omega_s} \tag{2.27}$$

The output torque (shaft torque) is

$$T_{out} = \frac{P_{out}}{\omega_m} \tag{2.28}$$

2.2.4.3 Efficiency equations

The efficiency of an induction motor can be determined from

$$\eta = \frac{P_{out}}{P_{in}} = \frac{P_{out}}{P_{out} + P_{loss}} \tag{2.29}$$

2.3 Transient and Dynamics

2.3.1 Mathematical description

A three-phase induction machine shown in Figure 2.8 has six windings, three distributed in the stator and three distributed in the rotor. Where the stator phases can be described them in letters a, b, and c, and the rotor phases are A, B, and C. The self and mutual inductances between the stator phases and rotor phases are constant if assumed that the machine is cylindrical. Moreover, the values of mutual inductances

between the stator and rotor coils are variables, and they are functions of rotor position.

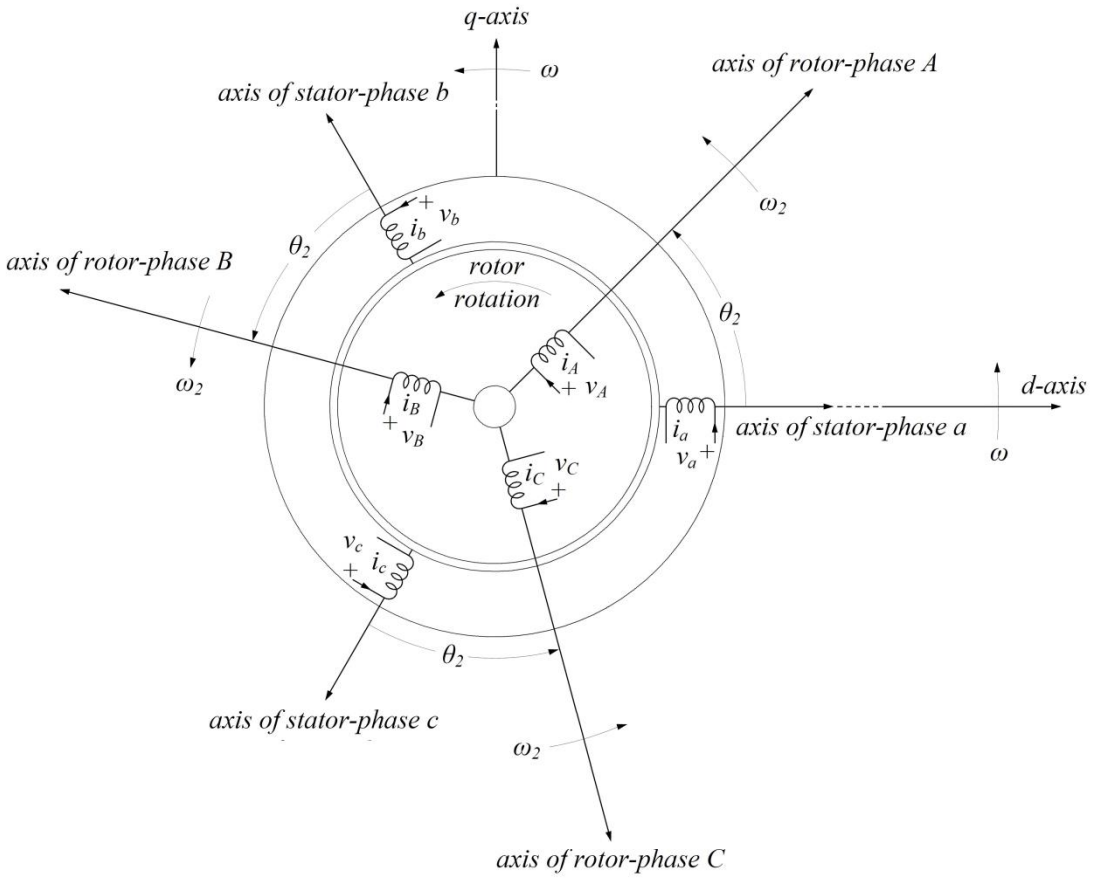

Figure 2.8 : Idealized three-phase induction machine.

The effect of teeth and slots considered to be neglected, thereby space mmf and flux waves are sinusoidally distributed. The stator and rotor phases are connected either a wye or a delta, and they are balanced. The rotor structure can be a squirrel-cage or a wound-rotor. For both structures, the rotor windings are short-circuited; thereby the rotor-terminal voltages V_A, V_B, and V_C become zero.

The Figure 2.8 shows that, the magnetic axes of the stator and rotor phases, and shows when the rotor turns there is displacement angle θ_2 between the rotor phases and the stator phases, it varies with time, at constant rotor angular velocity ω_2, or constant slip s.

$$\theta_2 = \omega_2 t = (1 - s)\omega t \tag{2.30}$$

The following equations give the voltage relations of the stator and rotor windings:

$$v_1 = \rho\lambda_1 + r_1 i_1 \tag{2.31.a}$$

$$v_2 = \rho\lambda_2 + r_2 i_2 \tag{2.31.b}$$

From values of the maximum mutual inductance between any stator phase and any rotor phase M, and the per phase and mutual inductances between the stator windings L_1 and M_1, and the rotor windings L_2 and M_2, the flux-linkage equations can be given as the following:

Stator:

$$\lambda_a = L_1 i_a + M_1(i_b + i_c) + M[i_A \cos\theta_2 + i_B \cos(\theta_2 + 120^\circ) + i_C \cos(\theta_2 - 120^\circ)] \tag{2.32.a}$$

$$\lambda_b = L_1 i_b + M_1(i_a + i_c) + M[i_A \cos(\theta_2 - 120^\circ) + i_B \cos\theta_2 + i_C \cos(\theta_2 + 120^\circ)] \tag{2.32.b}$$

$$\lambda_c = L_1 i_c + M_1(i_a + i_b) + M[i_A \cos(\theta_2 + 120^\circ) + i_B \cos(\theta_2 - 120^\circ) + i_C \cos\theta_2] \tag{2.32.c}$$

Rotor:

$$\lambda_A = L_2 i_A + M_2(i_B + i_C) + M[i_a \cos\theta_2 + i_b \cos(\theta_2 - 120^\circ) + i_c \cos(\theta_2 + 120^\circ)] \tag{2.33.a}$$

$$\lambda_B = L_2 i_B + M_2(i_A + i_C) + M[i_a \cos(\theta_2 + 120^\circ) + i_b \cos\theta_2 + i_c \cos(\theta_2 - 120^\circ)] \tag{2.33.b}$$

$$\lambda_C = L_2 i_C + M_2(i_A + i_B) + M[i_a \cos(\theta_2 - 120^\circ) + i_b \cos(\theta_2 + 120^\circ) + i_c \cos\theta_2] \tag{2.33.c}$$

In general, there are no zero-sequence currents in almost all induction machines because there is no neutral connection, and can be assumed that:

$$i_a + i_b + i_c = 0 \tag{2.34.a}$$

$$i_A + i_B + i_C = 0 \tag{2.34.b}$$

The self-inductance of stator windings and rotor windings can be describe them as

$$L_{11} = L_1 - M_1 \tag{2.35.a}$$

$$L_{22} = L_2 - M_2 \tag{2.35.b}$$

From equations 2.34 and 2.35, the flux-linkage can be simplified as

Stator:

$$\lambda_a = L_{11} i_a + M[i_A \cos\theta_2 + i_B \cos(\theta_2 + 120^\circ) + i_C \cos(\theta_2 - 120^\circ)] \tag{2.36.a}$$

$$\lambda_b = L_{11} i_b + M[i_A \cos(\theta_2 - 120^\circ) + i_B \cos\theta_2 + i_C \cos(\theta_2 + 120^\circ)] \tag{2.36.b}$$

$$\lambda_c = L_{11} i_c + M[i_A \cos(\theta_2 + 120^\circ) + i_B \cos(\theta_2 - 120^\circ) + i_C \cos\theta_2] \tag{2.36.c}$$

Rotor:

$$\lambda_A = L_{22} i_A + M[i_a \cos\theta_2 + i_b \cos(\theta_2 - 120^\circ) + i_c \cos(\theta_2 + 120^\circ)] \tag{2.37.a}$$

$$\lambda_B = L_{22} i_B + M[i_a \cos(\theta_2 + 120^\circ) + i_b \cos\theta_2 + i_c \cos(\theta_2 - 120^\circ)] \tag{2.37.b}$$

$$\lambda_C = L_{22} i_C + M[i_a \cos(\theta_2 - 120^\circ) + i_b \cos(\theta_2 + 120^\circ) + i_c \cos\theta_2] \tag{2.37.c}$$

Because θ_2 is a function of time, the flux-linkage expressions in equations 2.36 and 2.37 are an algebraically complicated set of nonlinear differential equations. However, this algebra can be simplified by applying the proper transformation to get linear equations for all constant-speed cases. One of the methods is to split the air-gap mmfs into two perpendicular axes (d-axis) and (q-axis). The properties of these axes are, the d-axis is synchronized with the phase-a axis at t = 0, the d-axis is displaced from the phase-a axis at any time by ωt, the q-axis is located 90 electrical degree ahead from the d-axis in the direction of rotation. From dq-axes, the new stator-current i_{1d} and i_{1q} are given as follows:

$$i_{1d} = k_d[i_a \cos \omega t + i_b \cos(\omega t - 120^\circ) + i_c \cos(\omega t + 120^\circ)] \quad (2.38.a)$$

$$i_{1q} = -k_q[i_a \sin \omega t + i_b \sin(\omega t - 120^\circ) + i_c \sin(\omega t + 120^\circ)] \quad (2.38.b)$$

By replacing the constant k_d and k_q by 2/3, can get the matrix form of the currents as

$$\begin{bmatrix} i_{1d} \\ i_{1q} \\ i_{10} \end{bmatrix} = \frac{2}{3} \begin{bmatrix} \cos \omega t & \cos(\omega t - 120^\circ) & \cos(\omega t + 120^\circ) \\ -\sin \omega t & -\sin(\omega t - 120^\circ) & -\sin(\omega t + 120^\circ) \\ 1/2 & 1/2 & 1/2 \end{bmatrix} \begin{bmatrix} i_a \\ i_b \\ i_c \end{bmatrix} \quad (2.39)$$

Because of the zero-sequence current component, i_{10} is zero due to equation 2.34.a, the phase current components can be given in terms of d, q, 0 components as follows:

$$\begin{bmatrix} i_a \\ i_b \\ i_c \end{bmatrix} = \begin{bmatrix} \cos \omega t & -\sin \omega t & 1 \\ \cos(\omega t - 120^\circ) & -\sin(\omega t - 120^\circ) & 1 \\ \cos(\omega t + 120^\circ) & -\sin(\omega t + 120^\circ) & 1 \end{bmatrix} \begin{bmatrix} i_{1d} \\ i_{1q} \\ i_{10} \end{bmatrix} \quad (2.40)$$

Because the currents i_{1d} and i_{1q} can produce the same magnetic field as the actual phase currents, the flux-linkage and voltage transformations can use the same transformation matrix of the currents. So, the equations 2.39 and 2.40 can be written for the flux-linkage λ by replacing i, and for voltage v by replacing i.

Let the displacement angle between the rotor phase-A and the d-axis is θ_s.

$$\frac{d\theta_s}{dt} = \rho\, \theta_s = s\omega \quad (2.41)$$

Now, the rotor-currents dq-component can be given as

$$\begin{bmatrix} i_{2d} \\ i_{2q} \\ i_{20} \end{bmatrix} = \frac{2}{3} \begin{bmatrix} \cos \theta_s & \cos(\theta_s - 120^\circ) & \cos(\theta_s + 120^\circ) \\ -\sin \theta_s & -\sin(\theta_s - 120^\circ) & -\sin(\theta_s + 120^\circ) \\ 1/2 & 1/2 & 1/2 \end{bmatrix} \begin{bmatrix} i_A \\ i_B \\ i_C \end{bmatrix} \quad (2.42)$$

Because of the zero-sequence current component, i_{20} is zero due to equation 2.34.b, the phase current components can be given in terms of d, q, 0 components as follows:

$$\begin{bmatrix} i_A \\ i_B \\ i_C \end{bmatrix} = \begin{bmatrix} \cos \theta_s & -\sin \theta_s & 1 \\ \cos(\theta_s - 120^\circ) & -\sin(\theta_s - 120^\circ) & 1 \\ \cos(\theta_s + 120^\circ) & -\sin(\theta_s + 120^\circ) & 1 \end{bmatrix} \begin{bmatrix} i_{2d} \\ i_{2q} \\ i_{20} \end{bmatrix} \quad (2.43)$$

Once again, the rotor flux-linkages and rotor voltages can be written in the same transformation matrix in the equations 2.42 and 2.43, by replacing once i with λ and once i with v.

Can replace the angle θ_2 in equation 2.30 with the following

$$\theta_2 = \omega t - \theta_s \tag{2.44}$$

By simplifying, the flux-linkage equations can get

Stator:

$$\lambda_{1d} = L_{11} i_{1d} + L_{12} i_{2d} \tag{2.45.a}$$

$$\lambda_{1q} = L_{11} i_{1q} + L_{12} i_{2q} \tag{2.45.b}$$

Rotor:

$$\lambda_{2d} = L_{22} i_{2d} + L_{12} i_{1d} \tag{2.46.a}$$

$$\lambda_{2q} = L_{22} i_{2q} + L_{12} i_{1q} \tag{2.46.b}$$

where L_{12} = (3/2) M. From the equations 2.31 and 2.39 can get the dq-component of stator and rotor voltages in terms of flux-linkages as below

Stator:

$$v_{1d} = r_1 i_{1d} + \rho\lambda_{1d} - \omega\lambda_{1q} \tag{2.47.a}$$

$$v_{1q} = r_1 i_{1q} + \rho\lambda_{1q} - \omega\lambda_{1d} \tag{2.47.b}$$

Rotor:

$$v_{2d} = r_2 i_{2d} + \rho\lambda_{2d} - \lambda_{2q}(\rho\theta_s) \tag{2.48.a}$$

$$v_{2q} = r_2 i_{2q} + \rho\lambda_{2q} - \lambda_{2d}(\rho\theta_s) \tag{2.48.b}$$

Equations 2.45 to 2.48 represent the idealized induction machine relations for the purpose of analysis in dq-variables. Induction machine works as a motor with a

positive value of the slip s, when ($\rho\theta_s$) is positive; as a generator with a negative value of slip s, when ($\rho\theta_s$) is negative. equations 2.47 and 2.48 become linear differential equations with constant coefficients if the rotor speed is constant and ($\rho\theta_s$) is constant.

In equations 2.47 the value of $\rho\lambda_{1d}$ and $\rho\lambda_{1q}$ are neglected because when are compare it with the value of $\omega\lambda_{1q}$ and $\omega\lambda_{1d}$ are usually small. Additionally, r_1 used in the steady-state analysis, while they are frequently neglected in the transient analysis.

The equation of instantaneous power input to the stator can be given by

$$p_1 = v_a i_a + v_b i_b + v_c i_c \tag{2.49}$$

The instantaneous power in terms of dq-variables, as following

$$p_1 = \frac{3}{2}(v_{1d} i_{1d} + v_{1q} i_{1q}) \tag{2.50}$$

Eremia and Shahidehpour (2013), "The electromagnetic torque developed is obtained as the power associated with the speed voltages (the instantaneous rotor power obtained by neglecting the winding losses and the transient mmf) divided by the shaft speed in mechanical radians per second." From equations 2.48 the power associated with speed-voltage can be given as

$$\frac{3}{2}\left[-\lambda_{2q} i_{2d}(\rho\theta_s) + \lambda_{2d} i_{2q}(\rho\theta_s)\right] \tag{2.51}$$

For the motor action, ($\rho\theta_s$) will be positive and rotor rotation goes inversely with the synchronously rotating of dq-axes; therefore, the quantity [-($\rho\theta_s$)2/p] is the corresponding speed. The electromagnetic torque can be expressed as

$$T = \frac{3}{2}.\frac{p}{2}(\lambda_{2q} i_{2d} - \lambda_{2d} i_{2q}) \tag{2.52}$$

The torque production can come from the interaction between the magnetic fields of dq-axes. The required acceleration for rotating mass can be given as

$$T_{inertia} = J\frac{d\omega_0}{dt} = J\frac{d^2\theta_0}{dt^2} \tag{2.53}$$

where J is the moment of inertia, θ_0 is the shaft-position angle, and ω_0 is the shaft angular velocity.

2.3.2 Transient of an induction machine

Let assume that a three-phase short-circuit occur at the terminals of an induction machine. The machine will feed the fault with current, by the time the fault current decay to zero due to the trapped flux-linkage with the rotor circuits. In this case, the voltage equations 2.47 and 2.48 can be simplified to get the initial magnitude. In equation 2.47, the stator-phase resistance r_1 and the $\rho\lambda_{1d}$ and $\rho\lambda_{1q}$ can be neglected, also ignoring the dc components in the short-circuit current. In equation 2.48, because the slip value is small, the speed-voltage terms $\lambda_{2q}(\rho\theta_s)$ and $\lambda_{2d}(\rho\theta_s)$ could be ignored. Now, the voltage equations 2.47 and 2.48 can be written as

Stator:

$$v_{1d} = -\omega\lambda_{1q} \tag{2.54.a}$$

$$v_{1q} = \omega\lambda_{1d} \tag{2.54.b}$$

Rotor:

$$v_{2d} = r_2 i_{2d} + \rho\lambda_{1d} = 0 \tag{2.55.a}$$

$$v_{2q} = r_2 i_{2q} + \rho\lambda_{1q} = 0 \tag{2.55.b}$$

The equations 2.55 are set to be equal zero to indicate which rotor type (squirrel-cage rotor or wound-rotor) with the short-circuit slip rings.

Solving for i_{2d} from equation 2.46.a can get

$$i_{2d} = \frac{\lambda_{2d} - L_{12} i_{1d}}{L_{22}} \tag{2.56}$$

and substitute it in equation 2.45.a, can get

$$\lambda_{1d} = \left(L_{11} - \frac{L_{12}^2}{L_{22}}\right) i_{1d} + \frac{L_{12}}{L_{22}}\lambda_{2d} = L' i_{1d} + \frac{L_{12}}{L_{22}}\lambda_{2d} \tag{2.57}$$

where

$$L' = L_{11} - \frac{L_{12}^2}{L_{22}} \tag{2.58}$$

Similarly, from equations 2.46.b and 2.45.b, can get

$$\lambda_{1q} = L' i_{1q} + \frac{L_{12}}{L_{22}} \lambda_{2q} \tag{2.59}$$

The quantity $L^{'}$ is known as "Transient inductance."

The voltages v_{1d} and v_{1q} and the stator-flux linkages λ_{1d} and λ_{1q} in equations 2.54 become zero when the three-phase short-circuit occur at the terminals. The dc component of the stator current is ignored by neglecting the terms $\rho\lambda_{1d}$ and $\rho\lambda_{1q}$, which is physically prevents λ_{1d} and λ_{1q} from the sudden changes. Under these conditions, λ_{1d} and λ_{1q} are equal to zero to maintain the rotor-flux linkage constant at their initial prefault values λ_{2d0} and λ_{2q0}. From equations 2.57 and 2.59, the stator components currents will be

$$i_{1d} = -\frac{(L_{12}/L_{22})}{L'} \lambda_{2d0} \tag{2.60.a}$$

$$i_{1q} = -\frac{(L_{12}/L_{22})}{L'} \lambda_{2q0} \tag{2.60.b}$$

After the short-circuit at t = 0, the equations 2.60 are reached their initial values immediately; these values will continue to exist if there is no rotor resistance to cause their decay. The rms stator current is given by

$$\bar{I_1} = I_{1d} + jI_{1q} = \frac{i_{1d}}{\sqrt{2}} + j\frac{i_{1q}}{\sqrt{2}} = -\frac{1}{X'}\omega\frac{L_{12}}{L_{22}}\left(\frac{\lambda_{2d0}}{\sqrt{2}} + j\frac{\lambda_{2q0}}{\sqrt{2}}\right) \tag{2.61}$$

where referred to $X^{'} = \omega L^{'}$ as (Transient reactance). The (Initial symmetrical short-circuit current) are called to the rms magnitude of $\bar{I}_1$, and its given by

$$|\bar{I_1}| = \frac{1}{X'}\omega\frac{L_{12}}{L_{22}}\frac{1}{\sqrt{2}}\sqrt{\lambda_{2d0}^2 + \lambda_{2q0}^2} \tag{2.62}$$

2.3.2.1 Decay of the short-circuit current

Short-circuit current decay at a time to zero due to the rotor resistance r_2. By studying the effect of the decay of rotor currents i_{2d} and i_{2q}, can find this decrement. Let substitute λ_{2d} from equation 2.46.a into equation 2.55.a, one gets

$$r_2 i_{2d} + L_{22}\rho i_{2d} + L_{12}\rho i_{1d} = 0 \tag{2.63}$$

By making $\lambda_{1d} = 0$ from equation 2.45.a

$$i_{1d} = -\frac{L_{12}}{L_{11}} i_{2d} \tag{2.64}$$

Substituting the above i_{1d} in equation 2.63 can get

$$r_2 i_{2d} + \frac{1}{L_{11}}\left(L_{11} - \frac{L_{12}^2}{L_{22}}\right) L_{22}\rho i_{2d} = 0 \tag{2.65}$$

or

$$i_{2d} + \frac{L'}{L_{11}} \frac{L_{22}}{r_2} \frac{di_{2d}}{dt} = 0 \tag{2.66}$$

The quantity $[(L'/L_{11}).(L_{22}/r_2)]$ is known as "Short-circuit time constant" T'. Moreover, the quantity (L_{22}/r_2) is known as "Time constant of the rotor circuit alone" T_0'. Once the stator is open-circuited, T_0' is responsible for the decay of rotor transient. Can express T' in terms of T_0' as

$$T' = \frac{L'}{L_{11}} . \frac{L_{22}}{r_2} = T_o' \frac{L'}{L_{11}} = T_o' \frac{X'}{X_{11}} \tag{2.67}$$

In the present discussion note that the DC component of the short-circuit current has been ignored.

2.3.2.2 Transient equivalent circuit

During the prefault operation conditions, can evaluate the flux-linkage λ_{2d0} and λ_{2q0} of the machine and develop a transient equivalent circuit of an induction machine.

Before short-circuit, let the rms stator-phase currents be I_{10} with its dq-components I_{1d0} and I_{1q0} given by $i_{1d0}/\sqrt{2}$ and $i_{1q0}/\sqrt{2}$, respectively. For prefault conditions, equation 2.57 can be written and multiply by ω and can get

$$\omega \frac{L_{12}}{L_{22}} \lambda_{2d0} = \omega \lambda_{1d0} - X' i_{1d0} \tag{2.68}$$

According to equation 2.54.b, $\omega\lambda_{1d0}$ can be replaced by v_{1q0}, and equation 2.68 can be expressed in phase form by

$$\omega \frac{L_{12}}{L_{22}} \frac{\overline{\lambda}_{2d0}}{\sqrt{2}} = \overline{V}_{1q0} - X' \overline{I}_{1d0} \tag{2.69}$$

where V_{1q0} is equal to $v_{1q0}/\sqrt{2}$. Similarly, equation 2.59 can be expressed by

$$\omega \frac{L_{12}}{L_{22}} \frac{\overline{\lambda}_{2q0}}{\sqrt{2}} = -\overline{V}_{1d0} - X' \overline{I}_{1q0} \tag{2.70}$$

By combining equations 2.69 and 2.70 can get

$$\begin{aligned} \omega \frac{L_{12}}{L_{22}} \left(\frac{\overline{\lambda}_{2d0}}{\sqrt{2}} + j \frac{\overline{\lambda}_{2q0}}{\sqrt{2}} \right) &= \frac{1}{j} \left[\left(\overline{V}_{1d0} + j \overline{V}_{1q0} \right) - jX' \left(\overline{I}_{1d0} + j \overline{I}_{1q0} \right) \right] \\ &= \frac{1}{j} \left(\overline{V}_{10} - jX' \overline{I}_{10} \right) = \frac{1}{j} \overline{E}_1' \end{aligned} \tag{2.71}$$

where $\overline{V}_{10}$ is the prefault rms terminal voltage. $\overline{E}_1'$ is known as "The initial voltage behind the transient reactance"; it is proportional to the rotor-flux linkages, is given by

$$\overline{E}_1' = \overline{V}_{10} - jX' \overline{I}_{10} \tag{2.72}$$

Equation 2.62 shows the rms magnitude of the initial symmetrical short-circuit current; now, in prefault conditions can be given by

$$I_1 = E_1'/X' \tag{2.73}$$

At any time t after the fault, the rms magnitude of the initial symmetrical short-circuit current can be expressed as

$$I_1' = \frac{E_1'}{X'} e^{-t/T'} \tag{2.74}$$

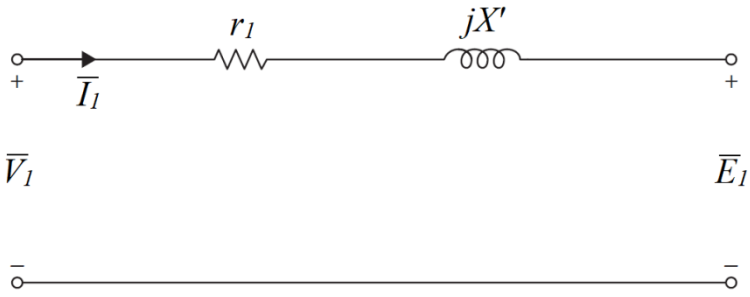

Figure 2.9 : Simple transient equivalent circuit of an induction machine (Sarma, 1985).

Since the transient behavior of an induction motor is foregoing discussed, Figure 2.9 can represent the simple transient equivalent circuit of the induction motor; r_1 is the stator-phase resistance and X' is the transient reactance.

2.4 NEMA Motor Standard Design

Performance characteristics are the key for NEMA to classify the squirrel-cage induction motor to 4 designs. Design A, designed to withstand full-voltage starting and develop a starting torque of 110-120%, starting locked rotor current of 6-10 times rated, and having a slip at rated load of less than 5%. Design B, similar to design A motor with the same starting torque, however, the locked rotor current is limited to five times. Design C, designed to withstand full-voltage starting, developing a high starting torque of 200% and locked rotor current less than the standard type of motor, and having a slip at rated load of less than 5%. Design D, designed to withstand full-voltage starting, developing a very high locked rotor torque of 300%, low lock rotor current, and having a slip at rated load of 5% or more.

Table 2.3 : NEMA classes of squirrel-cage induction motor (Karmakar et al. 2016)

	Design A	Design B	Design C	Design D
Properties	Normal starting torque. High starting current. Low operating slip.	Normal starting torque. Low starting current. Low operating slip.	High starting torque. Low starting current.	High starting torque. Low starting current. High operating slip.
Uses	Fan, pump load etc. where torque is low at the start	For constant speed drive such as a pump, blower	Compressor, conveyors, crashers etc.	For driving an intermittent load, e.g. punch press etc.

2.5 IEC Motor Standard Classification

Worldwide, energy saving and motor efficiency are crucial factors; thus, researchers and developers are continually working on. According to (Almeida et al., 2008), in a single year, the energy cost can be up to 10 times the purchase cost due to motor efficiency. The International Electrotechnical Commission (IEC) has published an International Efficiency (IE) standard that stipulates the energy efficiency of low-voltage AC motors, by established 4 efficiency classes for three-phase induction motors depending on efficiency as presented in the (Table 2.4).

Table 2.4 : Efficiency classes for induction motors (IEC 60034-30-1, 2014)

Class Number	Class Type
IE1	Standard efficiency
IE2	High efficiency
IE3	Premium efficiency
IE4	Super premium efficiency

The efficiency graphs of IE standards can be shown in (Figure 2.10). Each motor class has efficiency range; for instance, the motor that used in this thesis is 2.2 kW class IE2 and his efficiency is 84.3 %.

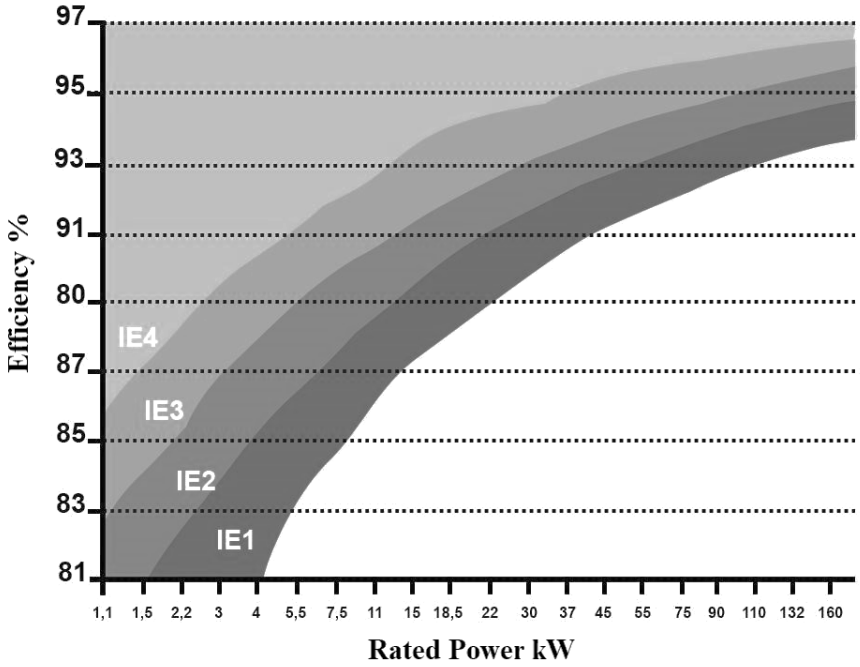

Figure 2.10 : IE efficiency classes of 4-poles motors (Url-3)

3. METHODOLOGY

3.1 Off-Line Parameters Estimation

To calculate the parameters of an induction motor understanding of equivalent circuit are important. In general, there are three common types of equivalent circuit as shown in (Figure 3.1).

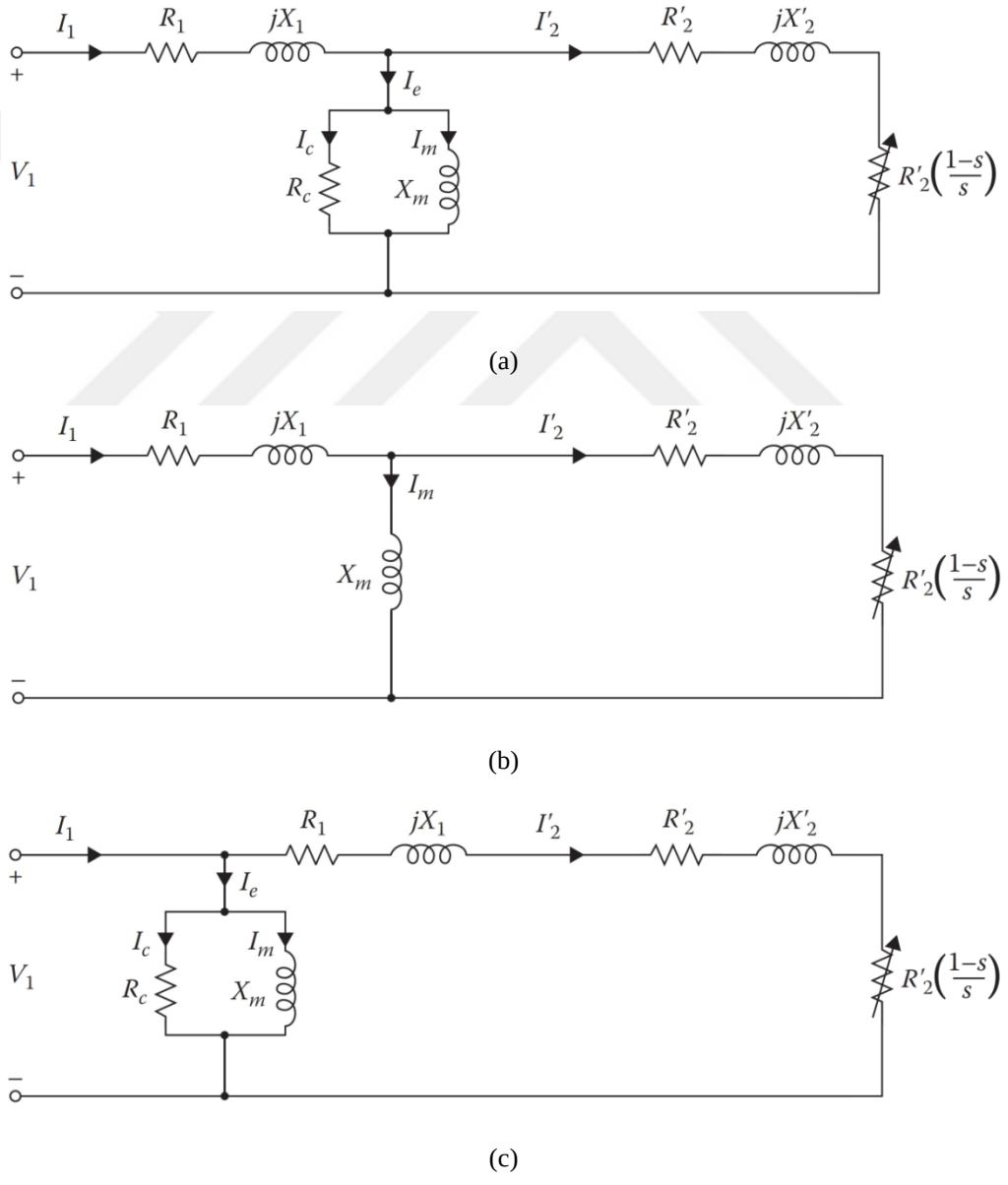

Figure 3.1 : Types of induction motor equivalent circuit (a) Exact equivalent circuit, (b) Exact equivalent circuit without core loss, (c) Approximate equivalent circuit.

3.1.1 DC test

From the DC test can calculate the winding dc resistance by applying DC voltage to the two phases of the induction motor and then increased the input DC voltage until the current reached the rated value.

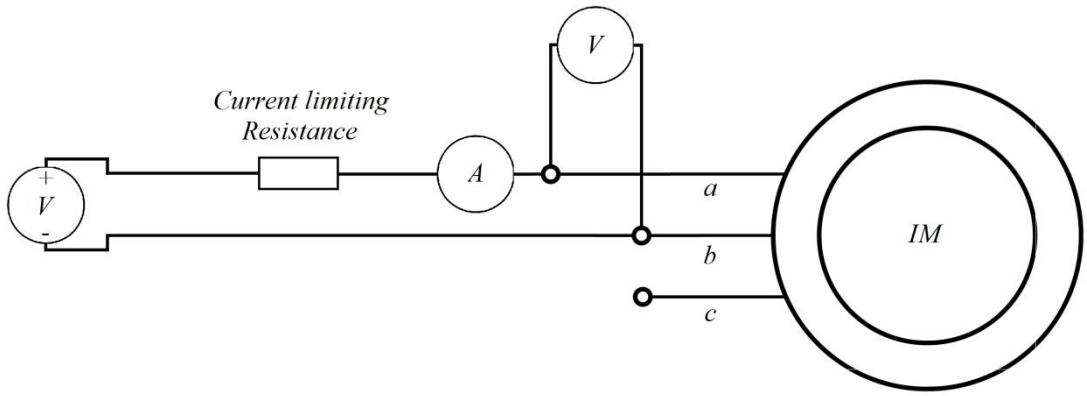

Figure 3.2 : Three-phase induction motor DC test.

Then from the measuring, the DC voltage and DC current can calculate the dc resistance. Bhattacharya (1998) mentioned that the AC effective resistance is higher than the DC resistance; thus, should multiply it by the factor between 0.9-1.8 depending on the motor size as in equations below

$$R_{dc} = \frac{V_{dc}}{2\, I_{dc}} \tag{3.1}$$

$$R_1 = 1.4 \times R_{dc} \tag{3.2}$$

3.1.2 No-load test

In the No-load test can measure the voltage, current, input power, and power factor, by applying a three-phase rated voltage to the motor stator and the motor run freely without any load.

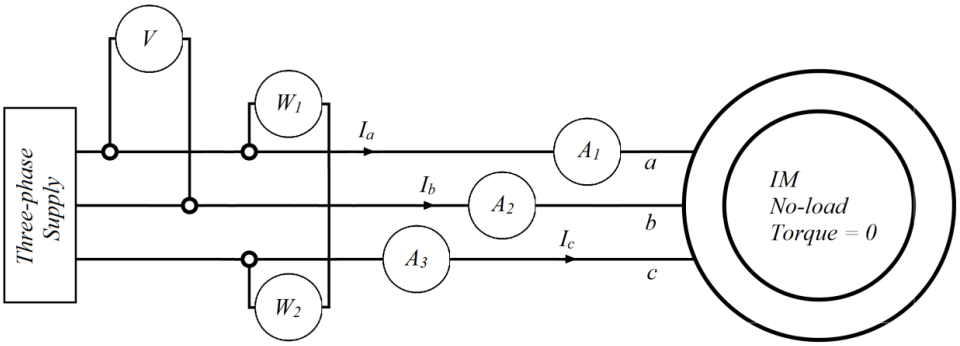

Figure 3.3 : Three-phase induction motor No-load test.

Then, calculate the parameters that related to the stator part, fixed losses (friction and winding + core losses) and the values in the magnetizing part.

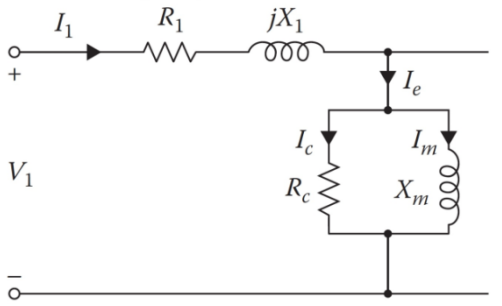

(a)

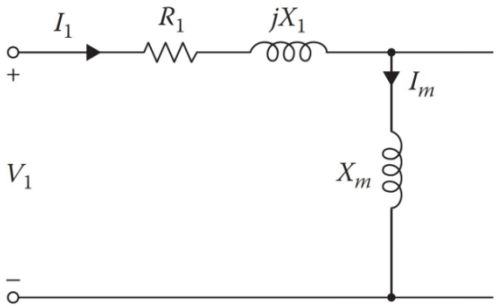

(b)

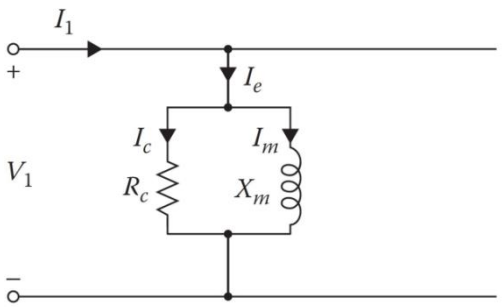

(c)

Figure 3.4 : No-load test equivalent circuit (a) Exact, (b) Exact without core loss, (c) Approximate.

3.1.2.1 Exact equivalent circuit

Calculate phase voltage for per phase circuit

$$V_{P-NL} = \frac{V_{L-NL}}{\sqrt{3}} \tag{3.3}$$

No-load Impedance = X_1+X_m

$$Z_{NL} = \frac{V_{P-NL}}{I_{NL}} \tag{3.4}$$

No-load power factor

$$PF_{NL} = \frac{P_{in-NL}}{\sqrt{3}V_{L-NL}I_{NL}} \tag{3.5}$$

Voltage across magnetizing branch

$$V_m = V_{P-NL} - I_{NL}R_1 \tag{3.6}$$

Magnetizing current through X_m

$$I_m = I_{NL} \times \sin(\text{acos}(PF_{NL})) \tag{3.7}$$

Core current through R_c

$$I_C = I_{NL} \times PF_{NL} \tag{3.8}$$

Value of core resistance

$$R_C = \frac{V_m}{I_C} \tag{3.9}$$

Value of magnetizing reactance

$$X_m = \frac{V_m}{I_m} \tag{3.10}$$

Calculation of X_1 using an approximation, i.e. Znl=X1+Xm

$$X_1 = Z_{NL} - X_m \tag{3.11}$$

3.1.2.2 Exact equivalent circuit without core loss

In this type of circuit the equations it will be the same of the exact circuit except that the magnetizing current will be

$$I_m = I_{NL} \tag{3.12}$$

and I_c and R_c will be zero.

3.1.2.3 Approximate equivalent circuit

Also here, the equations will be the same as the exact circuit, but the value of the voltage across the magnetizing branch will be

$$V_m = V_{P-NL} \tag{3.13}$$

and the X_1 will be found during the blocked-rotor test according to the motor class.

3.1.3 Second no-load test

From the first no-load test, the slip value is approximately zero, this might be not accurate to estimate the stator parameters. A second no-load test obtained to get more accurate results by rotating the induction motor in the synchronous speed via DC machine; consequently, the slip value now is exactly zero. Motor parameters can be calculated by the same equation in the first no-load test. Figure 3.5 illustrates the corrected no-load test.

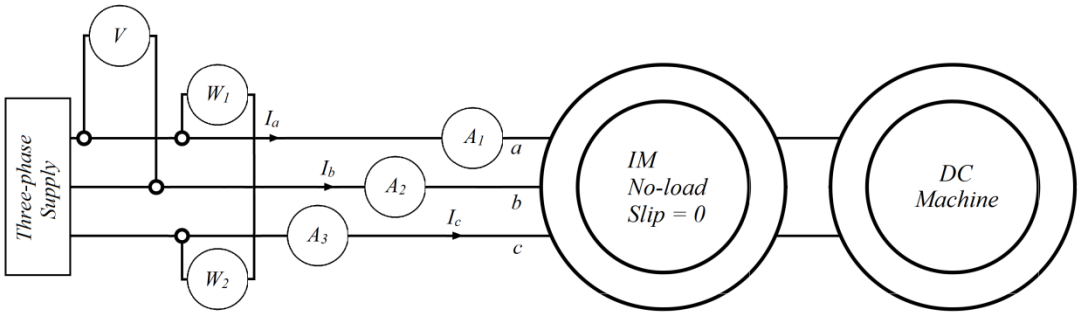

Figure 3.5 : Corrected no-load test

3.1.4 Blocked-rotor test

In blocked-rotor test can measure the line voltage, rated current, input power, power factor, and frequency, by applying a three-phase voltage to the motor stator until the current reached to the rated value with block the shaft rotation.

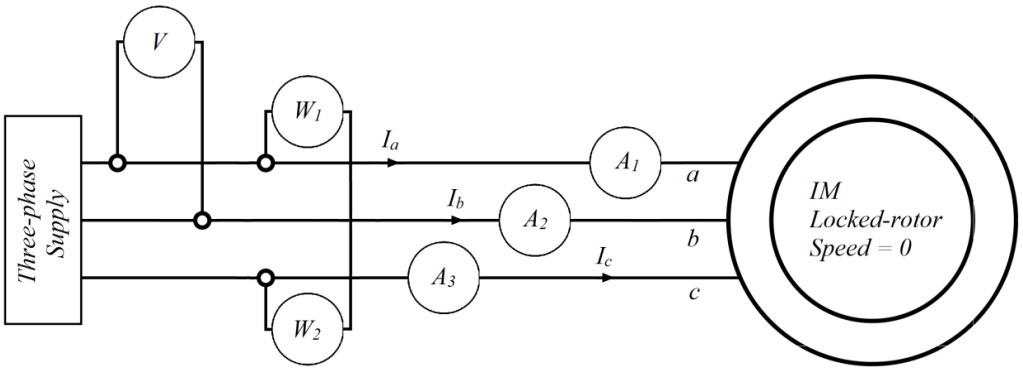

Figure 3.6 : Three-phase induction motor blocked-rotor test.

Then calculate all parameters that related to the rotor part. After finding the induction motor parameters, it is easy to find the performance of the motor by calculating the power relations and the efficiency.

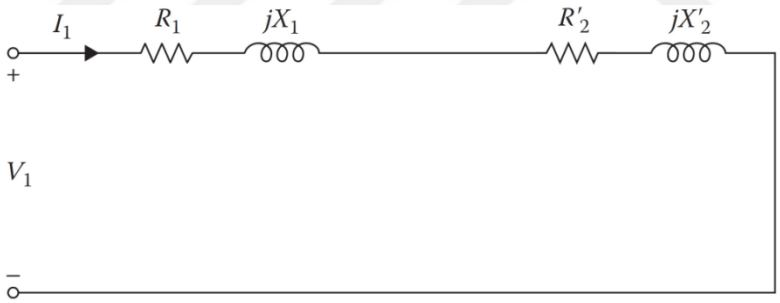

Figure 3.7 : Blocked-rotor test equivalent circuit.

3.1.4.1 Exact equivalent circuit

Full load phase voltage

$$V_{P-SC} = \frac{V_{L-SC}}{\sqrt{3}} \tag{3.14}$$

Calculating R_2 from copper losses

$$R_2 = \frac{P_{in-SC} - 3I_2^2 R_1}{3I_2^2} \tag{3.15}$$

Full load equivalent impedance

$$Z_{SC} = \frac{V_{P-SC}}{I_{SC}} \tag{3.16}$$

Full load power factor

$$PF_{SC} = \frac{P_{in-SC}}{\sqrt{3}V_{L-SC}I_{SC}} \tag{3.17}$$

Calculation of X_2

$$X_2 = \sqrt{Z_{SC}^2 - (R_1 + R_2)^2} - X_1 \tag{3.18}$$

3.1.4.2 Exact equivalent circuit without core loss

Equations are the same as the exact circuit.

3.1.4.3 Approximate equivalent circuit

Due to the same circuit in this test, the equations will be the same except that the full load reactance should be calculated

Full load equivalent reactance

$$X_{SC} = Z_{SC} \times \sin(\text{acos}(PF_{SC})) \tag{3.19}$$

then, Table 3.1 shows the relationship between X_1 and X_2 for the most common types of induction motors.

Table 3.1 : Empirical distribution of leakage reactances in induction motors (IEEE Standard 112).

Motor class	Fraction of X_1+X_2	
	X_1	X_2
A	0.5 X_{FL}	0.5 X_{FL}
B	0.4 X_{FL}	0.6 X_{FL}
C	0.3 X_{FL}	0.7 X_{FL}
D	0.5 X_{FL}	0.5 X_{FL}

3.1.5 Thevenin equivalent circuit

Thevenin's theorem states that “Any linear circuit that can be separated by two terminals from the rest of the system can be replaced by a single voltage source in series with an equivalent impedance” (Chapman, 2005). Calculating Thevenin equivalent voltage by open-circuited the end terminal, and calculating Thevenin equivalent impedance by short-circuited all voltage sources, as indicates in (Figure 3.8).

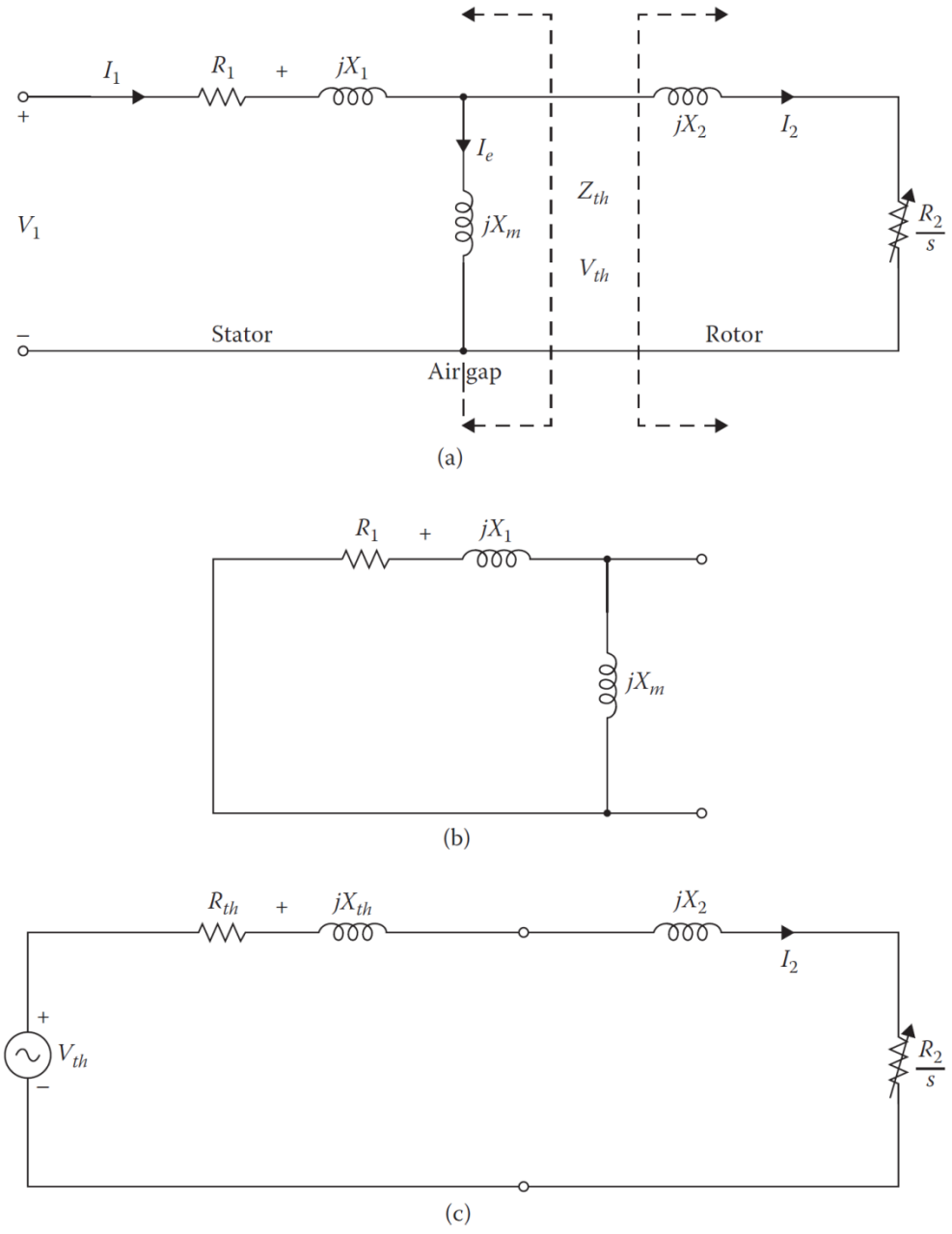

Figure 3.8 : (a) Thevenin equivalent circuit of the induction motor, (b) Thevenin equivalent circuit of the stator circuit, (c) The resultant Thevenin circuit (Turan, 2012).

Calculating Thevenin equivalent voltage

$$V_{th} = V_{P-NL}\left(\frac{X_m}{X_1 + X_m}\right) \tag{3.20}$$

Calculation of Thevenin resistance

$$R_{th} = R_1\left(\frac{X_m}{X_1 + X_2}\right)^2 \tag{3.21}$$

Calculation of Thevenin reactance

$$X_{th} = X_1 \tag{3.22}$$

Calculating starting torque of the motor

$$T_{start} = \frac{3V_{th}^2 R_2}{\omega_s[(R_{th} + R_2)^2 + (X_{th} + X_2)^2]} \tag{3.23}$$

Slip for maximum torque

$$S_{max} = \frac{R_2}{\sqrt{R_{th}^2 + (X_{th} + X_2)^2}} \tag{3.24}$$

Calculating maximum torque

$$T_{max} = \frac{3V_{th}^2}{2\omega_s\left[R_{th} + \sqrt{R_{th}^2 + (X_{th} + X_2)^2}\right]} \tag{3.25}$$

3.2 On-Line Parameters Identification

Walker (1921), was the first references that described on-line machine condition monitoring for diagnosis of motor faults by using a measurement system contain data and theoretical bases. By the time, the technological maturity in the area of sensing, DAQ, and integration communication equipment gives the possibilities for continuous monitoring. Table 3.2 shows the advantages and disadvantages of condition monitoring.

Table 3.2 : Advantages and disadvantages of condition monitoring

Advantage	Disadvantage
Predict failures before they occur	Higher upfront cost for monitoring equipment
Improves asset reliability	Necessity of employee training
Saves time, money, and energy in the long run	Significant time commitment to develop and implement program

3.2.1 Proposed system

In modern wireless telecommunication, Internet of Things (IoT) as an emerging technology has got attention with benefits to many applications. IoT provides industrial automation with the best way to remote access. IoT devices have the capability to communicate in bio direction with other devices; thus, gives them the ability to exchange the data, statistics, and information to improve their performance, which helps industries to have better productivity, management and increased throughput (Kande et al., 2017).

Figure 3.9 shows proposed system architecture of the on-line condition monitoring by using IoT network. The proposed system consists of voltage, current, temperature, vibration sensors that attached to the three-phase induction motor, IoT gateway, and the motor monitored and controlled through VisSim software.

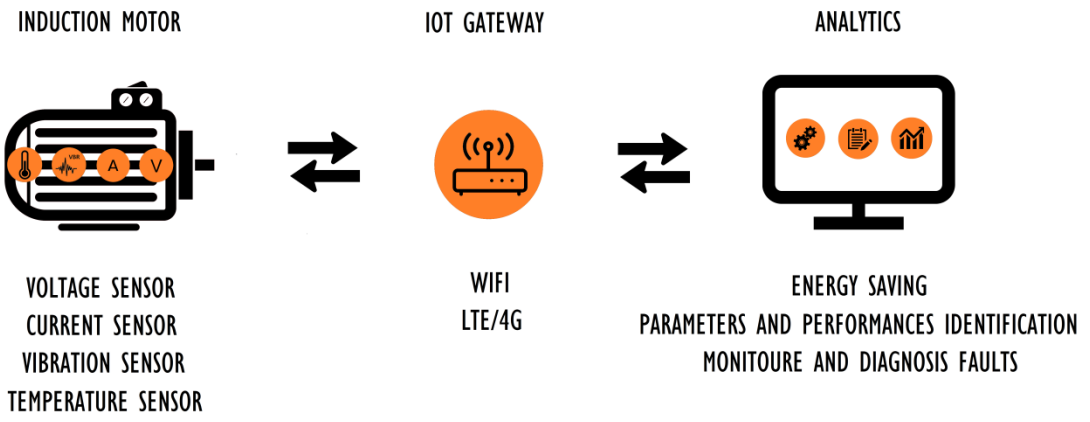

Figure 3.9 : Proposed on-line induction motor analysis using IoT network

3.2.2 Fast Fourier Transform (FFT)

Fast Fourier Transform (FFT) is a tool that used to evaluate the AC signals or waveforms in the frequency domain; it is one of the proposed methods that can check whether the waveforms are sinusoidal or not. Calculations produce of FFT one of signification of interest in Total Harmonic Distortion (THD). FFT can help to identify the noise interference, noise problems in power supply and analog device performance.

3.2.3 Total Harmonic Distortion (THD)

THD can measure the amount of distortion in voltage and current due to harmonics. A pure sinusoidal voltage and current waveforms have no harmonic distortion. High power factor, low peak currents, and high-efficiency advantages can be obtained from the lower value of THD. Because THD is an important feature, IEC put limits on several classes of equipment (IEC 61000-3-2, 2018).

3.2.4 Crest factor (CF)

According to (Keysight Technologies, 2011) defines “Crest Factor is a measure of how high the waveform peaks, relative to its rms value”, also known as “The ratio of instantaneous peak value to rms value” as shown in equation (3.26).

$$CF = \frac{Peak\ Value}{RMS\ Value} \tag{3.26}$$

CF is an important parameter when measuring accuracy or purity for a specific signal or waveform. An accurate AC measurement becomes more difficult when distortions take a place and result in higher CF. CF of a pure sinusoidal waveform has the value of 1.414 or near value, as shown in (Table 3.3).

Table 3.3 : Crest Factors for Different Wave Types.

Wave Type	Waveform	Crest Factor
Sine wave		$\sqrt{2} = 1.414$
Half-wave, Rectified sine		2
Full-wave, Rectified sine		$\sqrt{2} = 1.414$
Triangle wave		$\sqrt{3} = 1.732$
Square wave		2

4. EXPERIMENTAL WORK

4.1 Induction Motor Tests

In this chapter, the conducted fundamental tests of the motor under attention is explained. First, the fundamental tests of an induction motor are implemented to find out T – equivalent circuit lumped parameters. The fundamental tests are a no-load test and blocked-rotor test. A corrected version of no-load test is also done to provide the approximate real value of core loss resistance. Second, the performance test is completed and mechanical and electrical quantities of the motor are captured. All tests are accomplished according to IEC 60034-1 standard in which the detailed test procedure is given.

4.2 Manufacturer Data

Table 4.1 is showing the nameplate data of the motor which is provided by the manufacturer. Although the rated voltage is given as 380 V (220 V), nowadays in Turkey, the terminal voltage of the low voltage grid can be assumed 400 V (230 V).

Table 4.1 : Nameplate Manufacturer Data

Parameters	Value	Unit
Operation Voltage	380	V
Motor Nominal Frequency	50	Hz
Rated Speed	1430	rpm
Motor Output Power	2.2	kW
Power Factor	0.77	-
Nominal Current	5	A
Efficiency Value	84.3	%

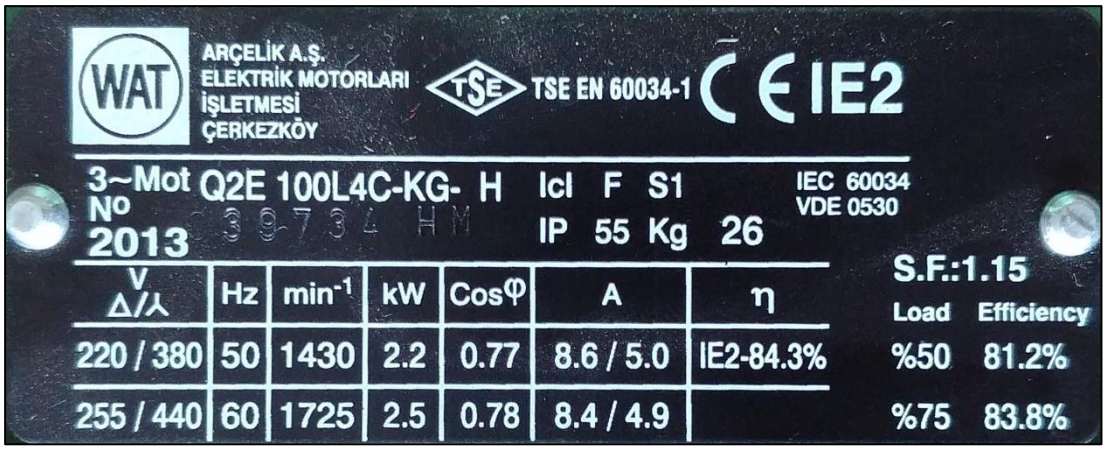

Figure 4.1 : Induction motor nameplate

4.3 Test Setup

For the detailed tests, many measurement devices are used. The list of the used meters and measuring units which are applied in test setup is given in Table 4.2. The high quality and precise measuring devices are used to get more accurate test results. And the picture of the test setup is shown in (Figure 4.2).

Table 4.2 : Equipment used for tests setup

Equipment
Current probes
DC power supply
Loading bank
Multimeter
Oscilloscope
PM loading generator
Power analyzer
Rectifier
Three-phase induction motor
Three-phase variable transformer
Torque meter
Torque meter monitoring device
Voltage probes

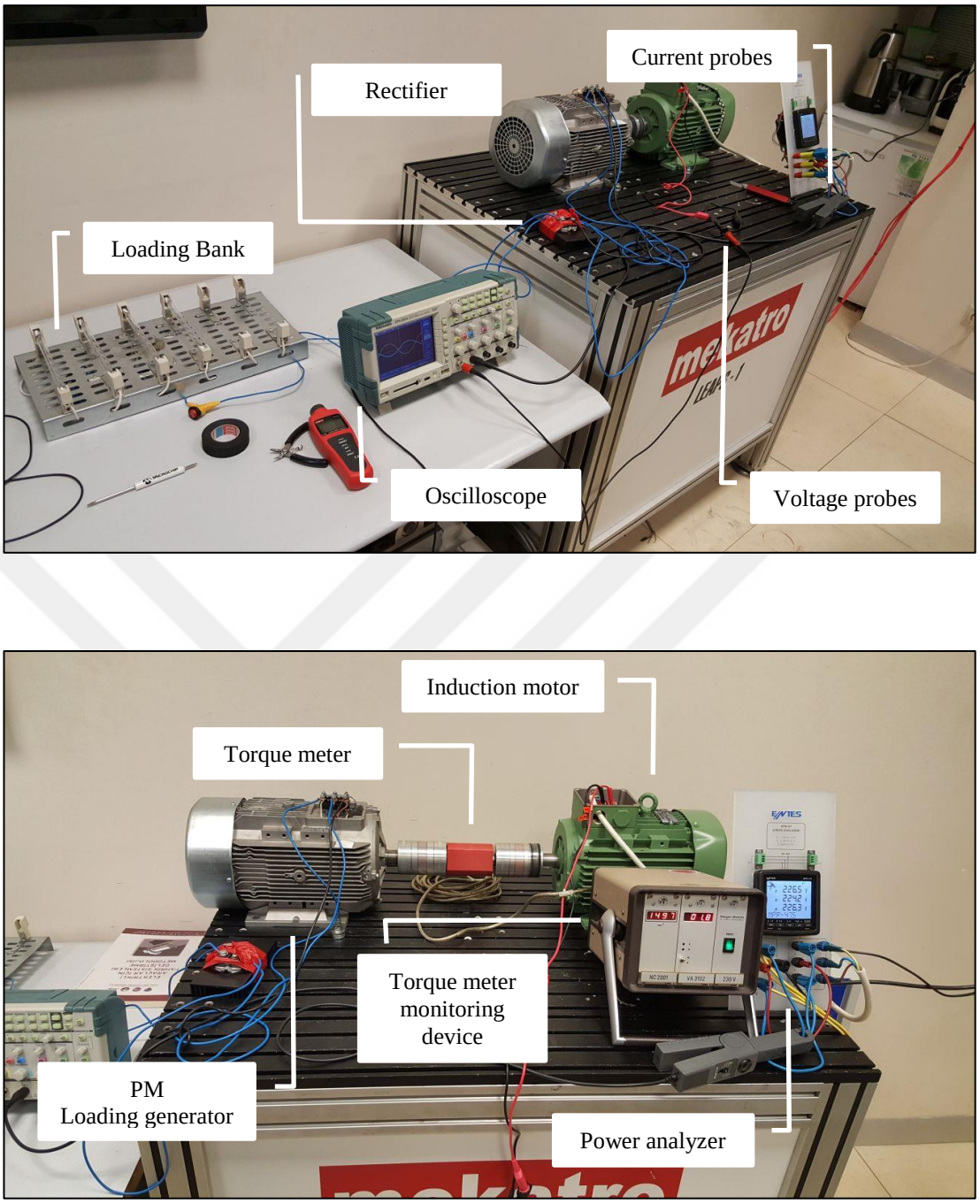

Figure 4.2 : Test setup

4.4 DC Stator Resistance Measurement Test

To measure the stator winding resistance, a voltage-current method is used. The motor terminal voltage (both phase-to-phase and phase-to-neutral) is monitored during a proper current is flowing through stator windings. The skin effect due to the input frequency is neglected.

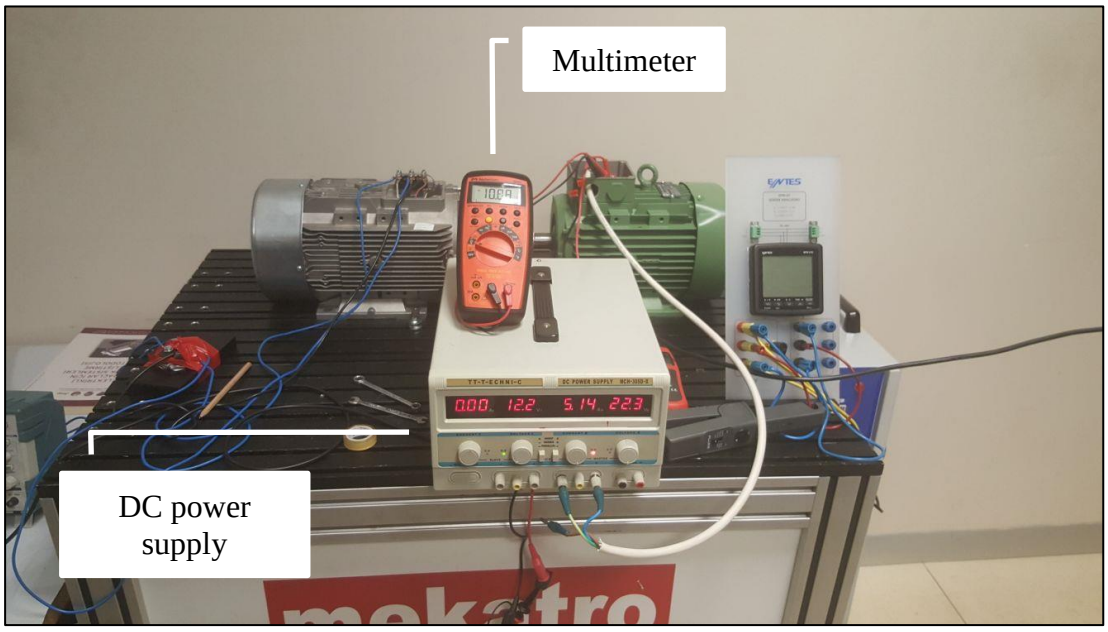

Figure 4.3 : DC stator winding resistance test

Table 4.3 : Laboratory DC Test Data

Parameters	Value	Unit
Voltage	10.58	V
Rated Current	5.03	A
Stator resistance R_1	2.105	Ω
Temperature	23.2	^{o}C

4.5 No-load Test

The no-load test is done while the motor is not driving any connected load to its shaft. The input voltage, current, and power are measured. So all the demanded power is for providing the iron (core) losses, frictional (mechanical) losses and stator copper losses. Stator copper losses cannot be neglected for small motors because of their substantial no-load currents. Because of the very high speed close to the synchronous speed and very low slip, the rotor is assumed as an open circuit which yields no rotor copper losses. And the input reactive power is for mainly magnetized and partly for stator leakage reactance. So core loss resistance, magnetizing reactance can be calculated both, of course, the stator resistance and reactance must be known beforehand. The problem with the conventional no-load test, the core losses cannot be determined for especially small motors because of relatively higher mechanical loss. In Table 4.4 the no-load test results are given. The test setup is shown in (Figure 4.4).

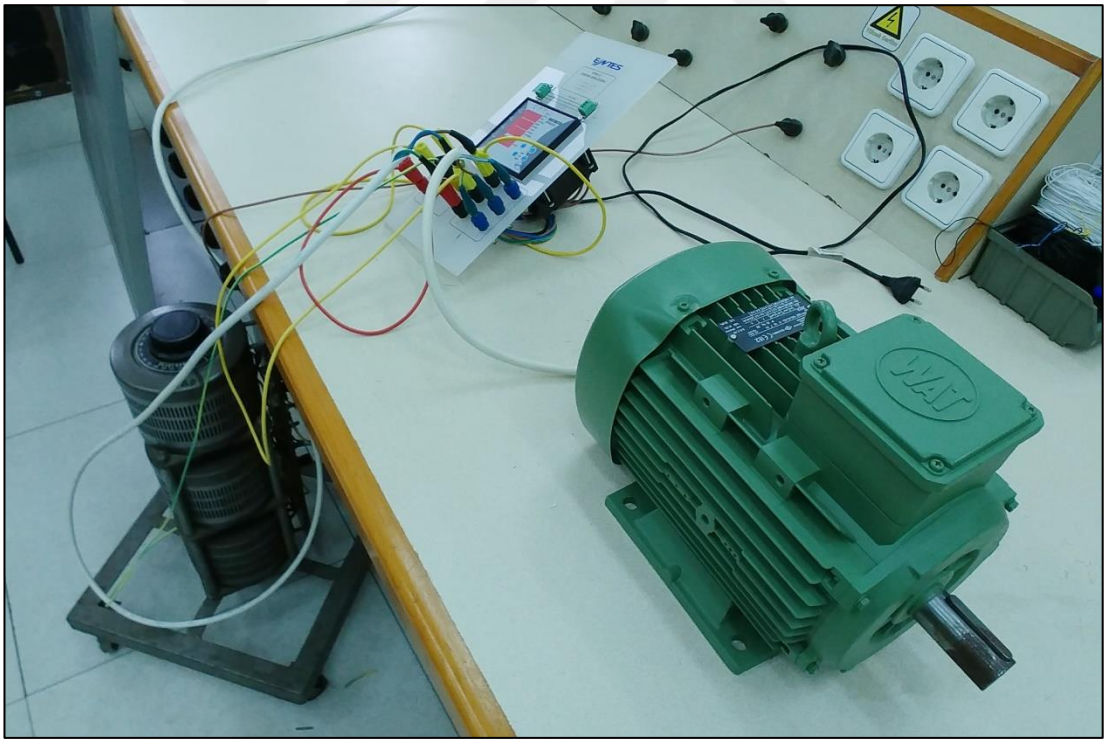

Figure 4.4 : No-load test

Table 4.4 : Laboratory no-load test data

Parameters	Value	Unit
Rated Voltage (Line)	400	V
Rated Voltage (Phase)	231	V
Rated Current	3.19	A
Input Power	218.2	W
Power Factor	0.098	-
Temperature	23.5	^{o}C

4.6 Corrected No-load Test

If the induction motor is driven by another motor at its synchronous speed while it is energized. The measured value of input active power is not containing the mechanical losses which are provided by driving motor. And also the mechanical power loss can be determined by the help of driving motor's demanded input power. Figure 4.5 shows the corrected no-load test. And Table 4.5 contains the corrected data of no-load test.

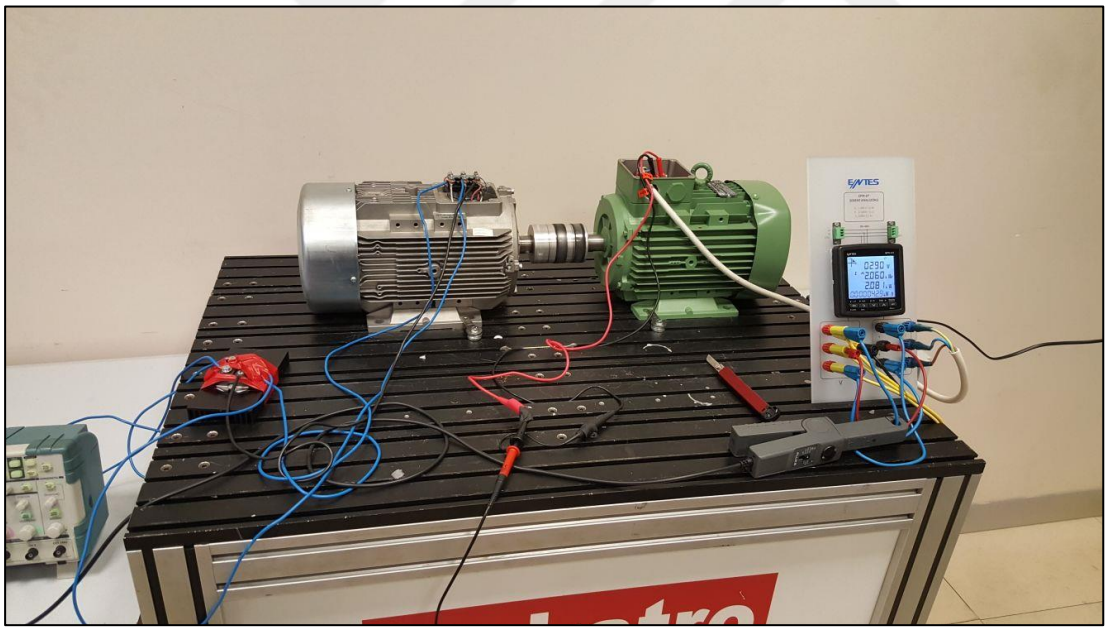

Figure 4.5 : Estimation tests without torque and speed measurements (Corrected no-load test)

Table 4.5 : Laboratory corrected no-load test data

Parameters	Value	Unit
Rated Voltage (Line)	400	V
Rated Voltage (Phase)	231	V
Rated Current	2.9	A
Input Power	171	W
Power Factor	0.085	-
Temperature	23	^{o}C

4.7 Blocked-rotor Test

The blocked-rotor test is conducted while the shaft of the motor is locked by a mechanical device. The input current is adjusted close to its rated value and all terminal parameters are measured. Due to the low input voltage because of short circuit operation, the no-load current can be omitted and with unit slip, all the current is assumed that it is flowing through stator and rotor equivalent circuit branches. The measured values are given in (Table 4.6). For deep-bar or multiple rotor cage induction motors, blocked-rotor test must be done at lower input frequencies, otherwise, the skin effect deteriorates rotor current distribution and eventually, both rotor resistance and reactance are calculated mistakenly.

Table 4.6 : Laboratory block-rotor test data

Parameters	Value	Unit
Rated Voltage (Line)	64.26	V
Rated Voltage (Phase)	37.1	V
Full Load Current	5.08	A
Input Power	341	W
Power Factor	0.606	-
Temperature	23.4	^{o}C

4.8 T-equivalent circuit calculation

By using the results of the fundamental tests of induction motors, e.g. no-load and blocked-rotor tests, it is possible to calculate all the lumped steady-state parameters which are shown in the T-equivalent circuit. The circuit can be formed for a certain temperature because of the temperature dependency of stator and rotor resistors.

The iron core loss resistor can be evaluated as no temperature dependent because it is showing a ferromagnetic loss content rather than a joule loss component.

First, the short circuit resistance which is containing both stator and rotor winding resistances can be found from short-circuit or blocked-rotor test. If P_{sc} the active input power captured during blocked-rotor test.

$$P_{sc} = 3I_{sc}^2 R_{sc} \tag{4.1}$$

so the R_{sc} is found as (ohm). The referred rotor resistance can be defined as

$$R_2' = R_{sc} - R_1 \tag{4.2}$$

R_1 is defined via DC stator resistance test. If Q_{sc} is the reactive input power during blocked-rotor test.

$$Q_{sc} = 3I_{sc}^2 X_{sc} \tag{4.3}$$

Both X_1 and X'_{250} can be found at the half of X_{sc}

$$X_1 \cong X'_{250} = \frac{X_{sc}}{2} \tag{4.4}$$

From the corrected no-load test, if P_o is the input power during no-load test

$$P_o = 3I_{10}^2 R_1 + 3I_{Fe}^2 R_{Fe} \tag{4.5}$$

To find out R_{fe} value, it is the proper way to use induced voltage E_1=E'_2

$$\overline{E_1} = \overline{V_1} - I_{10}(R_1 + jX_1) \tag{4.6}$$

where

$$I_{10} = I_{1P0} - jI_{1Q0} \tag{4.7}$$

E_1 is found as voltage V and it is phase angle is a degree, so

$$P_{Fe} = P_{10} - P_{cu10} \tag{4.8}$$

$$R_{Fe} = \frac{3E^2}{P_{Fe}} \tag{4.9}$$

and similarly, the magnetic reactance, if Q_{10} is the input reactive power, the reactive power necessary for magnetizing is as follows

$$Q_m = Q_{10} - Q_{X1} \tag{4.10}$$

Q_{X1} is the reactive power demanded by X_1, so

$$X_m = \frac{3E_1^2}{Q_m} \tag{4.11}$$

so for the given temperature (T≅23°C) the T-equivalent circuit is as

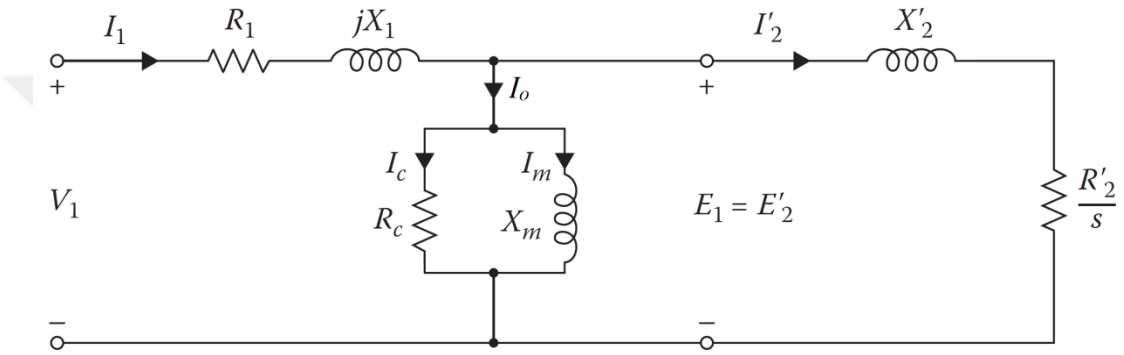

Figure 4.6 : T-equivalent circuit.

Table 4.7 shows the motor parameters of equivalent circuit.

Table 4.7 : Equivalent circuit parameters

Parameters	Value	Unit
Induced voltage $E_1=E_2'$	222.27-j5904	V
Induced voltage $\|E_1\|$	222.348	V
Stator resistance R_1	2.08	Ω
Short-circuit resistance R_{sc}	4.404	Ω
Rotor referred resistance R_2'	2.324	Ω
Short circuit reactance X_{sc}	5.824	Ω
Stator reactance $X_{1\sigma}$	2.912	Ω
Rotor referred reactance $X_{2\sigma 0}'$	2.912	Ω
Core loss resistance R_c	1106	Ω
Magnetizing reactance X_m	67.712	Ω
Temperature	20	°C

4.9 Performance Test

The performance test of the motor is realized by using a loading setup consisting of a PM synchronous motor and a resistor loading bank. The motor is driving the synchronous machine as a generator and generated three-phase voltages by synchronous machine are rectified via a three-phase bridge diode rectifier. The loading resistor is connected to the rectifier as a load bank. By adjusting the different resistor values by connecting them series or parallel the induction motor can be loaded with various shaft torque which reflects the output performance of the motor.

During the loading process, the motor shaft torque and speed are monitored and captured by a torque transducer and a speed sensor. Simultaneously, the motor terminal parameters such as the terminal voltage, terminal current and input active power are measured by an oscilloscope and a power analyzer. The motor's heating test is also done by using the same setup by loading the motor at its rated output power for a long time. The loading test setup can be shown in (Figure 4.2). and the measured values for same certain loading are given in (Table 4.8).

Table 4.8 : Performance test data

Parameters	Value						Unit
Rated Voltage	400.1	400.0	400.6	399.7	399.9	399.3	V
Full Load Current	6.75	5.82	5.01	4.27	3.69	3.30	A
Input Power	3932	3259	2626	1985	1380	784	W
Torque	21.969	18.304	14.632	10.975	7.321	3.661	Nm
Mechanical Speed	1410	1427	1443	1458	1473	1485	rpm
Output Power	3243.6	2735.1	2210.9	1675.6	1129.2	569.3	W
Efficiency	82.5	83.9	84.2	84.4	81.8	72.6	%
Power Factor	0.841	0.808	0.756	0.672	0.539	0.343	-

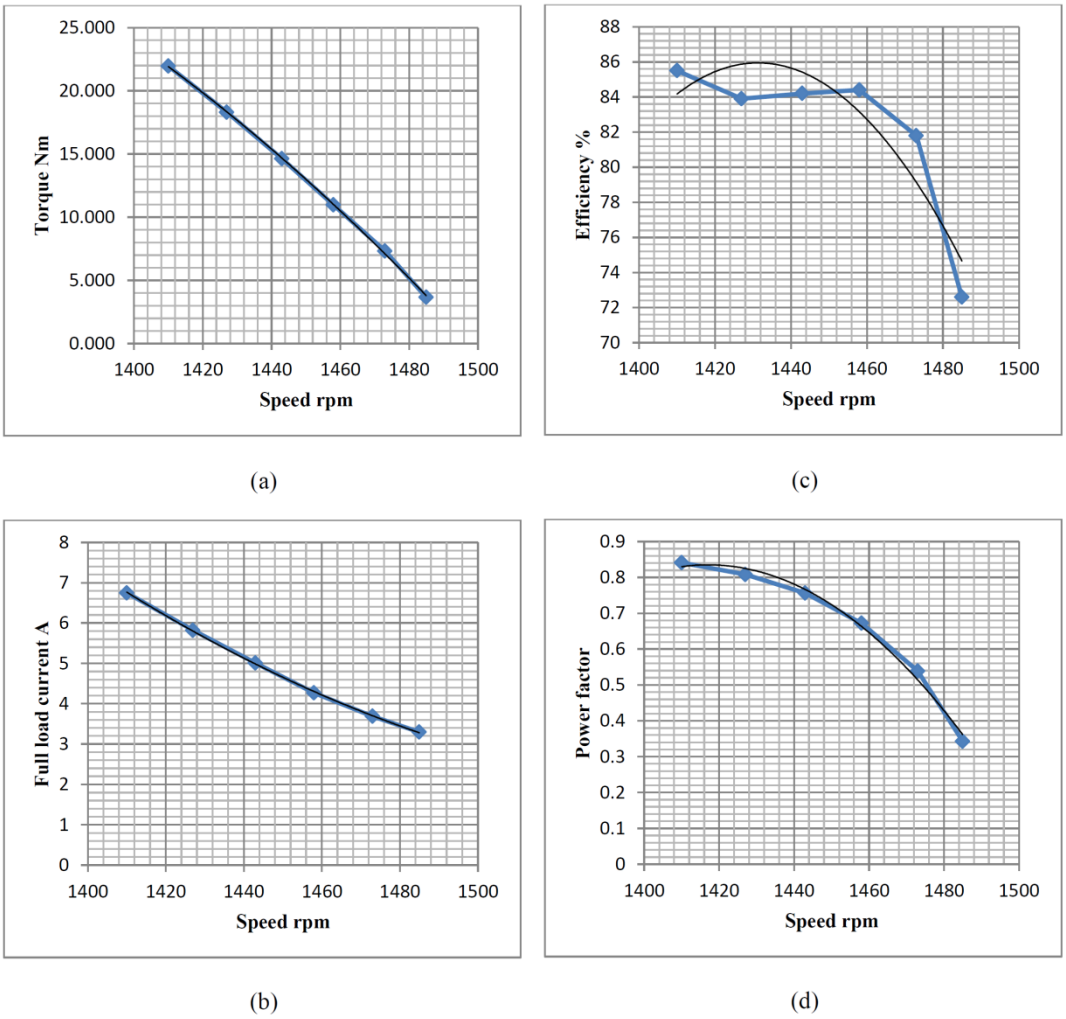

Figure 4.7 : Performance curves (a) torque-speed curve, (b) current-speed curve, (c) efficiency-speed curve, (d) power factor-speed curve.

5. PERFORMANCE ESTIMATION STUDY

5.1 Method Explained

The proposed method is based on the determination of equivalent impedance of the T-equivalent circuit as a function of slip. After the definition of exact T-equivalent circuit parameters, the equivalent impedance that is depicting the input power factor and input current is found. The equivalent impedance is given as:

$$Z_{eq} = Z_1 + (Z_2 // Z_{ab}) \tag{5.1}$$

This value is a function of slip and temperature. Both stator and rotor resistances are temperature dependent. The motor temperature can be found by using another estimation algorithm by using a simple temperature sensor, which is placed, on the motor surface or inside of the motor. The slip dependency of the total equivalent impedance is the essence of steady-state performance estimation of the induction motor under attention.

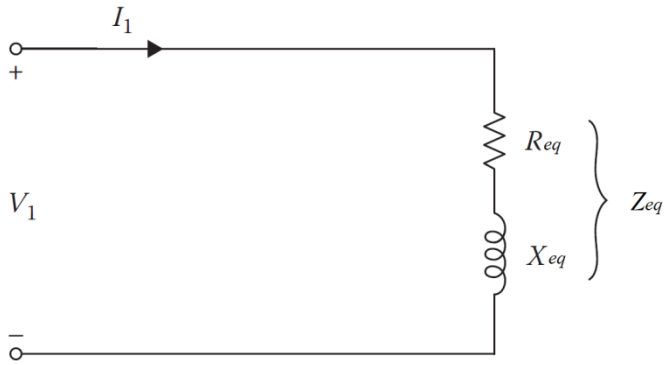

Figure 5.1 : Equivalent circuit of an induction motor

$$\overline{V_1} = \overline{Z_{eq}}.\overline{I_1} \tag{5.2}$$

$$Z_{eq} = R_{eq} + jX_{eq} \tag{5.3}$$

Equivalent impedance versus slip characteristic can be calculated by using a simple algorithm. For the meaningful values of motor operation slip, i.e. from break-down slip to zero slip, can be defined by using the calculation algorithm given in (Figure 5.11). If the motor is operated at unstable region, i.e. between unit slip (zero speed) and breakdown slip, the operation is labeled as a fault operation, which causes excessive current flow. In this condition, the performance estimation is no longer needed; the electrical energy input of the motor must be cut as soon as possible. After the definition of Z_{eq} = f(s) curve which is a non-linear function, a proper curve fitting process is applied to find out the related slip values. For the sake of simplification, a quadratic curve fitting is more proper to calculate slip value from the curve. Of course, the curve must be obtained for different temperature values.

Then the equivalent impedance – slip equation is given as follows:

$$Z_{eq}(s) = as^2 + bs + c \tag{5.4}$$

where a, b and c are the motor coefficients which are depending on the T-equivalent circuit parameters and temperature. These coefficients can be supplied from the manufacturer and embedded in performance estimation processor or simply can be found by means of fundamentals tests which are providing the equivalent circuit parameters. In addition, the similar process can be applied for the input power factor to verify the measured value from the terminal voltage and current.

$$Cos\varphi = ds^2 + fs + e \tag{5.5}$$

The total equivalent impedance of T-equivalent circuit is calculated by using the VisSim algorithm as given in (Figure 5.2). the algorithm is for calculating all subequivalent impedances of T-equivalent circuit, e.g. R_0 and X_0 are the equivalent resistance and reactance of no-load branch and, R_{20} and X_{20} are the parallel equivalent resistance and reactance values of no-load and rotor circuit branches. By using the given slip value, the numerical value of the total equivalent impedance can be found. By means of the calculated impedance and other lumped circuit resistors, all inner power values of the motor can be defined. The input power, stator copper loss, iron loss, rotor copper loss, and inner electromechanical powers can be calculated in the algorithm which is given in (Figure 5.3).

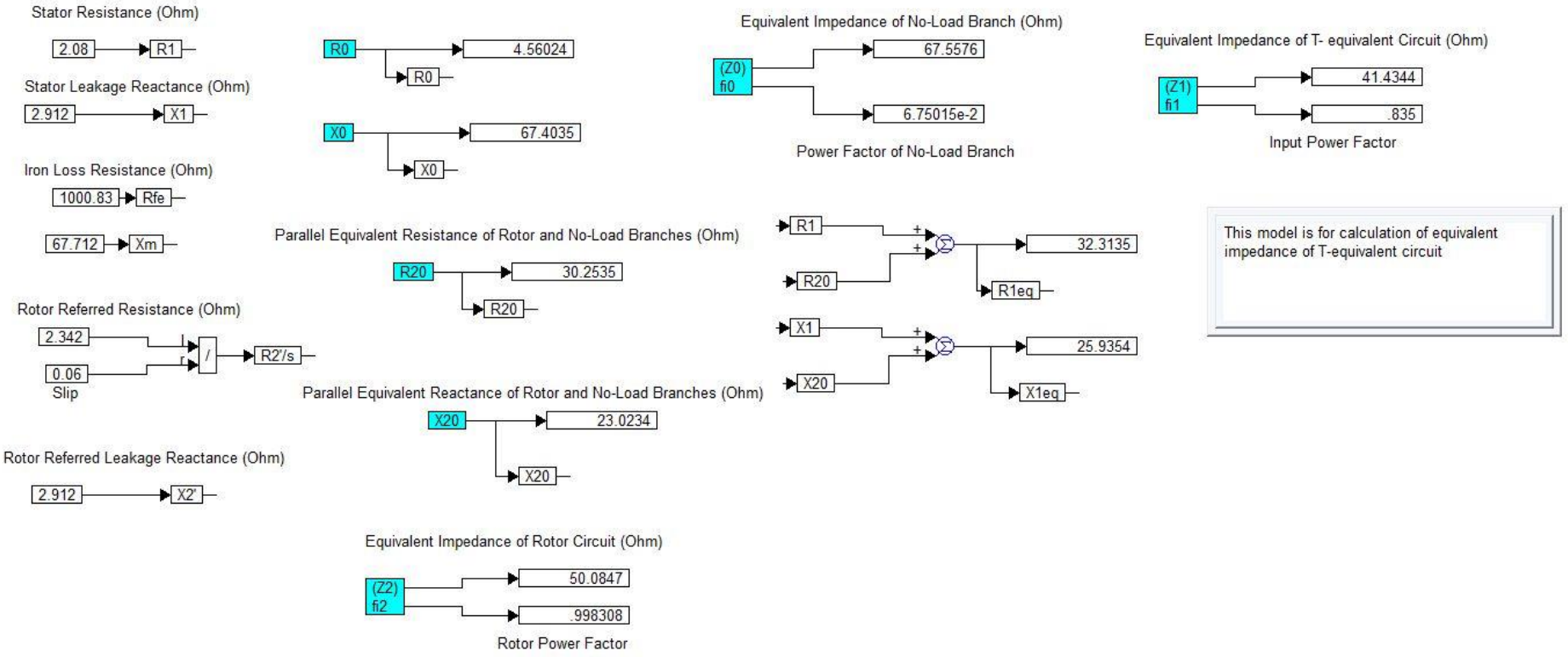

Figure 5.2 : VisSim algorithm of equivalent impedance

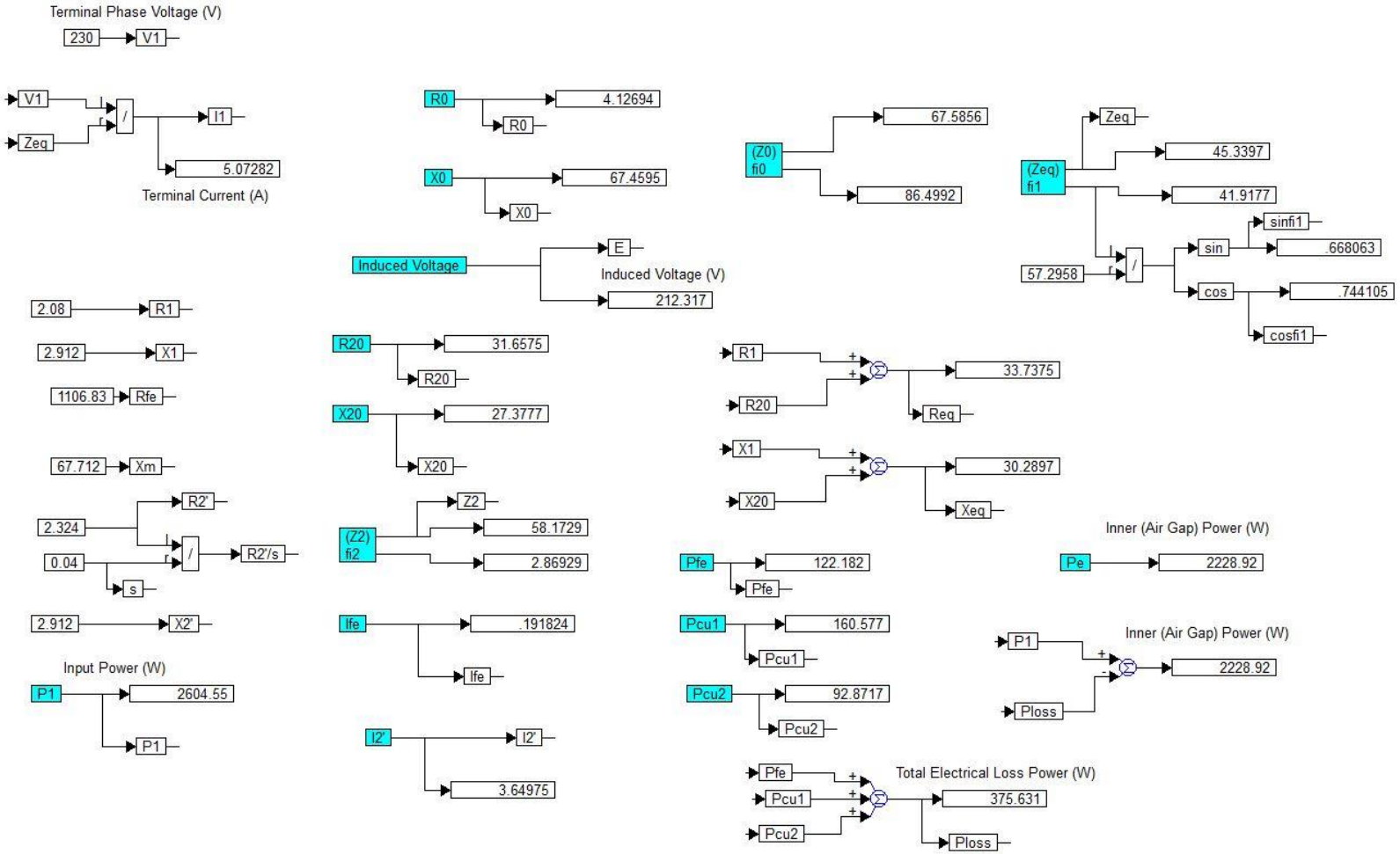

Figure 5.3 : VisSim algorithm of power calculations

5.2 Terminal Voltage - Current Measurements And Input Power Calculations

The motor terminal voltage and current waveforms are under attention have captured by an oscilloscope. The waveforms are obtained for each loading situation as an MS Excel file, so the data sets of measurements can be easily sent to any processor or computer to analyze their contents. The tests are conducted at 23 °C test ambient temperature and the signals are filtered substantially to overcome any calculating error. Anyhow, some calculation errors may arise due to the poor signal quality. The checking of waveforms which are whether near sinusoidal or not is done by two methods: FFT (Fast Fourier Transformation) and CF (Crest Factor). By multiplying the time-dependent voltage and current waveforms, the instantaneous power waveform is found for each loading situation. Moreover, by integrating the instantaneous power waveform, the active power value can be determined. Because apparent power can be calculated from the captured voltage and current waveforms, power factor and reactive power values can be defined consecutively. For FFT analysis, it is aimed that the THD of the waveform must be lower than 5% so that the signal can be assumed near sinusoidal and the power calculations that are founded on pure sinusoidal waveforms can be done with small calculation errors. Mostly the terminal motor voltage can be assumed as a pure sinusoidal unless an important AC mains disturbance is presented. The CF value check limits are determined as ± 10 % because of the unwanted superposed signals, i.e. noise. However, with proper analog and digital filtering, when the method is implemented in a microprocessor these limits can be decreased due to the signal capturing quality.

For a star (wye) connected motor, it is proper to capture the motor voltage and current waveform of a single-phase winding. The measurements must be done on the same phase’s voltage and current. The input power calculations from the terminal voltage and current capturing are connected by using an oscilloscope and evaluated off-line.

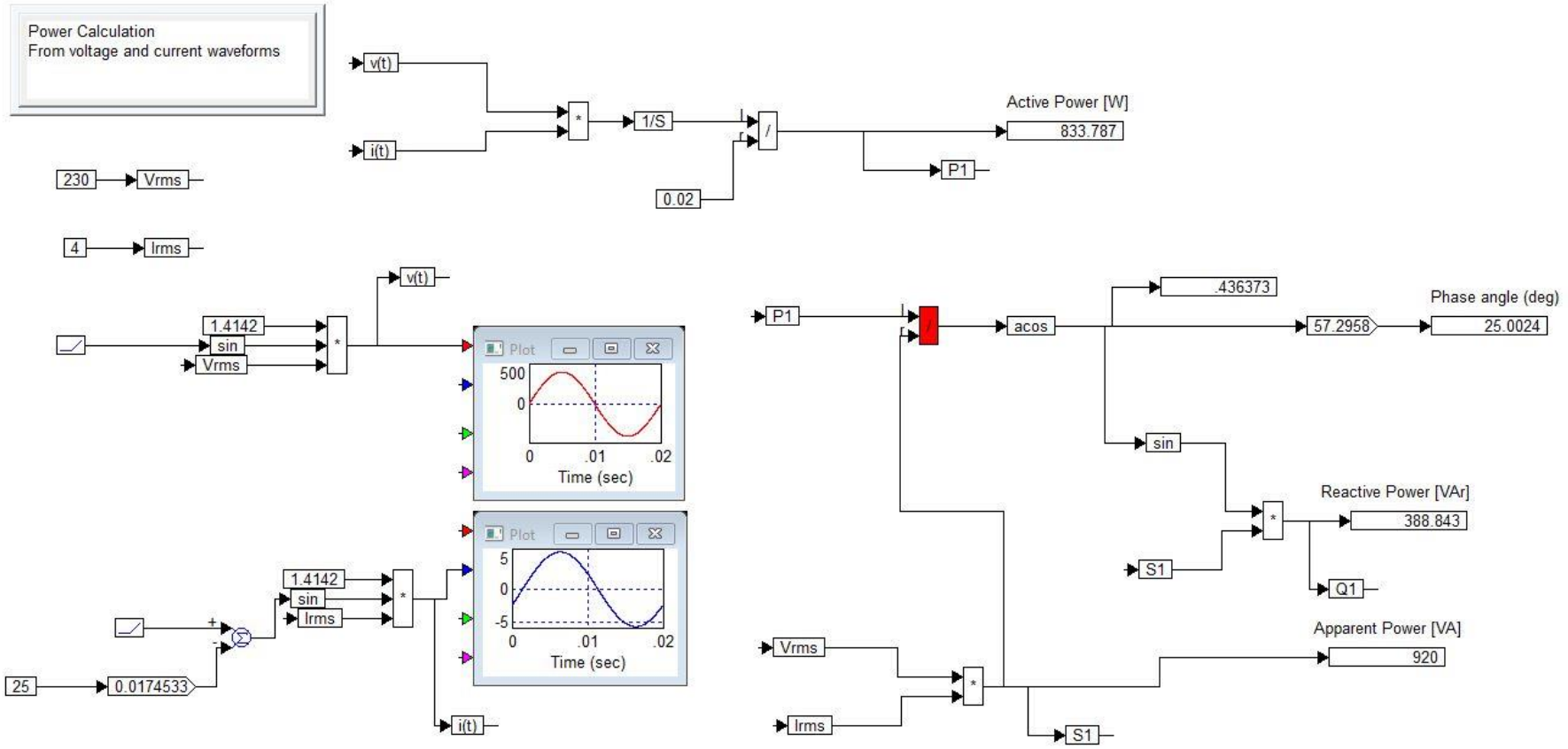

Figure 5.4 : VisSim algorithm of power calculation

5.2.1 Measurement 1

The voltage and current waveforms are monitored form the terminal box of the induction motor by means of voltage and current probes, and the obtained waveforms of single phase are shown in (Figure 5.5). The given waveforms are for a no-load operation whose power factor is quite low and the phase angle is close to 90°, but of course, lowers than that. As it can be seen, there is a small amount of noise content due to the measuring process, but it can be easily understood that both waveforms can be assumed pure sinusoidal.

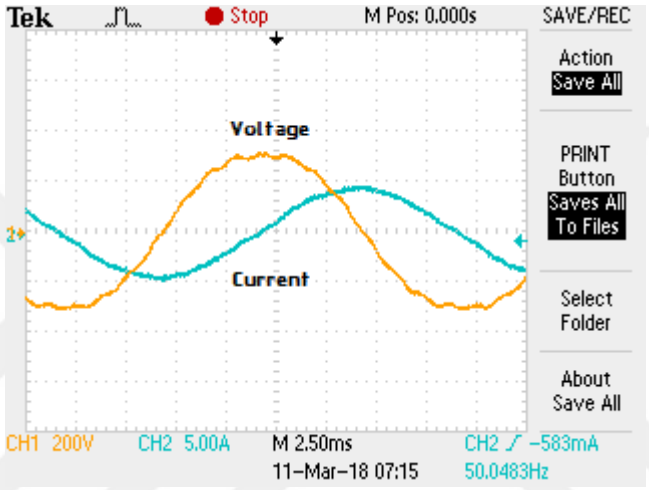

Figure 5.5 : Terminal voltage and current waveform from an oscilloscope

Also, the point-by-point graph of the waveform, e.g. an MS Excel file, can be taken via an oscilloscope. The terminal current waveform and the terminal voltage waveform are seen in Figures 5.6 and Figure 5.7, respectively.

The captured waveforms have some noises and harmonics due to the measurement conditions. But it can be seen in (Figure 5.8). so the calculations are somewhat deviated from the other measurements which are done by the power analyzer. But all calculated values are credible and agreement with the power analyzer measurements. And also it can be seen that the power factor can be found by means of conventional relation between the active power (P) and the apparent power (S) and also by determining the duration of negative power sections in the instantaneous power waveform.

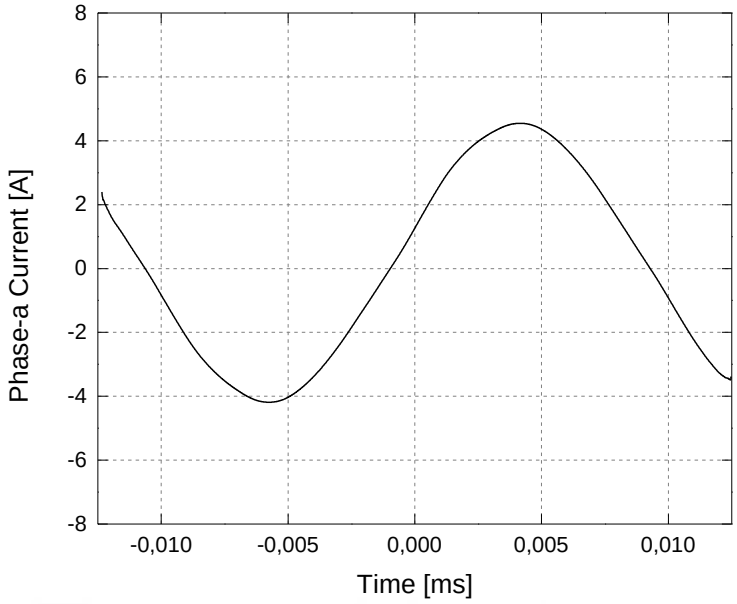

Figure 5.6 : Analyzed current waveform

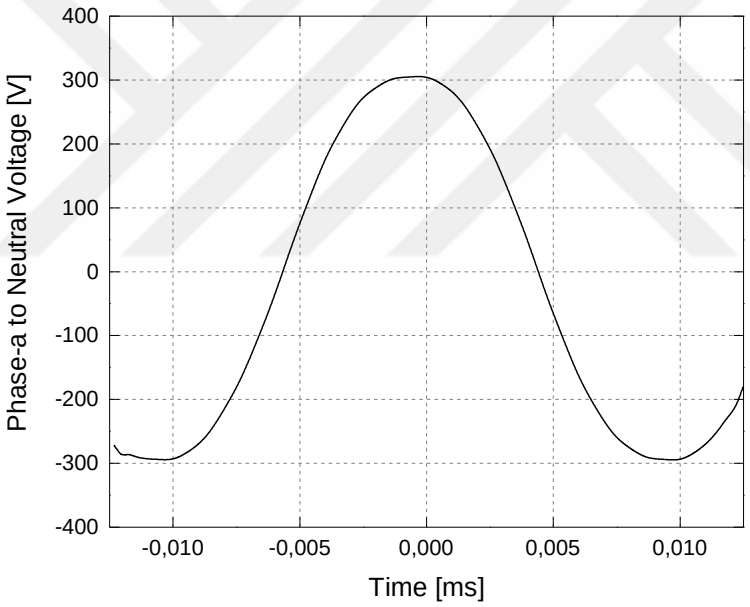

Figure 5.7 : Analyzed voltage waveform

After the data capturing, the measured waveforms are analyzed by an FFT process which can be implemented in a processor. The frequency distribution of harmonic content of terminal current is shown in (Figure 5.8). The harmonic order of terminal current can be seen in (Figure 5.9).

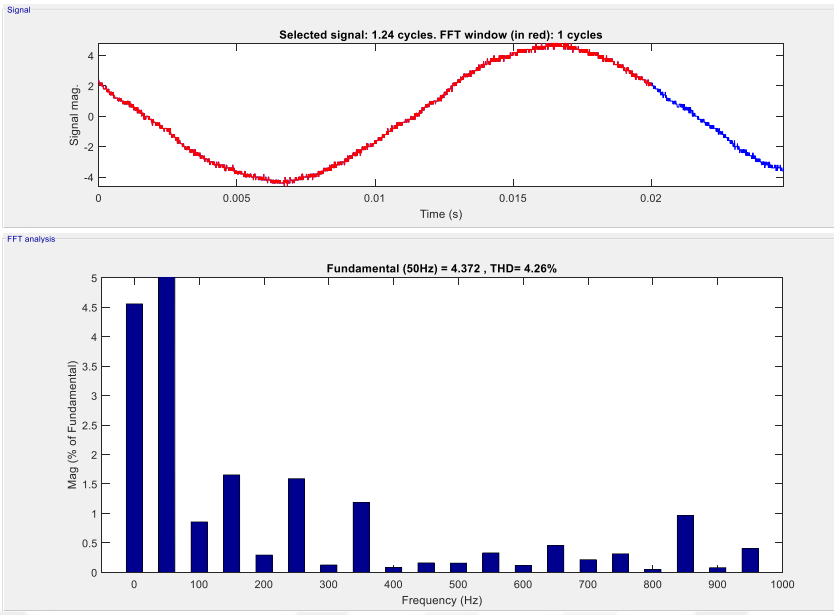

Figure 5.8 : FFT (harmonic content due to frequency) of terminal current

Another check for the suitability of captured waveform for sinusoidal calculations is the CF check. Because of the measurement noise, there are substantial deviations from 1.4142, but by using a proper filtering, this value can be satisfied accordingly. Mostly, for the regular grids, the terminal voltage can be assumed as pure sinusoidal directly and only the compatibility of current can be investigated.

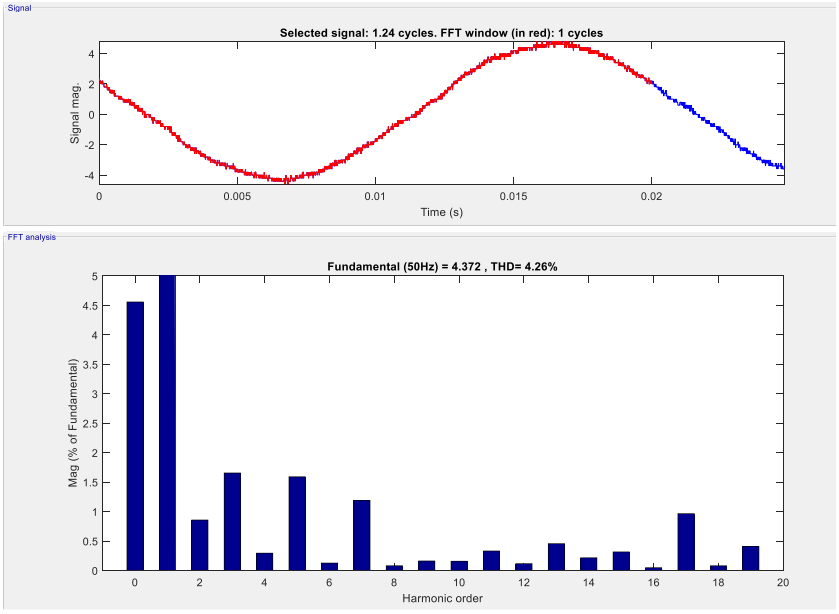

Figure 5.9 : Harmonic order content of terminal current

As can see, Table 5.1 shows the ratio values of the voltage and current waveforms.

Table 5.1 : CF check for voltage and current waveforms

Parameters	Value
V_{max}/V_{rms}	1,391129911
I_{max}/I_{rms}	1,554314754

The product of terminal voltage and terminal current gives the instantaneous power signal and the average of that signal yields the input active power. The single-phase input power variation is seen in (Figure 5.10). The area determined by integrating the waveform is given as V.s (Volts × seconds) and the mean value of the instantaneous power is input active power.

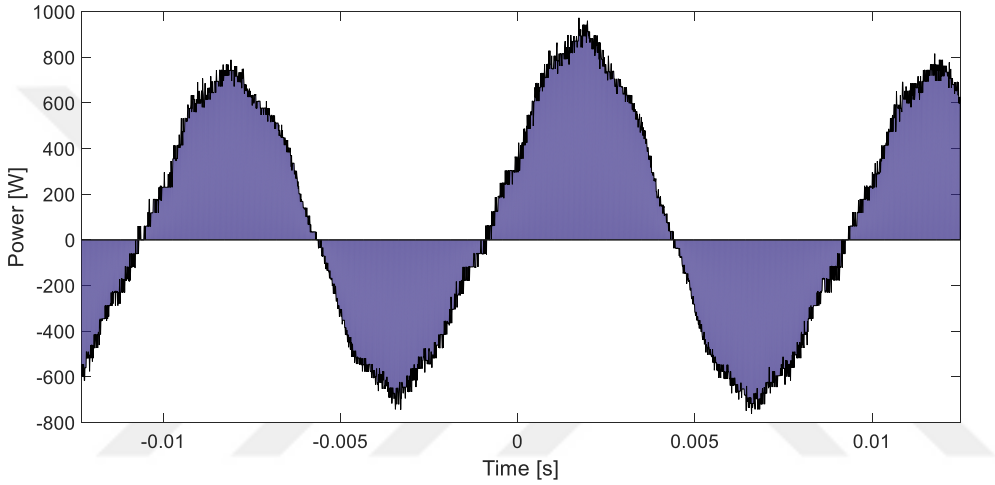

Figure 5.10 : Instantaneous input power waveform (v(t).i(t))

The integral of the area is 0.6935 whose period is 0.01 sec. The active power can be calculated by dividing this value by the period of 0.01 sec. This is reflecting 69.35 W for single phase and 208.05 W for three-phase which is very close to the measured value of 195 W.

As it can be calculated easily, the input apparent power:

$$S_1 = 3V_{rms}I_{rms} = 694.4\,VA \tag{5.6}$$

Power factor:

$$PF = \frac{P_1}{S_1} = 0.3 \tag{5.7}$$

5.2.2 The other measurements

The figures and tables for the rest of measurements are listed in Appendix A. Table 5.2 shows the CF check of the voltage and current waveforms for the 5 measurements to get nearly pure sinusoidal waveform.

Table 5.2 : CF check of voltage and current waveforms for the 5 measurements

Measurements	Parameters	
	V_{max}/V_{rms}	I_{max}/I_{rms}
Measurement 1	1,391129911	1,554314754
Measurement 2	1,406799	1,589338
Measurement 3	1,400209	1,36978
Measurement 4	1,408208	1,58372
Measurement 5	1,412712054	1,55062807

5.3 Curve Fitting

The total equivalent impedance Z_{eq} variation due to motor slip can be found by using the algorithm given in (Figure 5.11). After the determination of Z_{eq} = f(s) curve which is essential for the motor operation, that variation must be simplified to calculate the related slip value which is showing the motor's performance. The total equivalent impedance versus slip curve of the motor is given in (Figure 5.11). A quadratic curve fitting can be applied to the characteristic and resulted as:

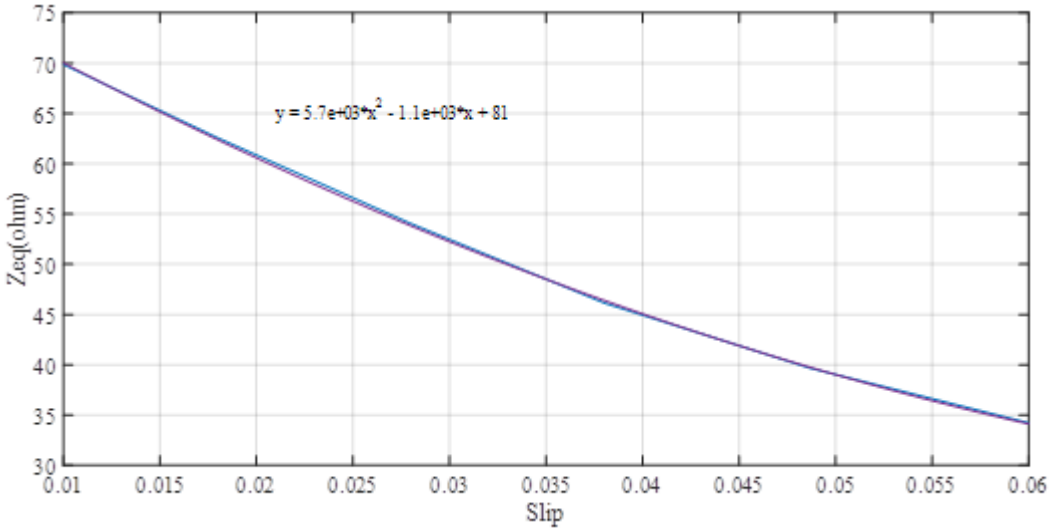

Figure 5.11 : Equivalent impedance - slip relation

$$Z_{eq} = 5700s^2 - 1100s + 81 \tag{5.8}$$

From the quadratic equation can be found the slip value.

$$x = \frac{-b \pm \sqrt{b^2 - 4ac}}{2a} \tag{5.9}$$

A root of the quadratic equation is the slip which is to be found. The similar curve fitting process can be applied to the input power factor of the motor. The power factor versus slip curve is shown in (Figure 5.12). Moreover, a quadratic approximation of this curve is as follows.

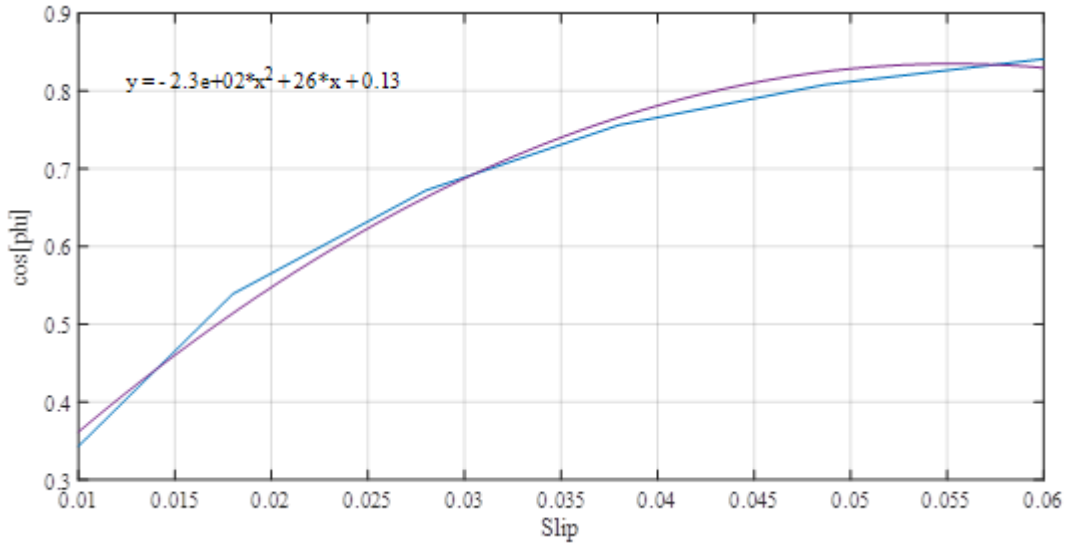

Figure 5.12 : Power factor - slip relation

$$Cos\varphi_1 = -230s^2 + 26s + 0.13 \tag{5.10}$$

Because the input power factor is already calculated from the terminal values during the monitoring process, this definition can be used for verification of the performance estimation. Both characteristics, of course, are temperature dependent and the temperature dependency must be considered during performance estimation computation.

5.4 Estimation Results

The measured parameters of some different loadings are given in (Table 5.3). The values are captured by using tachometer, torque meter and power analyzer for the motor that is not loaded previously, i.e. not heated.

Table 5.3 : Experimental results by using torque meter, tachometer, and power analyzer

Parameters	Loading no.				Unit
	1	2	3	4	
Input phase voltage V_1	230	230	230	230	V
Input current I_1	3.69	4.27	5.01	5.82	A
Input power P_1	1380	1985	2626	3259	W
Mechanical speed n_m	1473	1458	1443	1427	rpm
Mechanical torque T_m	7.32	10.97	14.63	18.30	Nm
Output power P_o	1130	1676	2211	2735	W
Power factor Cosφ	0.539	0.672	0.756	0.808	-
Efficiency η	81.8	84.4	84.2	83.9	%

As an example, the equivalent impedance of loading no.2 can be found as

$$Z_{eq} = \frac{V_1}{I_1} = 53.86\ \Omega \tag{5.11}$$

and from the given curve equation can be found as

$$s = \frac{-b \pm \sqrt{b^2 - 4ac}}{2a} = 0.0302 \tag{5.12}$$

By using this speed value the motor's shaft speed can be calculated as

$$n_m = n_s(1 - s) = 1452\ min^{-1} \tag{5.13}$$

To determine the output power, first, the inner electromechanical or air gap power must be calculated as

$$P_e = 3I_2'^2 R_2' \left(\frac{1 - s}{s}\right) = 1632\ W \tag{5.14}$$

The referred rotor current can be found or estimated by using the algorithms in Figure 5.2 and Figure 5.3.

Although it is depending on slip the mechanical friction loss can be assumed as measured which is 23W. And so the output shaft power can be estimated as:

$$P_m = P_e - P_{Fr} = 1655\ W \tag{5.15}$$

Then the estimated efficiency is;

$$\eta = \frac{P_m}{P_1} = 0.833\% \tag{5.16}$$

The shaft torque is simply as follows,

$$T_m = \frac{P_m}{\omega_m} = 13.14\ Nm \tag{5.17}$$

So the all estimated values of the loading situations are found properly. The other estimation calculations are given in (Table 5.4). As it can be seen the tested and estimated results are in agreement for cold motor. But the temperature dependency must also be investigated.

Table 5.4 : Input Measurements and Estimated Results

Parameters	Loading no.				Unit
	1	2	3	4	
Input phase voltage V_1	230	227	227	230	V
Input current I_1	3.64	4.25	4.98	5.77	A
Input power P_1	1363	1997	2618	3244	W
Mechanical speed n_m	1468	1452	1439	1420	rpm
Mechanical torque T_m	7.28	13.14	14.52	18.27	Nm
Output power P_o	1120	1655	2188	2717	W
Power factor Cosφ	0.543	0.690	0.772	0.815	-
Efficiency η	82.1	82.8	83.6	83.7	%

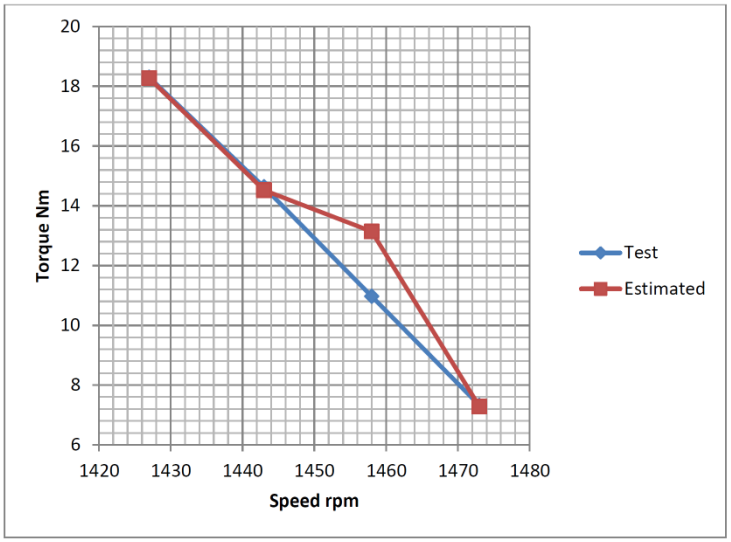

(a)

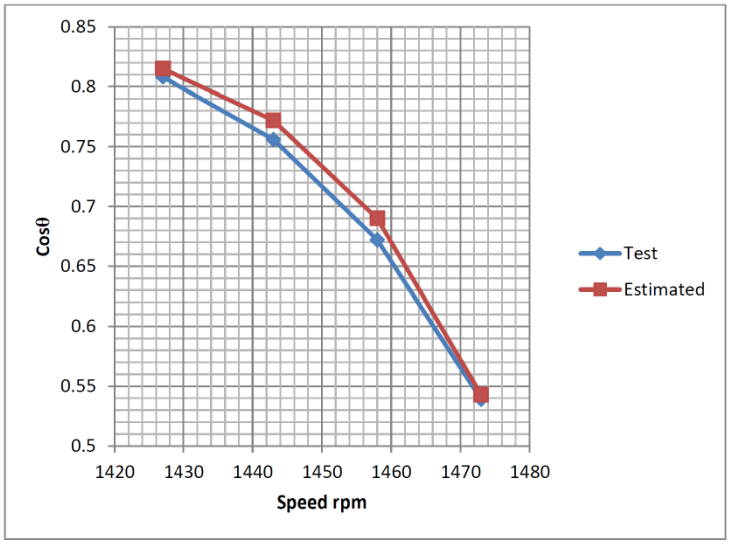

(b)

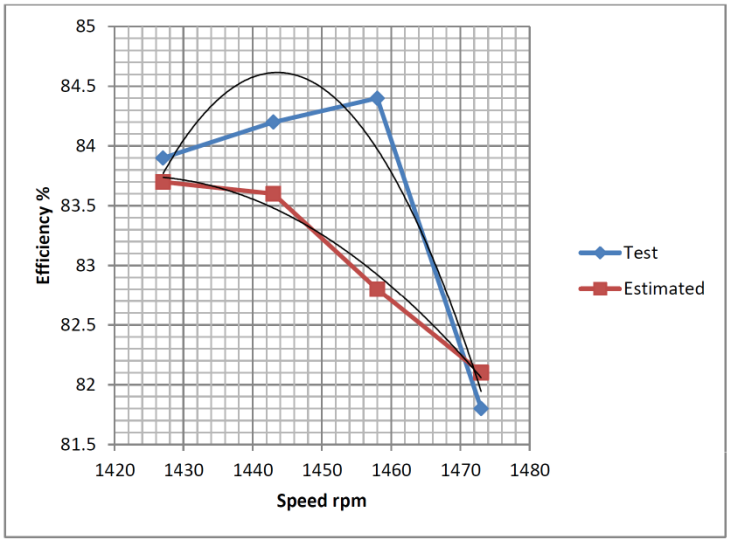

(c)

Figure 5.13 : Torque-speed curve of test and estimated measurements.

6. CONCLUSION AND FUTURE ASPECTS

In this thesis, a simple on-line steady-state performance estimation technique for three-phase induction motors is presented. The target is to define the approximate performance of induction motor, i.e. input power, shaft speed, shaft torque, output power, and efficiency, by using only terminal voltage and current measurements. The method is based on the T-equivalent circuit, which reflects motor performance by means of lumped parameters. The method uses slip value as a key parameter of induction motor, for power distribution and output mechanical quantities. The main aim is to find the operation slip of motor from the total equivalent impedance that can be defined by T-equivalent circuit. For this aim, first the well-approximated equivalent circuit parameters are obtained via fundamental tests. Then, the slip variation of total equivalent impedance is expressed by using a simple curve fitting process. This variation can be provided either by directly from manufacturer or by doing some tests.

The motor used in the study is a 2.2 kW, 380 V, IE2 class, 4-pole induction motor. The performance parameters are defined by conducting loading tests and are known beforehand. After that, a series of fundamental tests for obtaining induction motor equivalent circuit lumped parameters are done. For small induction motors, some assumptions such as omitting stator impedance during no-load test cannot be applied. So some corrections are accomplished due to the nature of small power induction motors.

After the definition of T- equivalent circuit parameters, the slip variation of the total equivalent impedance, which is simply equal to the division of input voltage and current, is extracted and a curve fitting is applied to find out slip vale from the impedance variation.

During performance estimation process, the input active power, apparent power and reactive power, power factor can be calculated from the terminal voltage and current

waveforms. The real-time calculation of powers is given. After the completion of input quantities, by help of the slip variation of equivalent impedance can obtain the output values. The slip value gives the shaft speed and inner (air gap) power, and by using proper values of frictional losses and stray losses the output power and shaft torque can be found approximately. So the efficiency and loading level of the motor can be monitored on-line. The real test results and the results from estimation calculations are agreeable. Some proper filtering is needed to get rid of unwanted noises during measurement.

Any substantial deviation from the expected operation mode can be assumed as a fault operation and some interventions can be done. By using Big Data via longtime monitoring data, a fault diagnosis can be applied.

For the future work, the analysis of temperature dependency of equivalent impedance will be considered by means of the information form cheap temperature sensors. Moreover, equivalent circuit parameters will be estimated from the on-site operation conditions instead of doing some separate tests. In addition, the waveforms with harmonic content will be considered for the estimation process.

REFERENCES

Aktaibi, A., Ghanim, D., & Rahman, M. A. (2011). Dynamic Simulation of a Three-Phase Induction Motor Using MATLAB Simulink. The 20th Annual Newfoundland Electrical and Computer Eng. Conference, (12), 1–5. https://doi.org/10.13140/RG.2.1.2705.4243

Almeida, A. T., Ferreira, F. J. T. E., Fong, J., & Fonseca, P. (2008). EUP Lot 11 Motors. University of Coimbra, (February), 137. Retrieved from http://www.eupnetwork.de/fileadmin/user_upload/Produktgruppen/Lots/Final_Documents/Lot11_Motors_FinalReport.pdf

Arçelik A.Ş. (2016). Three Phase & Single Phase Industrial Motors. Turkey - Istanbul: Arçelik A.Ş. Retrieved from http://www.tee.com.tr/Documents/IM en 16_1.pdf

Ayasun, S., & Nwankpa, C. O. (2005). Induction motor tests using MATLAB/Simulink and their integration into undergraduate. IEEE Transactions on Education, 48(1), 37–46. https://doi.org/10.1109/TE.2004.832885

Baranwal, A., Chahal, N., & Goley, R. (2014). Designing of Three Phase Induction Motor Using MATLAB GUI. MIT International Journal Of Electrical and Instrumentation Engineering, 4(1), 42–44.

Basu, J. B. (2015). MATLAB based Performance Prediction of a Three-Phase Induction Motor Utilising its Test Results, 4(9), 8–10.

Bhattacharya, S. K. (1998). Electrical Machines. Tata McGraw-Hill Education (2nd ed.).

Calis, H., & Caki, E. (2014). LabVIEW Based Laboratory Typed Test Setup for the Determination of Induction Motor Performance Characteristics. Journal of Electrical Engineering and Technology (JEET), 9(6), 1928–1934.

Chapman, S. J. (2005). Electric Machinery Fundamentals. McGraw-Hill Companies (4th ed.). Singapore.

Daut, I., Anayet, K., Irwanto, M., Gomesh, N., Muzhar, M., & Asri, M. (2009). Parameters Calculation of 5 HP AC Induction Motor. October, (October), 11–13.

Eremia, M., & Shahidehpour, M. (2013). Handbook of electrical power system dynamics modeling, stability, and control. Wiley. https://doi.org/10.1002/9781118516072

Gastli, A. (1999). Identification of induction motor equivalent circuit parameters using the single-phase test. IEEE Transactions on Energy Conversion, 14(1), 51–56. https://doi.org/10.1109/60.749147

Ghule, C. V, Mrssuhasini, S. D., & Samanta, J. (2013). An Off-Line Technique for Prediction of Performance Characteristics of Three Phase Induction Motor, 2(1), 1–6.

Guimarães, J. M. C., Bernardes Jr, J. V., Hermeto, A. E., & Bortoni, E. C. (2014). Determination of Three-phase Induction Motors Model Parameters from Catalog Information. IEEE PES General Meeting | Conference & Exposition, 1–5.

Haque, M. H. (1993). Estimation of three-phase induction motor parameters. Electric Power Systems Research, 26(3), 187–193. https://doi.org/10.1016/0378-7796(93)90012-4

Haque, M. H. (2008). Determination of NEMA design induction motor parameters from manufacturer data. IEEE Transactions on Energy Conversion, 23(4), 997–1004. https://doi.org/10.1109/TEC.2008.2001451

Hidayah, R., Siti, S., Binti, H., Kadir, A., Rizam, S., Shah, M., & Ismail, F. (2013). Parameter Identification of Three-Phase Induction Motor using MATLAB-Simulink, (June), 647–651.

Hindmarsh, J., & Renfrew, a. (1996). Electrical machines and drive systems.

IEC 60034-30-1 (2014). Rotating electrical machines - Part 30-1: Efficiency classes of line operated AC motors (IE code).

IEC 61000-3-2 (2018). Electromagnetic compatibility (EMC) - Part 3-2: Limits - Limits for harmonic current emissions (equipment input current ≤16 A per phase).

IEEE Std 112™ (2004). IEEE Standard Test Procedure for Poly-phase Induction Motors and Generators.

Imecs, M., & Incze, I. I. (2001). A simple approach to induction machine parameter estimation. Workshop on Electrical Machines' Parameters, (May), 73–80.

Jones, D. (2013). The Workhorse of Industry: The Induction Motor, (December 2013), 76–77. Retrieved from http://www.powertransmission.com/issues/1213/induction_motor.pdf

Jurkovic, S. (2005). Induction Motor Parameters Extraction. Michigan State University College of Engineering.

Kande, M., Isaksson, A., Thottappillil, R., & Taylor, N. (2017). Rotating Electrical Machine Condition Monitoring Automation—A Review. Machines, 5(4), 24. https://doi.org/10.3390/machines5040024

Karmakar, S., Chattopadhyay, S., Mitra, M., & Sengupta, S. (2016). Induction Motor Fault Diagnosis: Approach through Current Signature Analysis. Singapore: Springer Singapore. https://doi.org/10.1007/978-981-10-0624-1

Keysight Technologies (2011). Make Better AC RMS Measurements with Your Digital Multimeter - Application Note. NCSL International Workshop and Symposium. Retrieved from http://literature.cdn.keysight.com/litweb/pdf/5988-6916EN.pdf

Lee, K., Frank, S., Sen, P. K., Polese, L. G., Alahmad, M., & Waters, C. (2012). Estimation of induction motor equivalent circuit parameters from nameplate data. 2012 North American Power Symposium, NAPS 2012. https://doi.org/10.1109/NAPS.2012.6336384

Natarajan, R., & Misra, V. K. (1989). Parameter estimation of induction motors using a spreadsheet program on a personal computer. Electric Power Systems Research, 16(2), 157–164. https://doi.org/10.1016/0378-7796(89)90008-4

NEMA Standards Publication No. MG-1 (2012). American National Standard Motors and Generators.

Pandey, K. K., & Zope, P. H. (2013). Estimating Parameters of a Three-Phase induction motor using MATLAB/Simulink. International Journal of Scientific and Engineering Research (IJSER), 4(12), 425–431.

Parekh, R. (2003). AC Induction Motor Fundamentals. Microchip Technology Inc, 1–24. Retrieved from http://jimfranklin.co.uk/microchipdatasheets/00887a.pdf

Ratnani, P. L., & Thosar, A. G. (2014). Mathematical Modelling of an 3 Phase Induction Motor Using MATLAB/Simulink\n. International Journal of Modern Engineering Research (IJMER), 4(6), 62–67. Retrieved from http://www.ijmer.com/papers/Vol4_Issue6/Version-2/IJMER-46026267.pdf

Research and Markets. (2015). Induction Motor Market by Type (Single Phase, Three Phase), Application (Residential, Industrial, Commercial), Geography (North America, Europe, Asia-Pacific, Row) - Analysis and Forecasts to 2019, 67. Retrieved from https://www.researchandmarkets.com/research/9tsf77/induction_motor

Salleh, Z., Patakor, F. A., & Rashid, A. N. A. (2013). Study on Parameter Determination for 1.5 kW AC Induction Motor.

Sangani, C. P. (2015). New Parameters Estimation Using Numerical Method and Steady-State Performance for Convensional and Converter Fed Induction Motor. International Journal of Science and Research (IJSR), 4(6), 469–474.

Sangwan, V. (2014). Normalized Dynamic Simulation of 3-phase Induction Motor using MATLAB / SIMULINK. The International Journal of Emerging Technology and Advanced Engineering (IJETAE), 4(3), 43–48.

Sarma, M. S. (1985). Electric Machines: Steady-state Theory and Dynamic Performance. West Publishing Company.

Say, M. G. (1976). Alternating Current Machines (4th ed.). Pitman Publishing Ltd.

Sehra, S., Gautam, k.k., & Bhuria, V. (2012). Performance Evaluation of Three Phase Induction Motor Based on No Load and Blocked Rotor Test Using MATLAB, 1(5), 541–547.

Shaw, S. R., & Leeb, S. B. (1999). Identification of induction motor parameters from transient stator current measurements. IEEE Transactions on Industrial Electronics, 46(1), 139–149. https://doi.org/10.1109/41.744405

Siemens. (2003). Low-voltage Motors. Catalogue M 11. Siemens.

Singhal, A., & Garg, A. (2012). Online Parameter Determination and Performance Analysis of Three Phase Induction Motor using Virtual Instrumentation. IEEE International Conference on Power Electronics, Drivers and Energy Systems, 1–6.

Soe, N. N., Yee, T. T. H., & Aung, S. S. (2008). "Dynamic Modeling and Simulation of Three-phase Small Power Induction Motor." World Academy of Science, Engineering & Technolog (WASET), 2(6), 1139–1142.

Turan, N. E. N. (2012). Electrical Machines with MATLAB. Taylor & Francis Group. https://doi.org/10.1038/236184b0

Url-1 <*https://www.electrical4u.com*>. https://www.electrical4u.com/construction-of-three-phase-induction-motor

Url-2 <*http://circuitglobe.com*>. http://circuitglobe.com/difference-between-single-phase-and-three-phase-induction-motor.html

Url-3 <*https://www.inverterdrivesystems.com*>. https://www.inverterdrivesystems.com/mandatory-efficiency-requirements-for-low-voltage-electric-motors

Waide, P., & Brunner, C. U. (2011). Energy-Efficiency Policy Opportunities for Electric Motor-Driven Systems. Internationale Energy Agency, 132. https://doi.org/10.1787/5kgg52gb9gjd-en

Walker, M. (1921). The Diagnosing of Troubles in Electrical Machines; Longmans Green and Co.: Harlow, UK.

Wengerkievicz, C. A. C., Elias, R. de A., Batistela, N. J., Sadowski, N., Kuo-Peng, P., Lima, S. C., Beltrame, A. Y. (2017). Estimation of Three-Phase Induction Motor Equivalent Circuit Parameters from Manufacturer Catalog Data. Journal of Microwaves, Optoelectronics, and Electromagnetic Applications, 16(1), 90–107.

Zamora, J. L., & Garcia-Cerrada, A. (2000). Online estimation of the stator parameters in an induction motor using only voltage and current measurements. Conference Record of the 1999 IEEE Industry Applications Conference Thirty Forth IAS Annual Meeting Cat No99CH36370, 2(3), 805–816. https://doi.org/10.1109/28.845056

APPENDICES

APPENDIX A

Measurement 2

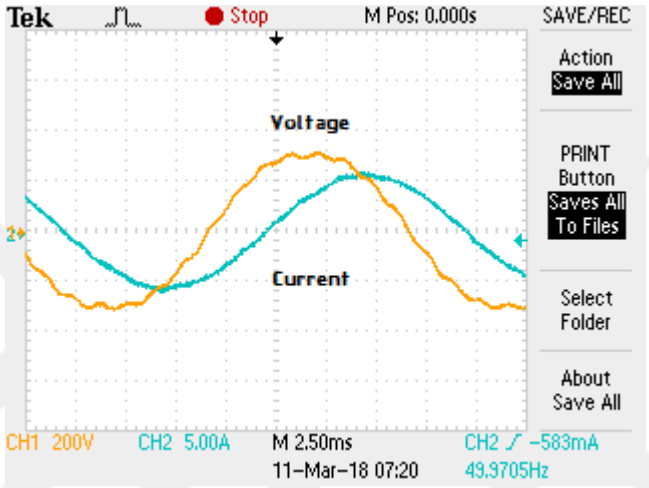

Figure A.1 : Terminal voltage and current waveform from an oscilloscope

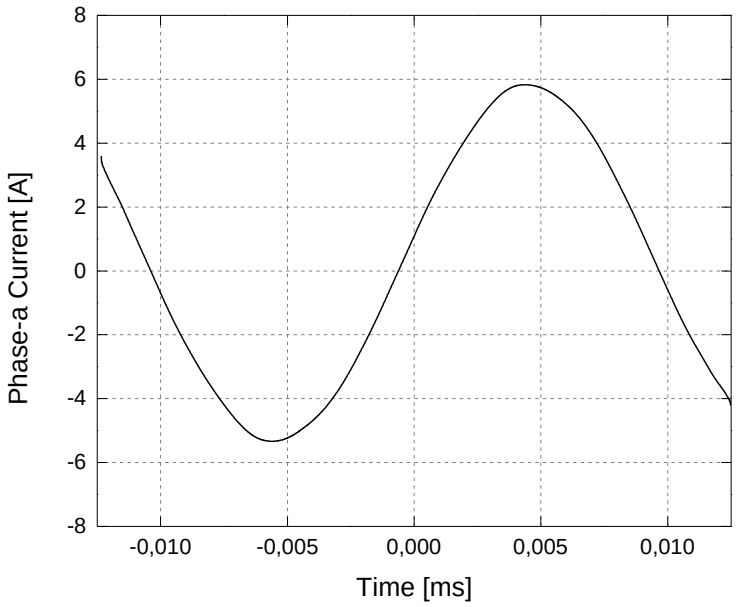

Figure A.2 : Analyzed current waveform

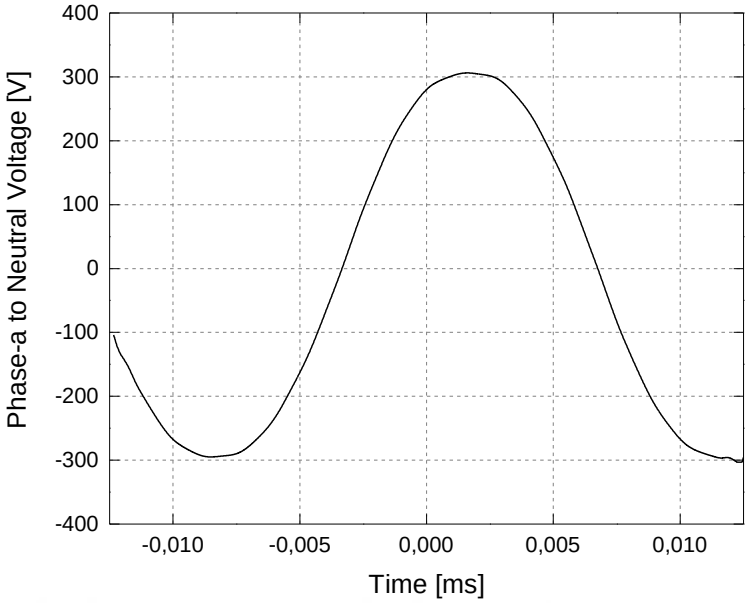

Figure A.3 : Analyzed voltage waveform

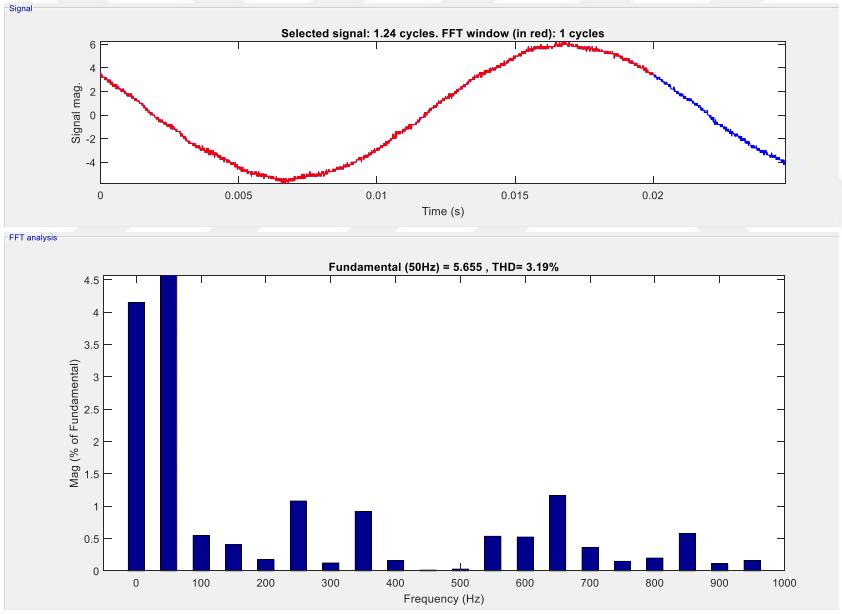

Figure A.4 : FFT (harmonic content due to frequency) of terminal current

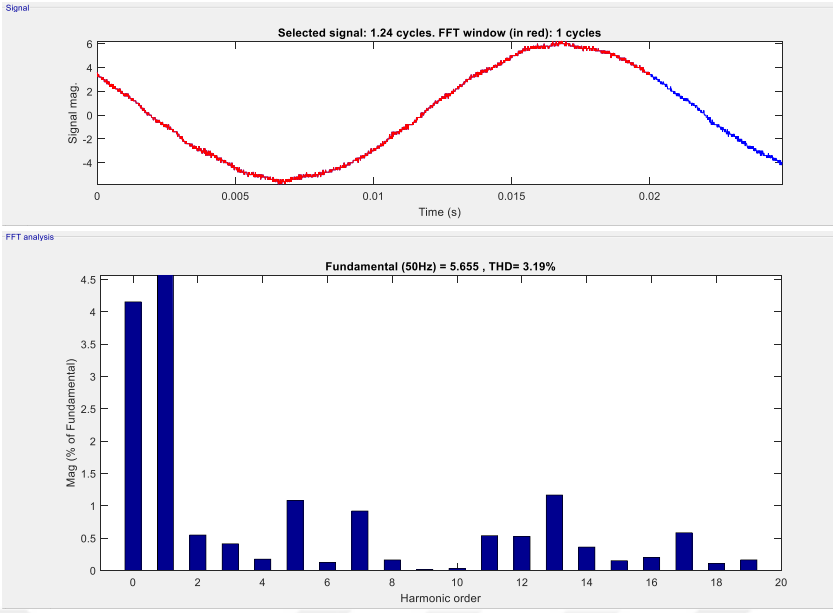

Figure A.5 : Harmonic order content of terminal current

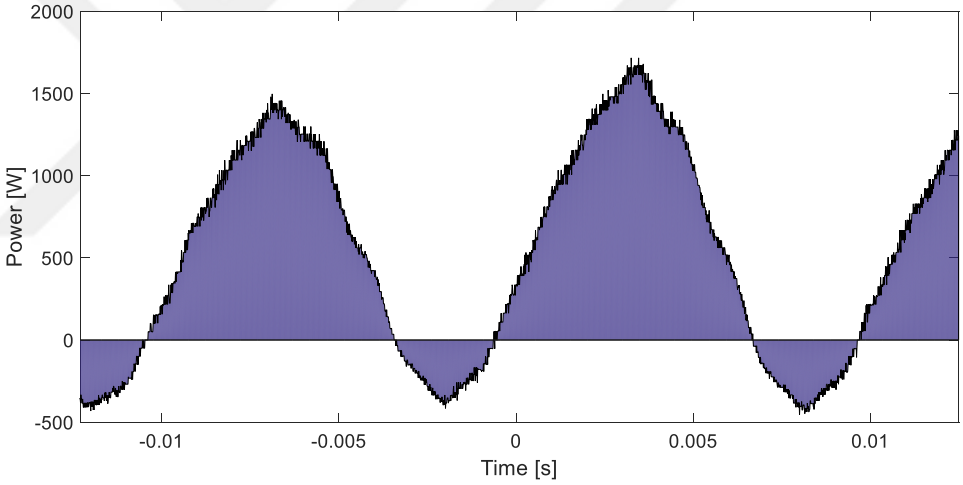

Figure A.6 : Instantaneous input power waveform (v(t).i(t))

The integral of the area is 5.433 which is valid for 0.01 sec. This is reflecting 543.3 W for single phase and 1629.9 W for three-phase which is very close to the measured value of 1.61 kW.

As it can be calculated easily, the input apparent power:

$$S = 2.57565 \text{ kVA}$$

Power factor:

$$PF = 0.6326$$

Table A.1 : CF check for voltage and current waveforms

Parameters	Value
V_{max}/V_{rms}	1,406799
I_{max}/I_{rms}	1,589338

Measurement 3

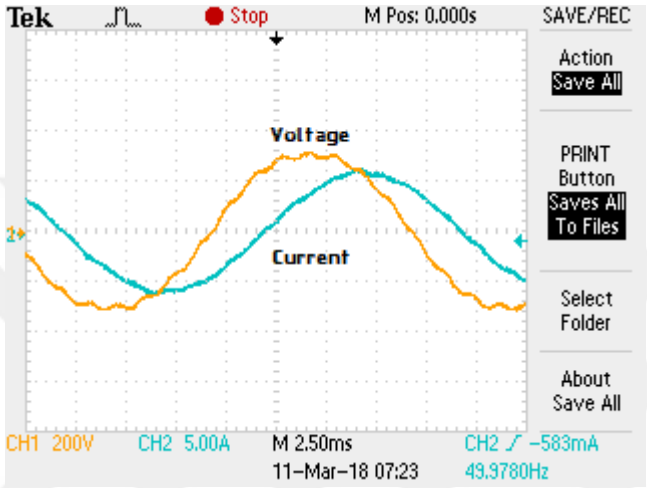

Figure A.7 : Terminal voltage and current waveform from an oscilloscope

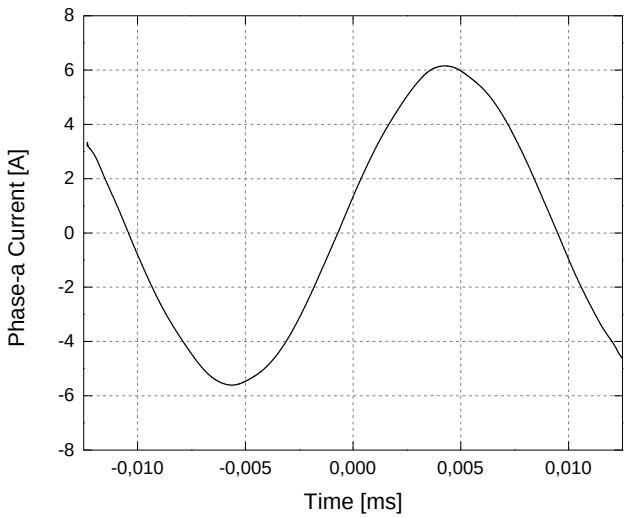

Figure A.8 : Analyzed current waveform

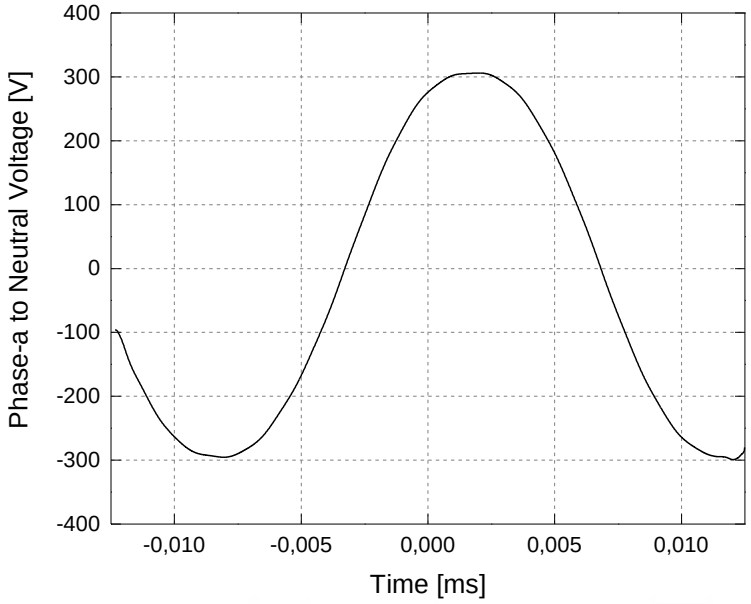

Figure A.9 : Analyzed voltage waveform

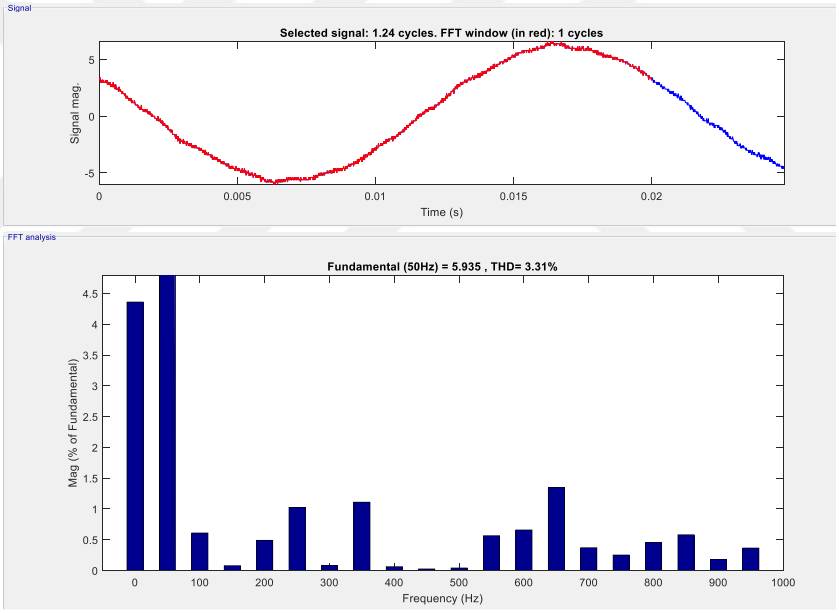

Figure A.10 : FFT (harmonic content due to frequency) of terminal current

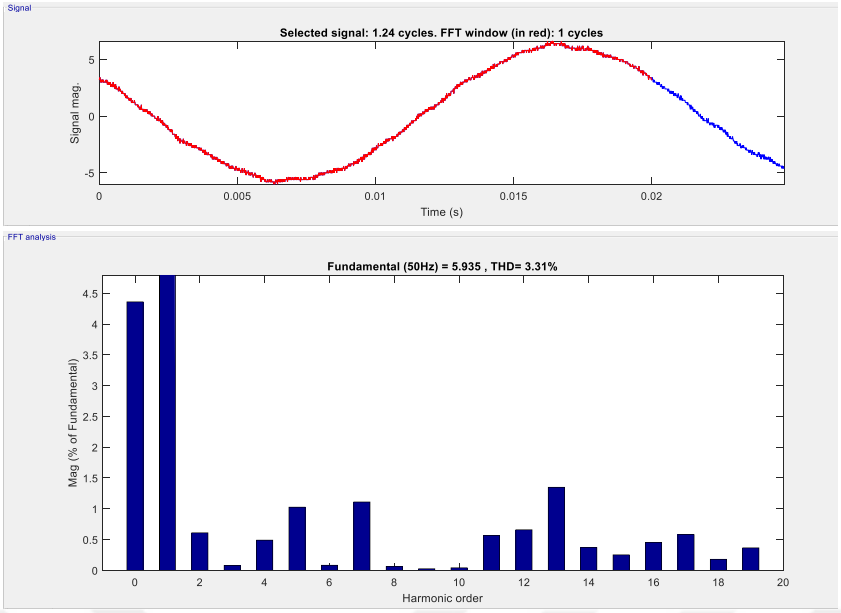

Figure A.11 : Harmonic order content of terminal current

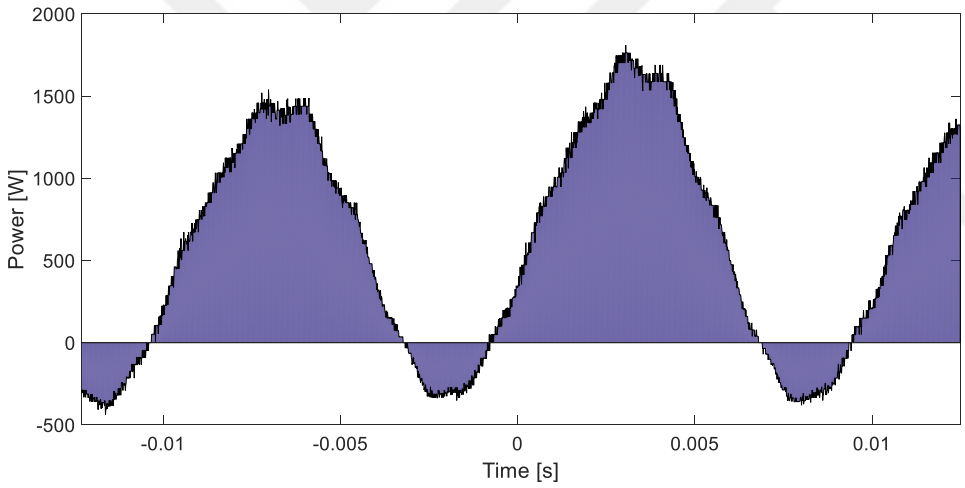

Figure A.12 : Instantaneous input power waveform (v(t).i(t))

The integral of the area is 6.08 which is valid for 0.01 sec. This is reflecting 608 W for single phase and 1824 W for three-phase which is very close to the measured value of 1.8 kW.

As it can be calculated easily, the input apparent power:

$$S = 2.7429 \text{ kVA}$$

Power factor:

$$PF = 0.665$$

Table A.2 : CF check for voltage and current waveforms

Parameters	Value
V_{max}/V_{rms}	1,400209
I_{max}/I_{rms}	1,36978

Measurement 4

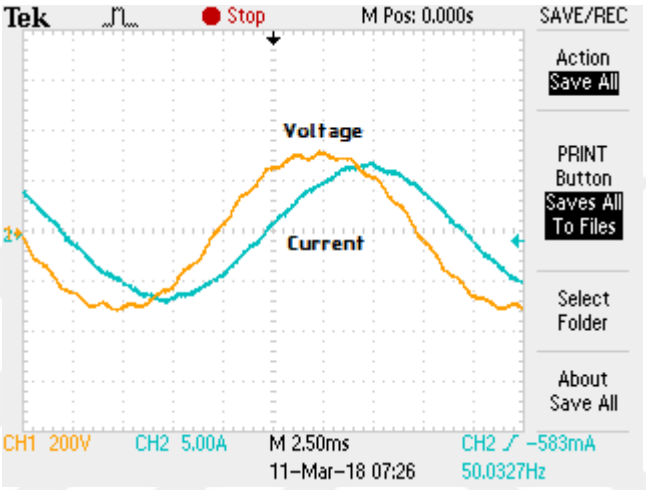

Figure A.13 : Terminal voltage and current waveform from an oscilloscope

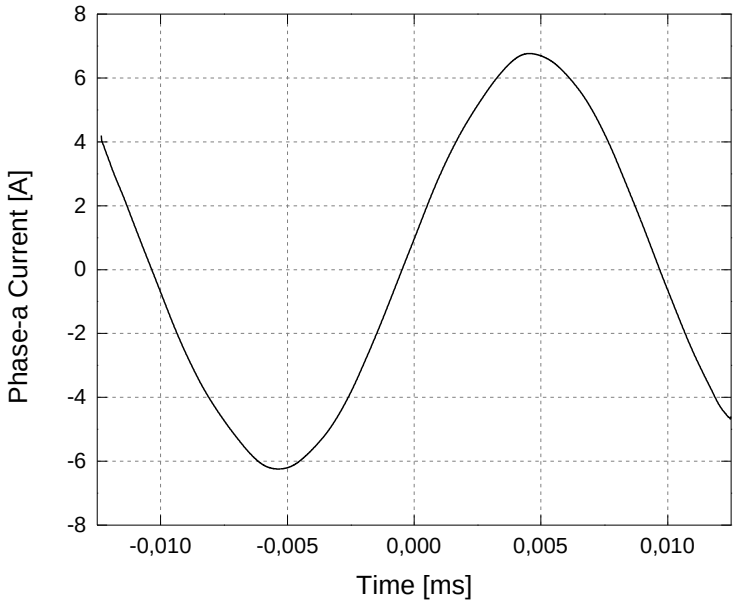

Figure A.14 : Analyzed current waveform

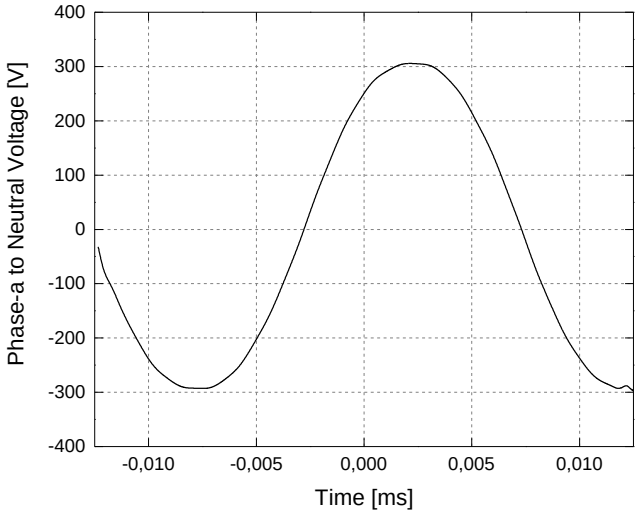

Figure A.15 : Analyzed voltage waveform

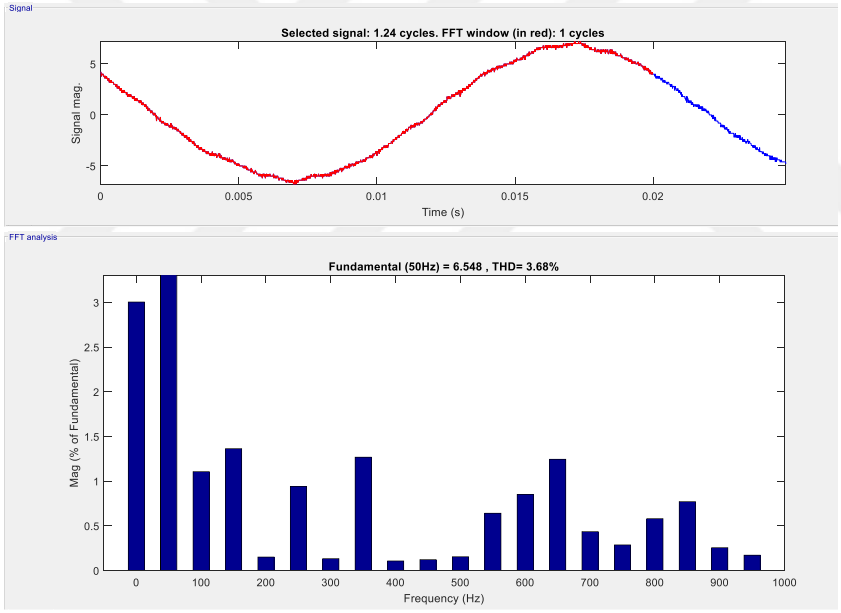

Figure A.16 : FFT (harmonic content due to frequency) of terminal current

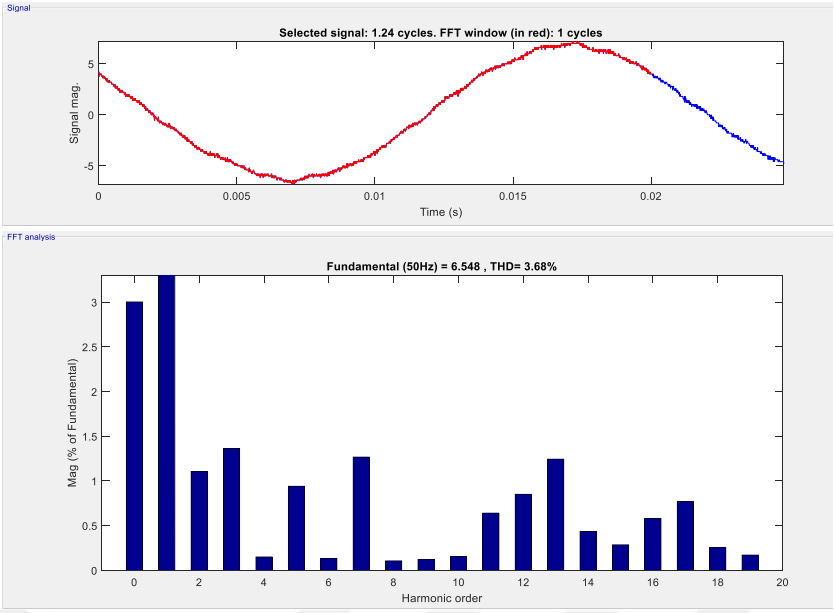

Figure A.17 : Harmonic order content of terminal current

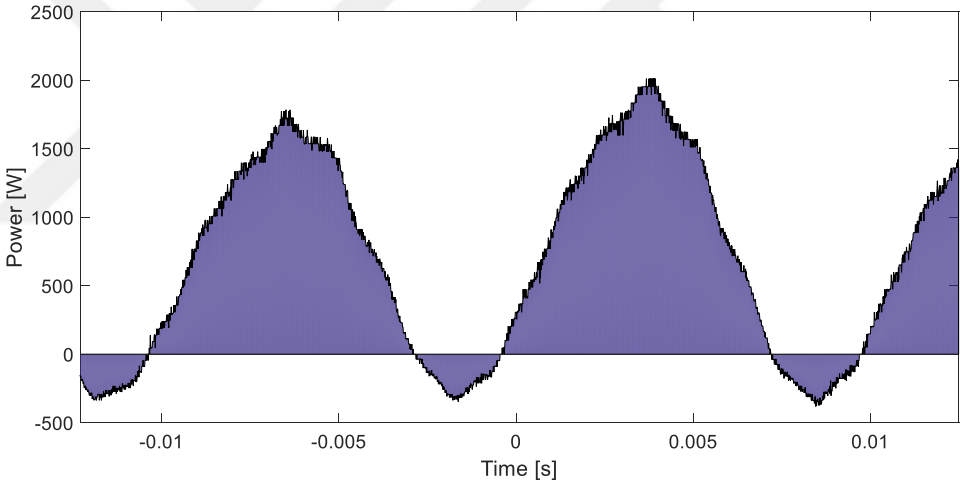

Figure A.18 : Instantaneous input power waveform (v(t).i(t))

The integral of the area is 7.35 which is valid for 0.01 sec. This is reflecting 735 W for single phase and 2205 W for three-phase which is very close to the measured value of 2.19 kW.

As it can be calculated easily, the input apparent power:

$$S = 2.997 \text{ kVA}$$

Power factor:

$$PF = 0.735$$

Table A.3 : CF check for voltage and current waveforms

Parameters	Value
V_{max}/V_{rms}	1,408208
I_{max}/I_{rms}	1,58372

Measurement 5

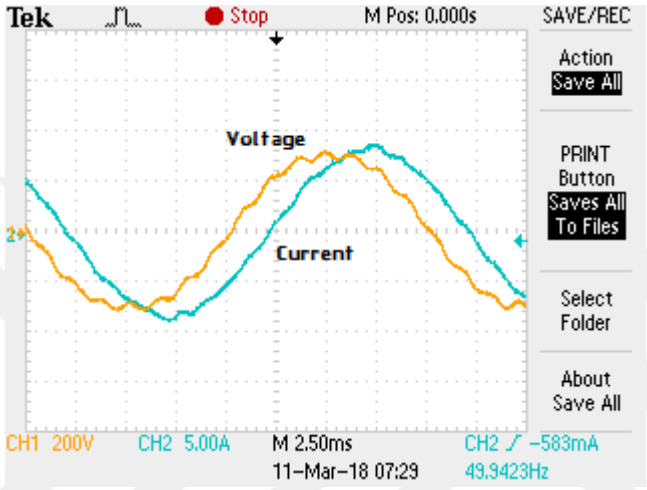

Figure A.19 : Terminal voltage and current waveform from an oscilloscope

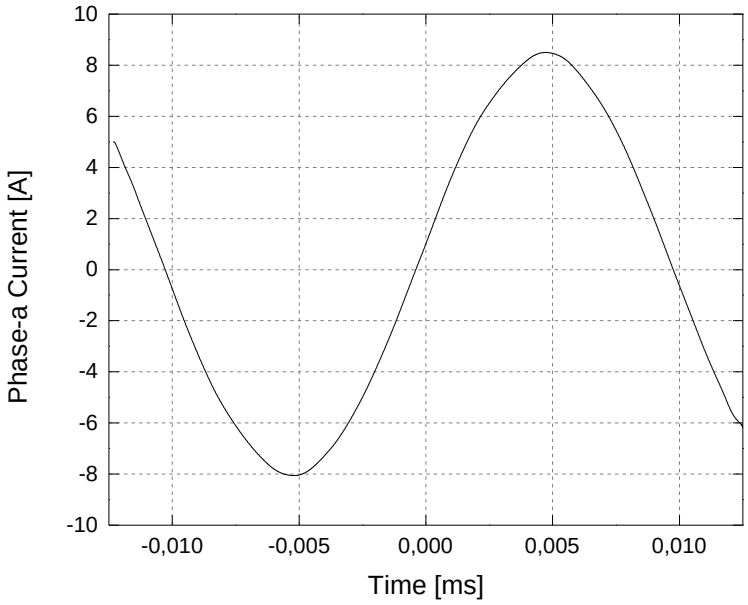

Figure A.20 : Analyzed current waveform

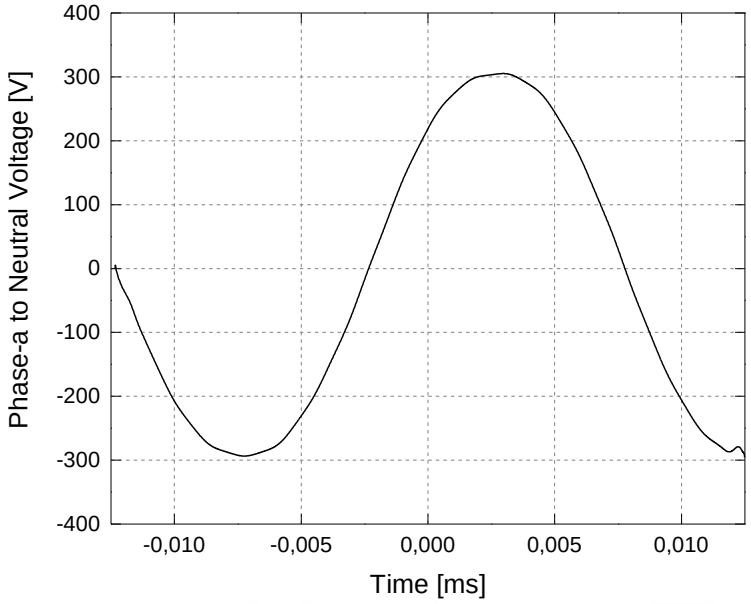

Figure A.21 : Analyzed voltage waveform

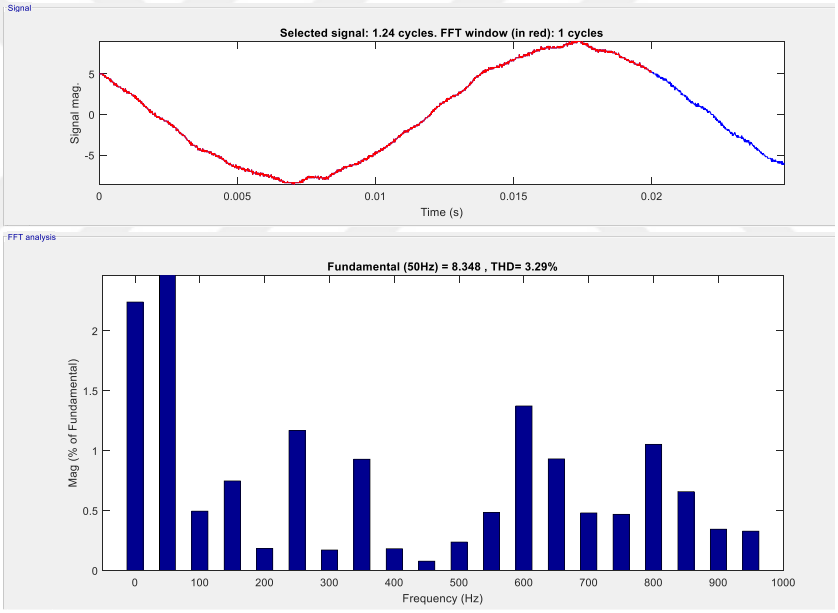

Figure A.22 : FFT (harmonic content due to frequency) of terminal current

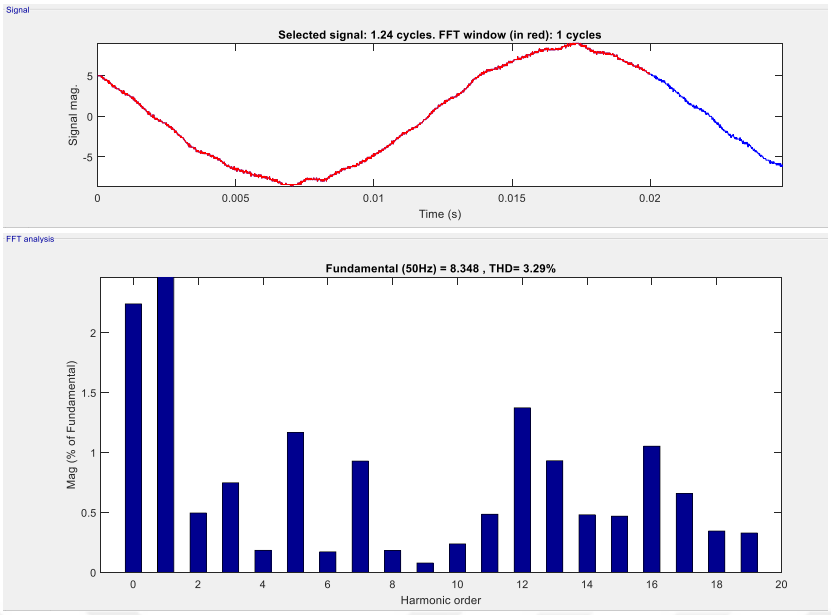

Figure A.23 : Harmonic order content of terminal current

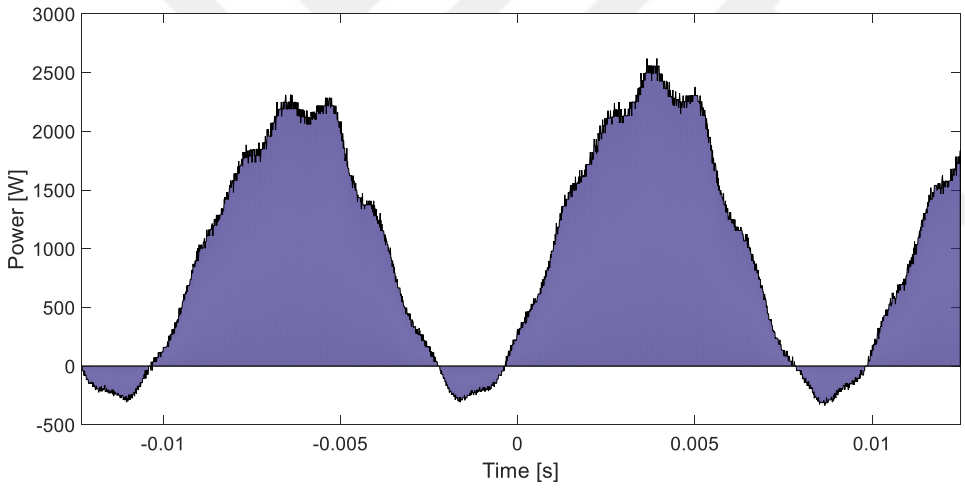

Figure A.24 : Instantaneous input power waveform (v(t).i(t))

The integral of the area is 10.04 which is valid for 0.01 sec. This is reflecting 1004 W for single phase and 3012 W for three-phase which is very close to the measured value of 3.09 kW.

As it can be calculated easily, the input apparent power:

$$S = 3.7791 \text{ kVA}$$

Power factor:

$$PF = 0.797$$

Table A.4 : CF check for voltage and current waveforms

Parameters	Value
V_{max}/V_{rms}	1,412712054
I_{max}/I_{rms}	1,55062807

CURRICULUM VITAE

Name Surname **: Rami Al-Samaraae**

Place and Date of Birth **: Baghdad – 01/04/1991**

E-Mail **: ramirafel1991@gmail.com**

EDUCATION **:**

- **B.Sc.** **:** 2013, College of Electrical and Electronic Technology, Electrical Engineering, Electrical Power Engineering

PROFESSIONAL EXPERIENCE AND REWARDS:

- 2011-2012 member of the maintenance department in Qaswaa Al-Bararry General Trading Company
- 2012-2013 internship on Al-Doura thermal power plant
- 2013-2014 member of the heat exchange department in Al-Usool Engineering Services Company Ltd
- 2017 Preparing to complete a master degree in Istanbul Technical University